WADC TECHNICAL REPORT 54-592, Part 1

EFFECTS OF STRUCTURAL FLEXIBILITY ON GUST LOADING OF AIRCRAFT

Part 1 - GUST LOADS ON SWEPT-WING AIRPLANES FREE TO PITCH AND TO DEFORM STATICALLY

K. A. Foss
Massachusetts Institute of Technology

March 1955

Aircraft Laboratory
Contract No. AF 33(616)-2425
RDO No. R451-344 SR-1g

Wright Air Development Center
Air Research and Development Command
United States Air Force
Wright-Patterson Air Force Base, Ohio

FOREWORD

The trend toward highly flexible aircraft with swept wings has raised some questions as to the applicability of existing methods for calculating the structural stresses due to gust loading. It was consequently decided by the Wright Air Development Center, U.S. Air Force, to initiate research to provide information on the effects of structural flexibility on the gust loading of swept-wing aircraft and to develop methods for computing these effects.

The present report is one of a series to be issued on this research. It was prepared by the Aeroelastic and Structures Research Laboratory, Massachusetts Institute of Technology, under U.S.A.F. Contract No. 33(616)-2425 with Professor T.H.H. Pian as project supervisor and Mr. K.A. Foss as project leader. The contract is being administered by the Aircraft Laboratory, Directorate of Laboratories, Wright Air Development Center, with Mr. H.E. Kugel acting as project engineer and Mr. W. Boccius as scientist advisor.

The author wishes to acknowledge the assistance of Mr. A.A. Kirsch and Mr. R. Storey in checking part of the formulation. He would also like to thank Mr. R.R. Staley for editing the manuscript, the personnel of the Computing Section of the Aeroelastic and Structures Research Laboratory for performing the computations, Mr. W. Marchant for drawing the figures, and Miss F. Miller for typing the report.

ABSTRACT

A simplified numerical method is presented for finding the gust loads on swept-wing airplanes free to pitch and to deform statically. The effects of the swept wing and the fuselage penetrating a gust front and the effects of unsteady downwash from the wing on the horizontal tail are included. Some sample calculations indicate that the combination of wing sweep and pitching motion increases the gust loads on a rigid airplane, particularly the loads on the horizontal tail.

PUBLICATION REVIEW

This report has been reviewed and is approved.

FOR THE COMMANDER:

E H Schwartz
for D. D. McKee
Colonel, USAF
Chief, Aircraft Laboratory
Directorate of Laboratories

TABLE OF CONTENTS

LIST OF ILLUSTRATIONS

LIST OF ILLUSTRATIONS (Cont.)

LIST OF TABLES

GLOSSARY OF SYMBOLS

A	Cross-sectional area of body of revolution equivalent to fuselage
AR	Aspect ratio
a	Lift-curve slope
b	Span of lifting surface
C_L	Lift coefficient, based on wing area
$\frac{dC_{m_f}}{d\alpha}$	Moment-curve slope of fuselage, based on wing area and wing mean geometric chord
c	Chord
$\bar{c}$	Mean geometric chord
F	Gust profile function $= \frac{w}{w_{max}}$
f, g	Gust forcing functions
K_y	Dimensionless radius of gyration of airplane $= \frac{k_y}{\bar{c}/2}$
k_y	Pitching radius of gyration of airplane
L	Lift
l	Distance in streamwise direction, measured in mean geometric wing semichords

GLOSSARY OF SYMBOLS (Cont.)

M	Mass of airplane
$\mathfrak{M}$	Pitching moment
P_t	Tail parameter $= \frac{S_t a_t}{S_w a_w}$
s	Dimensionless time $= \frac{Ut}{\bar{c}/2}$
s_g	Gust-gradient distance, distance to gust peak in mean geometric wing semichords
S	Area of lifting surface
t	Time from beginning of gust penetration
U	True airspeed of airplane
V_f	Volume of body of revolution equivalent to fuselage
w	Vertical velocity of gust
y	Spanwise coordinate, measured perpendicular from center line of airplane
z	Vertical displacement of center of gravity of airplane, positive up
α	Angle of attack
β	Sweep parameter
γ	Ratio of mean geometric wing chord to mean geometric tail chord $= \bar{c}_w / \bar{c}_t$

GLOSSARY OF SYMBOLS (Cont.)

ϵ	Increment of s for numerical integration
$\frac{d\epsilon}{d\alpha}$	Downwash parameter
ζ	Indicial lift growth on horizontal tail due to downwash from wing
η	Dimensionless spanwise coordinate $= \frac{y}{b/2}$
θ	Pitch angle of airplane, positive nose up
Λ	Sweep angle
λ	Taper ratio
μ	Dimensionless mass parameter $= \frac{M}{\rho S_w \frac{\bar{c}}{2} a_w}$
ζ	Dimensionless vertical displacement coordinate $= \frac{z}{c/2}$
ρ	Mass density of air
ϕ	Wagner lift-growth function
ψ	Kussner lift-growth function

Subscripts

f	Fuselage
w	Wing
t	Horizontal tail
Λ	Includes effects of sweep

Superscripts

A	Due to apparent mass effects
G	Due to gust
L	For lift
m	For pitching
α	Due to angle of attack (or motion)

Notation

$( )'$	Differentiation with respect to s
$(\dot{})$	Differentiation with respect to t
$[\,]$	Rectangular matrix
$\{\,\}$	Column matrix

INTRODUCTION

Considerable research has been conducted to determine the effect of longitudinal stability on the gust loading of unswept-wing aircraft, e.g., References 1, 2 and 3. These investigations showed that the inclusion of a pitching degree of freedom in a gust analysis often increases the gust loads on an airplane, but the amount of the increase is never very significant. When the airplane has a sweptback wing, however, the initial entry of the forward inboard sections of the wing into a gust front may produce a pitching motion which is large enough to have a significant effect on the resulting gust loads, and the present report is concerned with this effect.

In Section I the equations of motion are formulated for the response of a swept-wing airplane to a discrete gust. The effects of the swept wing and the fuselage penetrating a gust front and the effects of unsteady downwash from the wing on the horizontal tail are taken into account. The effects of flexibility can be included when the gradient distance of the gust is long enough to consider the structural response as quasi-steady.

To develop a method of solution suitable for engineering use, many possible simplifications have been investigated. For instance, expressions for the growth of lift and pitching moment on swept wings are greatly simplified with little loss of accuracy by using an average gust penetration distance for the entire portion of the wing which is enveloped by the gust.

A simplified numerical procedure for computing the time histories of the gust loads is presented in Section II. Since this method involves a

step-by-step recurrence relationship, it is particularly adaptable to automatic digital computing machinery. The computing steps involved in this numerical method are illustrated by a numerical example in Section III, and the accuracy, convergence and stability of this numerical technique are investigated in Appendix B.

I. EQUATIONS OF MOTION

For coördinate axes fixed in space, the equations of motion of a rigid airplane after entry into a discrete gust are

$$M\ddot{z} - L^A(\ddot{z}, \ddot{\theta}, \dot{\theta}) - L^\alpha(\dot{z}, \dot{\theta}, \theta) = L^G(w) \tag{1.1}$$

and

$$k_y^2 M\ddot{\theta} - \mathcal{M}^A(\ddot{z}, \ddot{\theta}, \dot{\theta}) - \mathcal{M}^\alpha(\dot{z}, \dot{\theta}, \theta) = \mathcal{M}^G(w) \tag{1.2}$$

where

z	is the vertical displacement of the center of gravity
θ	is the nose-up pitch angle
M	is the mass of the airplane
k_y	is the pitching radius of gyration of the airplane
w	is the vertical gust velocity
L^G	is the lift due to the gust
L^α	is the lift due to the angle of attack (or motion)
L^A	is the lift due to the apparent mass of the surrounding air
$\mathcal{M}^G$	is the pitching moment due to the gust
$\mathcal{M}^\alpha$	is the pitching moment due to the angle of attack
$\mathcal{M}^A$	is the pitching moment due to the apparent mass effects.

Equations (1.1) and (1.2) are based on forces and displacements which have incremental values above those necessary for level flight. An assumption inherent in these equations is that the forward velocity of the airplane, U, remains constant.

The expressions for the lifts and pitching moments in equations (1.1) and (1.2) are derived in Appendix A with the effects of unsteady aerodynamics and wing sweep included. When substituting these expressions into equations (1.1) and (1.2), it is convenient to make these equations dimensionless by the use of the dimensionless time,

$$s = \frac{Ut}{\bar{c}/2} \tag{1.3}$$

and by dividing equation (1.1) through by

$$\tfrac{1}{2}\rho U^2 S_w a_w$$

and equation (1.2) by

$$\tfrac{1}{2}\rho U^2 S_w \tfrac{\bar{c}}{2} a_w$$

Equations (1.1) and (1.2) then become,

$$\begin{aligned} &2\mu \xi'' + 2\mu_A \left[\xi'' - \theta' - \bar{l}_A \theta''\right] + \int_0^s \left[\xi'' - \theta' - \bar{l}_3 \theta''\right] \phi(s-\sigma)\, d\sigma \\ &+ P_t \int_0^s \left[\xi'' - \theta' - \left(l_t + \tfrac{1}{\gamma}\right)\theta''\right] \phi(\gamma s - \gamma\sigma)\, d\sigma \\ &- P_t \frac{d\epsilon}{d\alpha} \int_0^s \left[\xi'' - \theta' - l_3 \theta''\right] \zeta^{\alpha}(s-\sigma)\, d\sigma = f(s) \end{aligned} \tag{1.4}$$

$$\begin{aligned} &2K_y^2 \mu \theta'' + 2\mu_A \left[K_A^2 \theta'' - \bar{l}_A (\xi'' - l_\theta \theta')\right] - l_w \int_0^s \left[\xi'' - \theta' - \frac{\bar{l}_2}{l_w}\theta''\right] \phi(s-\sigma)\, d\sigma \\ &- l_t P_t \int_0^s \left[\xi'' - \theta' - \left(l_t + \tfrac{1}{\gamma}\right)\theta''\right] \phi(\gamma s - \gamma\sigma)\, d\sigma \\ &+ l_t P_t \frac{d\epsilon}{d\alpha} \int_0^s \left[\xi'' - \theta' - l_3 \theta''\right] \zeta^{\alpha}(s-\sigma)\, d\sigma \\ &- \frac{2}{a_w} \frac{dC_{m_f}}{d\alpha} \left[\theta - \xi' + \left(\bar{l}_f - l_{CG}\right)\theta'\right] = g(s) \end{aligned} \tag{1.5}$$

respectively, where

$$\bar{z} = \frac{z}{\bar{c}/2}$$

$$\mu = \frac{M}{\rho S_w \frac{\bar{c}}{2} a_w}$$

$$K_y = \frac{k_y}{\bar{c}/2}$$

$$\mu_A = \mu_{A_w} + \mu_{A_t} + \mu_{A_f}$$

$$\mu_{A_w} = \frac{\pi}{2 a_w} \left[1 + \frac{1}{3} \left(\frac{1-\lambda}{1+\lambda} \right)^2 \right]$$

$$\mu_{A_t} = \frac{\pi}{2 a_w} \frac{1}{\gamma} \frac{S_t}{S_w} \left[1 + \frac{1}{3} \left(\frac{1-\lambda_t}{1+\lambda_t} \right)^2 \right]$$

$$\mu_{A_f} = \frac{V_f}{S_w \frac{\bar{c}}{2} a_w}$$

$$\bar{l}_A = \frac{k_1 \mu_{A_w} + \left(l_t + \frac{1}{2\gamma} \right) \mu_{A_t} + \left(\bar{l}_f - l_{CG} \right) \mu_{A_f}}{\mu_{A_w} + \mu_{A_f} + \mu_{A_t}}$$

$$K_A^2 = \frac{k_3 \mu_{A_w} + \left(l_t + \frac{1}{2Y}\right)^2 \mu_{A_t} + \left[k_f^2 + \left(\bar{l}_f - l_{CG}\right)^2\right] \mu_{A_f}}{\mu_{A_w} + \mu_{A_f} + \mu_{A_t}}$$

$$l_{\dot{\theta}} = \frac{k_2 \mu_{A_w} + \left(l_t + \frac{1}{2Y}\right) \mu_{A_t} + \left(\bar{l}_f - l_{CG}\right) \mu_{A_f}}{k_1 \mu_{A_w} + \left(l_t + \frac{1}{2Y}\right) \mu_{A_t} + \left(\bar{l}_f - l_{CG}\right) \mu_{A_f}}$$

$$P_t = \frac{S_t \, a_t}{S_w \, a_w}$$

$$f(s) = \frac{L^G(s)}{\frac{1}{2} \rho U^2 S_w \, a_w}$$

$$g(s) = \frac{m^G(s)}{\frac{1}{2} \rho U^2 S_w \frac{\bar{c}}{2} a_w}$$

$\phi(s)$ is the Wagner function

$\zeta^{\alpha}(s)$ is the normalized lift growth function for the horizontal tail due to the downwash from the wing

l_w is the distance that the wing center of pressure lies aft of the airplane center of gravity in mean geometric wing semichords (usually negative)

l_t is the tail length, i.e., the distance that the tail center of pressure lies aft of the airplane center of gravity in mean geometric wing semichords

$\frac{d\epsilon}{d\alpha}$ is the steady-state downwash parameter

$\frac{dC_{m_f}}{d\alpha}$ is the moment-curve slope for the fuselage.

The remaining symbols are defined in the glossary of symbols in the front of this report and in Appendix A. The prime marks used in equations (1.4) and (1.5) denote differentiation with respect to s. Expressions for the forcing functions, $f(s)$ and $g(s)$, are given in Appendix A.4, for a sharp-edged gust per unit w/U. Forcing functions for other gust profiles can be found by the use of Duhamel's integral as shown in Appendix A. In the present paper, however, the equations of motion are solved for a sharp-edged gust, and Duhamel's integral is applied to these responses to obtain results for a one-minus-cosine gust.

The solution of equations (1.4) and (1.5) by analytical means is impractical because of the convolution integrals which contain the unknown responses in their integrands and because of the complexity of the forcing functions. The solution of these equations by numerical integration is described in the following section.

II. NUMERICAL INTEGRATION OF THE EQUATIONS OF MOTION

The numerical integration technique described in this section is a combination of the methods presented in References 3, 4 and 5. In this numerical procedure, the unknown responses, ξ'' and θ'', are found only at the discrete times, $s = n\epsilon$, where ϵ is a chosen small interval of time and n takes on the integral values,

$$n = 0, 1, 2, \ldots$$

For a particular time, $s = n\epsilon$, equations (1.4) and (1.5) can be written in matrix form as follows:

$$[A]\begin{Bmatrix} \xi'' \\ \theta'' \\ \xi' \\ \theta' \\ \theta \\ T^{(1)} \\ T^{(2)} \\ T^{(3)} \\ T^{(4)} \end{Bmatrix}_n + [B]\begin{Bmatrix} \xi'' \\ \theta'' \\ \xi' \\ \theta' \\ \theta \\ T^{(1)} \\ T^{(2)} \\ T^{(3)} \\ T^{(4)} \end{Bmatrix}_{n-n_r} = \begin{Bmatrix} f \\ g \end{Bmatrix}_n \tag{2.1}$$

where

$$[A] = \begin{bmatrix} A_{11} & A_{12} & \cdots & A_{19} \\ A_{21} & A_{22} & \cdots & A_{29} \end{bmatrix} \tag{2.2}$$

$$[B] = \begin{bmatrix} B_1 & B_2 & \cdots & B_9 \\ -l_t B_1 & -l_t B_2 & \cdots & -l_t B_9 \end{bmatrix} \qquad (2.3)$$

$$A_{11} = 2\mu + 2\mu_A$$

$$A_{12} = -2\bar{l}_A \mu_A$$

$$A_{13} = 1 + P_t + 0.2\, P_t \frac{d\epsilon}{d\alpha}$$

$$A_{14} = -2\mu_A - \bar{l}_3 - P_t\left(l_t + \frac{1}{\gamma}\right) - 0.2\, l_3 P_t \frac{d\epsilon}{d\alpha}$$

$$A_{15} = -A_{13}$$

$$A_{16} = 1$$

$$A_{17} = 1$$

$$A_{18} = P_t$$

$$A_{19} = P_t$$

$$A_{21} = A_{12}$$

$$A_{22} = 2K_y^2 \mu + 2K_A^2 \mu_A$$

$$A_{23} = -l_w - l_t P_t - 0.2\, l_t P_t \frac{d\epsilon}{d\alpha} + \frac{2}{a_w} \frac{dC_{m_f}}{d\alpha}$$

$$A_{24} = 2\bar{l}_A l_{\dot{\theta}} \mu_A + \bar{l}_2 + l_t P_t \left(l_t + \frac{1}{y}\right) + 0.2\, l_t l_3 P_t \frac{d\epsilon}{d\alpha} - \left(\bar{l}_f - l_{CG}\right)\frac{2}{a_w}\frac{dC_{m_f}}{d\alpha}$$

$$A_{25} = -A_{23}$$

$$A_{26} = -l_w$$

$$A_{27} = -l_w$$

$$A_{28} = -l_t P_t$$

$$A_{29} = -l_t P_t$$

$$B_1 = 0$$

$$B_2 = 0$$

$$B_3 = -1.2\, P_t \frac{d\epsilon}{d\alpha}$$

$$B_4 = 1.2\, l_3 P_t \frac{d\epsilon}{d\alpha}$$

$$B_5 = -B_3$$

$$B_6 = 0$$

$$B_7 = 0$$

$$B_8 = 0$$

$$B_9 = 0$$

The $T^{(i)}$ functions are defined by

$$T_n^{(1)} = .165 \int_0^{n\epsilon} \left(\theta' - \gamma'' + \bar{l}_3 \theta''\right) e^{-.045(n\epsilon - \sigma)} d\sigma \tag{2.4}$$

$$T_n^{(2)} = .335 \int_0^{n\epsilon} \left(\theta' - \gamma'' + \bar{l}_3 \theta''\right) e^{-.30(n\epsilon - \sigma)} d\sigma \tag{2.5}$$

$$T_n^{(3)} = .165 \int_0^{n\epsilon} \left[\theta' - \gamma'' + \left(l_t + \frac{1}{\gamma}\right)\theta''\right] e^{-.045\gamma(n\epsilon - \sigma)} d\sigma \tag{2.6}$$

$$T_n^{(4)} = .335 \int_0^{n\epsilon} \left[\theta' - \gamma'' + \left(l_t + \frac{1}{\gamma}\right)\theta''\right] e^{-.30\gamma(n\epsilon - \sigma)} d\sigma \tag{2.7}$$

These functions are the result of using the exponential approximation of the Wagner function,

$$\phi(s) = 1 - .165\, e^{-.045s} - .335\, e^{-.30s} \tag{2.8}$$

Any other exponential expression for the Wagner function could be used, e.g., one of those given in Reference 6 for subsonic compressible flow.

The second term on the left-hand side of equation (2.1) represents the lag in downwash at the horizontal tail due to the motion of the wing. This term was obtained by using the step-function approximation of $\zeta^{\alpha}(s)$ given by equation (A.61). The number n_r must be taken as the nearest integer to

$$n_r = \frac{l_{tw} + \frac{\beta_t}{2\gamma} + 1.6}{\epsilon} \tag{2.9}$$

Equation (2.1) can be integrated approximately by assuming that the time histories of β'' and θ'' are formed by straight-line segments between each of the points, $s = n\epsilon$. The integration of this straight-line relationship between the points, $n-1$ and n , yields

$$\beta'_n = \beta'_{n-1} + \frac{\epsilon}{2}\beta''_n + \frac{\epsilon}{2}\beta''_{n-1} \tag{2.10}$$

$$\theta'_n = \theta'_{n-1} + \frac{\epsilon}{2}\theta''_n + \frac{\epsilon}{2}\theta''_{n-1} \tag{2.11}$$

$$\theta_n = \theta_{n-1} + \epsilon\,\theta'_{n-1} + \frac{\epsilon^2}{6}\theta''_n + \frac{\epsilon^2}{3}\theta''_{n-1} \tag{2.12}$$

In addition, the application of the trapezoidal rule of integration to equation (2.4) yields

$$\begin{aligned} T^{(i)} &= e^{-.045\epsilon}T^{(i)}_{n-1} + .165\frac{\epsilon}{2}\left(\theta'_n - \beta''_n + \bar{l}_3\,\theta''_n\right) \\ &\quad + .165\frac{\epsilon}{2}e^{-.045\epsilon}\left(\theta'_{n-1} - \beta''_{n-1} + \bar{l}_3\,\theta''_{n-1}\right) \\ &= e^{-.045\epsilon}T^{(i)}_{n-1} + .165\frac{\epsilon}{2}\left(\theta'_{n-1} + \left(\bar{l}_3 + \frac{\epsilon}{2}\right)\theta''_n + \frac{\epsilon}{2}\theta''_{n-1} - \beta''_n\right) \\ &\quad + .165\frac{\epsilon}{2}e^{-.045\epsilon}\left(\theta'_{n-1} - \beta''_{n-1} + \bar{l}_3\,\theta''_{n-1}\right) \end{aligned} \tag{2.13}$$

Similar expressions for the other $T^{(i)}$ - functions can be obtained by analogy.

Equations (2.10), (2.11), (2.12) and (2.13) can be combined in matrix form as follows:

$$\begin{Bmatrix} \xi'' \\ \theta'' \\ \xi' \\ \theta' \\ \theta \\ T^{(1)} \\ T^{(2)} \\ T^{(3)} \\ T^{(4)} \end{Bmatrix}_n = [C] \begin{Bmatrix} \xi'' \\ \theta'' \end{Bmatrix}_n + [D] \begin{Bmatrix} \xi'' \\ \theta'' \\ \xi' \\ \theta' \\ \theta \\ T^{(1)} \\ T^{(2)} \\ T^{(3)} \\ T^{(4)} \end{Bmatrix}_{n-1} \tag{2.14}$$

The matrices $[C]$ and $[D]$ are defined by

$$[C] = \begin{bmatrix} 1 & 0 \\ 0 & 1 \\ \epsilon/2 & 0 \\ 0 & \epsilon/2 \\ 0 & \epsilon^2/6 \\ -.165\frac{\epsilon}{2} & .165\frac{\epsilon}{2}\left(\bar{l}_3 + \frac{\epsilon}{2}\right) \\ -.335\frac{\epsilon}{2} & .335\frac{\epsilon}{2}\left(\bar{l}_3 + \frac{\epsilon}{2}\right) \\ -.165\frac{\epsilon}{2} & .165\frac{\epsilon}{2}\left(l_t + \frac{1}{y} + \frac{\epsilon}{2}\right) \\ -.335\frac{\epsilon}{2} & .335\frac{\epsilon}{2}\left(l_t + \frac{1}{y} + \frac{\epsilon}{2}\right) \end{bmatrix} \tag{2.15}$$

$$[D] = \begin{bmatrix} 0 & & & & & & & & \\ 0 & 0 & & & & & & & \\ \epsilon/2 & 0 & 1 & & & & & & \\ 0 & \epsilon/2 & 0 & 1 & & & & & \\ 0 & \epsilon^2/3 & 0 & \epsilon & 1 & & & & \\ D_{61} & D_{62} & 0 & D_{64} & 0 & e^{-.045\epsilon} & & & \\ D_{71} & D_{72} & 0 & D_{74} & 0 & 0 & e^{-.30\epsilon} & & \\ D_{81} & D_{82} & 0 & D_{84} & 0 & 0 & 0 & e^{-.045\gamma\epsilon} & \\ D_{91} & D_{92} & 0 & D_{94} & 0 & 0 & 0 & 0 & e^{-.30\gamma\epsilon} \end{bmatrix} \quad (2.16)$$

where

$$D_{61} = -.165\frac{\epsilon}{2}e^{-.045\epsilon} \qquad D_{81} = -.165\frac{\epsilon}{2}e^{-.045\gamma\epsilon}$$

$$D_{62} = .165\left(\frac{\epsilon}{2}\right)^2 - \bar{l}_3 D_{61} \qquad D_{82} = .165\left(\frac{\epsilon}{2}\right)^2 - \left(l_t + \frac{1}{\gamma}\right) D_{81}$$

$$D_{64} = .165\frac{\epsilon}{2} - D_{61} \qquad D_{84} = .165\frac{\epsilon}{2} - D_{81}$$

$$D_{71} = -.335\frac{\epsilon}{2}e^{-.30\epsilon} \qquad D_{91} = -.335\frac{\epsilon}{2}e^{-.30\gamma\epsilon}$$

$$D_{72} = .335\left(\frac{\epsilon}{2}\right)^2 - \bar{l}_3 D_{71} \qquad D_{92} = .335\left(\frac{\epsilon}{2}\right)^2 - \left(l_t + \frac{1}{\gamma}\right) D_{91}$$

$$D_{74} = .335\frac{\epsilon}{2} - D_{71} \qquad D_{94} = .335\frac{\epsilon}{2} - D_{91}$$

The substitution of equation (2.14) into equation (2.1) gives

$$[A][C]\begin{Bmatrix} \ddot{\beta} \\ \ddot{\theta} \end{Bmatrix}_n + [A][D] \begin{Bmatrix} \ddot{\beta} \\ \ddot{\theta} \\ \dot{\beta} \\ \dot{\theta} \\ \theta \\ T^{(1)} \\ T^{(2)} \\ T^{(3)} \\ T^{(4)} \end{Bmatrix}_{n-1} + [B] \begin{Bmatrix} \ddot{\beta} \\ \ddot{\theta} \\ \dot{\beta} \\ \dot{\theta} \\ \theta \\ T^{(1)} \\ T^{(2)} \\ T^{(3)} \\ T^{(4)} \end{Bmatrix}_{n-n_r} = \begin{Bmatrix} f \\ g \end{Bmatrix}_n \qquad (2.17)$$

Since $[A][C]$ is a square matrix of order two, it is easily inverted, and equation (2.17) can be solved for the accelerations, $\ddot{\beta}_n$ and $\ddot{\theta}_n$. The multiplication of equation (2.17) by the inverse of $[A][C]$ gives

$$\begin{Bmatrix} \ddot{\beta} \\ \ddot{\theta} \end{Bmatrix}_n = [K]\begin{Bmatrix} f \\ g \end{Bmatrix}_n - [E] \begin{Bmatrix} \ddot{\beta} \\ \ddot{\theta} \\ \dot{\beta} \\ \dot{\theta} \\ \theta \\ T^{(1)} \\ T^{(2)} \\ T^{(3)} \\ T^{(4)} \end{Bmatrix}_{n-1} - [F] \begin{Bmatrix} \ddot{\beta} \\ \ddot{\theta} \\ \dot{\beta} \\ \dot{\theta} \\ \theta \\ T^{(1)} \\ T^{(2)} \\ T^{(3)} \\ T^{(4)} \end{Bmatrix}_{n-n_r} \qquad (2.18)$$

where

$$[K] = \left[[A][C]\right]^{-1} \tag{2.19}$$

$$[E] = [K][A][D] \tag{2.20}$$

$$[F] = [K][B] \tag{2.21}$$

When used alternatively, equations (2.18) and (2.14) form a recurrence relationship which can be used to compute the time histories of $\ddot{\zeta}$ and $\ddot{\theta}$. The velocities, $\dot{\zeta}$ and $\dot{\theta}$, the pitch angle, θ, and the $T^{(i)}$ functions are also obtained automatically in the computing process. These quantities are needed to find the gust loads on the airplane. The initial condition for this recurrence relationship is that

$$\left\{\begin{array}{c} \ddot{\zeta} \\ \ddot{\theta} \\ \dot{\zeta} \\ \dot{\theta} \\ \theta \\ T^{(1)} \\ T^{(2)} \\ T^{(3)} \\ T^{(4)} \end{array}\right\}_0 = 0 \tag{2.22}$$

The accelerations at $n = 0$ are zero because the forcing functions, $f(s)$ and $g(s)$, are always zero at $s = 0$.

The accuracy of the numerical integration technique used in deriving

this recurrence solution is investigated in Appendix B. An integration interval of $\epsilon = 2$ is found to provide good accuracy for the problem at hand. If quasi-steady aerodynamics were used, the numerical solution given above would be greatly simplified because it would then be unnecessary to carry along the $T^{(i)}$ functions in the computations. The effect of neglecting unsteady aerodynamics in the damping terms of the equations of motion is illustrated in Appendix C. These results show that it is much more important to include the pitching degree of freedom than to include the effects of unsteady flow on the damping terms insofar as the gust loads on the example swept-wing airplane are concerned. The conclusion is reached in Appendix C that the use of quasi-steady aerodynamics in the damping terms is probably always justifiable when computing the gust loads on swept-wing airplanes free to pitch.

With the assumption of quasi-steady damping, the air forces due to apparent mass effects are zero, i.e., $L^A = \mathcal{M}^A = 0$ and the Wagner function, $\phi(s)$, in the expressions for the air forces due to angle of attack, can be replaced by a unit step function, $T^{(i)} = 0$. In addition, a quasi-steady expression for the lift on the tail due to the downwash used in stability analyses is

$$L_{tw} = -\frac{1}{2}\rho U^2 S_t a_t \frac{d\epsilon}{d\alpha}\left(\alpha_w - l_t \alpha_w'\right)$$

$$= -\frac{1}{2}\rho U^2 S_t a_t \frac{d\epsilon}{d\alpha}\left[\left(\theta - \zeta' + l_3 \theta'\right) - l_t\left(\theta' - \zeta'' + l_3 \theta''\right)\right] \qquad (2.23)$$

These modifications reduce equations (2.14) and (2.18) to

$$\begin{Bmatrix} y'' \\ \theta'' \\ y' \\ \theta' \\ \theta \end{Bmatrix}_n = [C] \begin{Bmatrix} y'' \\ \theta'' \end{Bmatrix}_n + [D] \begin{Bmatrix} y'' \\ \theta'' \\ y' \\ \theta' \\ \theta \end{Bmatrix}_{n-1} \tag{2.24}$$

and

$$\begin{Bmatrix} y'' \\ \theta'' \end{Bmatrix}_n = [K] \begin{Bmatrix} f \\ g \end{Bmatrix}_n - [E] \begin{Bmatrix} y'' \\ \theta'' \\ y' \\ \theta' \\ \theta \end{Bmatrix}_{n-1} \tag{2.25}$$

respectively, where, as before,

$$[K] = \left[[A][C]\right]^{-1} \tag{2.26}$$

$$[E] = [K][A][D] \tag{2.27}$$

The matrices $[A]$, $[C]$ and $[D]$ must now be redefined as

$$[A] = \begin{bmatrix} A_{11} & A_{12} & \cdots & A_{15} \\ A_{21} & A_{22} & \cdots & A_{25} \end{bmatrix} \tag{2.28}$$

$$[C] = \begin{bmatrix} 1 & 0 \\ 0 & 1 \\ \epsilon/2 & 0 \\ 0 & \epsilon/2 \\ 0 & \epsilon^2/6 \end{bmatrix} \tag{2.29}$$

$$[D] = \begin{bmatrix} 0 & & & & \\ 0 & 0 & & & \\ \epsilon/2 & 0 & 1 & & \\ 0 & \epsilon/2 & 0 & 1 & \\ 0 & \epsilon^2/3 & 0 & \epsilon & 1 \end{bmatrix} \tag{2.30}$$

where

$$A_{11} = 2\mu + l_t P_t \frac{d\epsilon}{d\alpha}$$

$$A_{12} = -l_3 l_t P_t \frac{d\epsilon}{d\alpha}$$

$$A_{13} = 1 + P_t \left(1 - \frac{d\epsilon}{d\alpha}\right)$$

$$A_{14} = -\bar{l}_3 - P_t \left(l_t + \frac{1}{\nu}\right) + (l_3 - l_t) P_t \frac{d\epsilon}{d\alpha}$$

$$A_{15} = -A_{13}$$

$$A_{21} = -\bar{l}_t^2 P_t \frac{d\epsilon}{d\alpha}$$

$$A_{22} = 2K_y^2 \mu + \bar{l}_3 \bar{l}_t^2 P_t \frac{d\epsilon}{d\alpha}$$

$$A_{23} = -\bar{l}_w - \bar{l}_t P_t \left(1 - \frac{d\epsilon}{d\alpha}\right) + \frac{2}{a_w} \frac{dC_{m_f}}{d\alpha}$$

$$A_{24} = \bar{l}_2 + \bar{l}_t P_t \left(\bar{l}_t + \frac{1}{\gamma}\right) - \bar{l}_t \left(\bar{l}_3 - \bar{l}_t\right) P_t \frac{d\epsilon}{d\alpha} - \left(\bar{l}_f - \bar{l}_{cg}\right) \frac{2}{a_w} \frac{dC_{m_f}}{d\alpha}$$

$$A_{25} = -A_{23}$$

The loads on the airplane can be found from the matrix equation,

$$\frac{1}{a_w} \begin{Bmatrix} C_{L_w} \\ C_{L_t} \\ C_{L_f} \end{Bmatrix}_n = \begin{Bmatrix} f_w \\ f_t \\ f_f \end{Bmatrix}_n - [G] \begin{Bmatrix} \xi'' \\ \theta'' \\ \xi' \\ \theta' \\ \theta \end{Bmatrix}_n \tag{2.31}$$

where

$$C_L(s) = \frac{L(s)}{\frac{1}{2}\rho U^2 S_w} \tag{2.32}$$

The functions, f_w , f_t and f_f , are those parts of the forcing function, $f(s)$, due to the wing, horizontal tail and fuselage, respectively. The matrix $[G]$ is defined by

$$[G] = \begin{bmatrix} G_{11} & G_{12} & \cdots & G_{15} \\ G_{21} & G_{22} & \cdots & G_{25} \\ 0 & 0 & \cdots & 0 \end{bmatrix} \tag{2.33}$$

where

$$G_{11} = 0 \qquad G_{21} = \lambda_t P_t \frac{d\epsilon}{d\alpha}$$

$$G_{12} = 0 \qquad G_{22} = -\lambda_3 \lambda_t P_t \frac{d\epsilon}{d\alpha}$$

$$G_{13} = 1 \qquad G_{23} = P_t \left(1 - \frac{d\epsilon}{d\alpha}\right)$$

$$G_{14} = -\bar{\lambda}_3 \qquad G_{24} = -P_t \left(\lambda_t + \frac{1}{V}\right) + \left(\lambda_3 - \lambda_t\right) P_t \frac{d\epsilon}{d\alpha}$$

$$G_{15} = -1 \qquad G_{25} = -P_t \left(1 - \frac{d\epsilon}{d\alpha}\right)$$

The total air load on the airplane is given by

$$\frac{C_L(s)}{a_w} = 2\mu f''(s) \tag{2.34}$$

The maximum value given by equation (2.34) is the quantity commonly designated as the alleviation factor, i.e., the ratio of the actual maximum acceleration of the airplane to that given by the sharp-edged gust formula (based on the wing lift-curve slope in this case).

III. NUMERICAL EXAMPLE OF THE INTEGRATION TECHNIQUE

A swept-wing airplane will be used as an example to illustrate the numerical procedure of the preceding section. The planform of this airplane is shown in Figure 3.1. The present analysis is based on a rigid aircraft structure whereas the example airplane is actually very flexible. Nevertheless, the method can be used if the stability parameters are corrected for aeroelasticity and if the gradient distance of the gust is long enough to exclude the possibility of any dynamic response of the structure. Therefore, in this numerical example, the response of the airplane to a long-graded gust is found, and since the response of the airplane is slow, quasi-steady damping is used.

The stability derivatives for the example airplane with corrections for aeroelasticity are given in Reference 7, and the pertinent derivatives for the present analysis are repeated in Table 3.1. These parameters were calculated for an airspeed of $U = 490$ mph and contain corrections for compressibility. The stability parameters for an equivalent rigid airplane are also included for comparison, and they will be used to obtain some of the results presented in Section IV. In both elastic and rigid cases, the values of l_w and l_t correspond to center-of-gravity positions which give neutral static stability. This condition is critical for gust loads because the most rearward center-of-gravity position results in the maximum pitching motion.

The stability parameters, $\frac{d\epsilon}{d\alpha}$ and $\frac{dC_{m_f}}{d\alpha}$, were assumed to be unaffected by quasi-steady flexibility. They are as follows:

$$\frac{d\epsilon}{d\alpha} = 0.326 \qquad \frac{dC_{m_f}}{d\alpha} = 0.363 \text{ per rad}$$

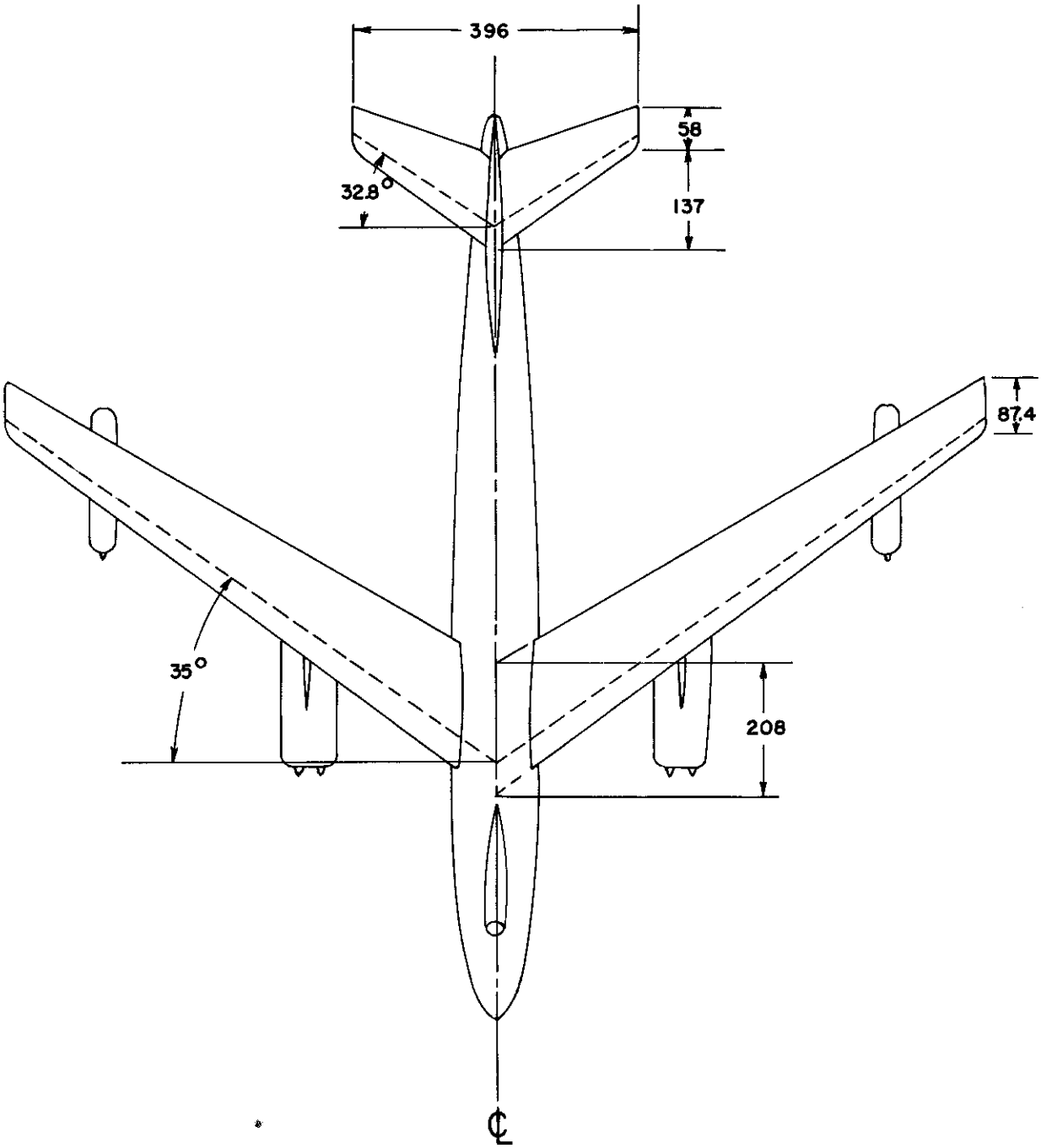

FIGURE 3.1 PLANFORM OF EXAMPLE AIRPLANE

TABLE 3.1

STABILITY PARAMETERS FOR EXAMPLE AIRPLANE

AND EQUIVALENT RIGID AIRPLANE

	Elastic	Rigid
a_w	4.13 per rad	6.01 per rad
l_w	-0.364	-0.517
a_t	2.45 per rad	4.25 per rad
l_t	7.20	7.04

As indicated in Appendix A.3, the over-all steady-state downwash at the tail due to a linear twist on the wing is very small, and the same statement for wing deformations in general is probably true.

In addition to the deformations caused by the air stream, there are also deformations caused by inertia forces which are, in turn, altered by the air stream. These deformations produce changes in the steady-state lift and pitching moment on the airplane. Additional stability parameters due to inertia deformations for the example airplane were also computed in Reference 7. They are as follows:

$$\frac{\partial L^i}{\partial \ddot{z}} = 383 \text{ slugs}$$

$$\frac{\partial L^i}{\partial \ddot{\theta}} = -10{,}120 \text{ slug-ft}$$

$$\frac{\partial m^i}{\partial \ddot{z}} = -6{,}290 \text{ slug-ft}$$

$$\frac{\partial m^i}{\partial \ddot{\theta}} = 216{,}000 \text{ slug-ft}^2$$

To include these inertia deformation parameters in the rigid airplane analysis, one must add the following increments to some of the elements in matrix [A] of equation (2.28):

$$\Delta A_{11} = - \frac{2}{\rho S_w \frac{\bar{c}}{2} a_w} \frac{\partial L^i}{\partial \ddot{z}} \tag{3.1}$$

$$\Delta A_{12} = - \frac{2}{\rho S_w \left(\frac{\bar{c}}{2}\right)^2 a_w} \frac{\partial L^i}{\partial \ddot{\theta}} \tag{3.2}$$

$$\Delta A_{14} = + \frac{2}{\rho S_w \frac{\bar{c}}{2} a_w} \frac{\partial L^i}{\partial \ddot{z}} \tag{3.3}$$

$$\Delta A_{21} = - \frac{2}{\rho S_w \left(\frac{\bar{c}}{2}\right)^2 a_w} \frac{\partial m^i}{\partial \ddot{z}} \tag{3.4}$$

$$\Delta A_{22} = - \frac{2}{\rho S_w \left(\frac{\bar{c}}{2}\right)^3 a_w} \frac{\partial m^i}{\partial \ddot{\theta}} \tag{3.5}$$

$$\Delta A_{24} = + \frac{2}{\rho S_w \left(\frac{\bar{c}}{2}\right)^2 a_w} \frac{\partial m^i}{\partial \ddot{z}} \tag{3.6}$$

The remaining parameters required in this analysis are given in Table 3.2.

TABLE 3.2

PARAMETERS FOR EXAMPLE ANALYSIS

Basic Parameters

M	= 4000 slugs	Λ_0	= $36^\circ\ 38'$
ρ	= 0.001702 slugs/ft^3	Λ_1	= 35°
$\bar{c}_w$	= 12.30 ft	Λ_2	= $33^\circ\ 18'$
$\bar{c}_t$	= 8.12 ft	Λ_3	= $31^\circ\ 32'$
S_w	= 1428 ft^2	Λ_{0_t}	= $36^\circ\ 40'$
S_t	= 268 ft^2	l_1	= -2.83 (-3.36)*
k_y	= 20.1 ft	l_2	= -2.13 (-2.66)*
AR_w	= 9.43	l_3	= -1.424 (-1.955)*
AR_t	= 4.06	l_{cg}	= 7.85 (8.38)*
λ_w	= 0.420	$\bar{l}_f$	= 7.44
λ_t	= 0.423	A_{max}	= $1.893\left(\frac{\bar{c}}{2}\right)^2$
		V_f	= $23.02\left(\frac{\bar{c}}{2}\right)^3$

Derived Parameters

μ	= 64.8 (44.5)*	γ	= 1.515
K_y^2	= 10.67	P_t	= 0.1113 (0.1327)*
β	= 7.01	$\bar{l}_2$	= 2.615 (2.725)*
β_t	= 3.02	$\bar{l}_3$	= 1.075 (0.544)*

* The corresponding values for the equivalent rigid airplane

The required matrices are defined by equations (2.27), (2.28), (2.29), (2.30), (2.31) and (2.34). For $\epsilon = 2$, they are

$$[A] = \begin{bmatrix} 117.37 & 53.61 & 1.0750 & 10.142 & -1.0750 \\ 31.24 & 1194.2 & 0 & -21.88 & 0 \end{bmatrix}$$

$$[C] = \begin{bmatrix} 1 & 0 \\ 0 & 1 \\ 1 & 0 \\ 0 & 1 \\ 0 & 2/3 \end{bmatrix}$$

$$[D] = \begin{bmatrix} 0 & & & & \\ 0 & 0 & & & \\ 1 & 0 & 1 & & \\ 0 & 1 & 0 & 1 & \\ 0 & 4/3 & 0 & 2 & 1 \end{bmatrix}$$

$$[K] = 10^{-3}\begin{bmatrix} 8.5642 & -0.4605 \\ -0.2282 & 0.8653 \end{bmatrix}$$

$$[E] = 10^{-3}\begin{bmatrix} 9.206 & 84.66 & 9.206 & 78.52 & -9.206 \\ -0.2453 & -20.92 & -0.2453 & -20.76 & 0.2453 \end{bmatrix}$$

$$[G] = \begin{bmatrix} -12.40 & 53.24 & 1.0 & 11.325 & -1.0 \\ 0.257 & 0.366 & 0.0750 & -1.183 & -0.750 \\ 0 & 0 & 0 & 0 & 0 \end{bmatrix}$$

The equations of motion could be solved directly for the response to a long-graded gust by integrating the forcing functions, $f(s)$ and $g(s)$, given in Appendix A.4 for a sharp-edged gust in convolution with the gust profile. Because of the complexity of $f(s)$ and $g(s)$, however, it would appear easier to solve directly for a sharp-edged gust and then to integrate any desired results in convolution with the gust profile. For the example airplane per

unit $\frac{w}{U}$, the expressions for $f(s)$ and $g(s)$ given by equations (A.64) and (A.65) become

$$f(s) = \psi_\Lambda^L + 0.0243\,\psi_f^L + 0.1113\,\psi_{\Lambda_t} - 0.0363\,\zeta^G$$

$$g(s) = 2.832\,\psi_\Lambda^L - 2.468\,\psi_\Lambda^m + 0.1758\,\psi_f^m - 0.801\,\psi_{\Lambda_t} + 0.261\,\zeta^G$$

where, for $s = 0$ at the nose of the fuselage,

$$\psi_\Lambda^L = 0 \qquad \text{when} \quad 0 \le s \le 4.31$$

$$= \left[1.408\left(\frac{s-4.31}{7.01}\right) - 0.408\left(\frac{s-4.31}{7.01}\right)^2\right] \psi\left(\frac{s-4.31}{2}\right) \quad \text{when} \quad 4.31 \le s \le 11.32$$

$$= \psi(s-7.82) \qquad \text{when} \quad s \ge 11.32$$

$$\psi_\Lambda^m = 0 \qquad \text{when} \quad 0 \le s \le 4.31$$

$$= \left[1.630\left(\frac{s-4.31}{7.01}\right)^2 - 0.630\left(\frac{s-4.31}{7.01}\right)^3\right] \psi\left(\frac{s-4.31}{2}\right) \quad \text{when} \quad 4.31 \le s \le 11.32$$

$$= \psi_\Lambda^L(s) \qquad \text{when} \quad s \ge 11.32$$

$$\psi_f^L = \frac{A(s)}{A_{max}}$$

$$\psi_f^m = \frac{V(s)}{V_f} - 0.0822\,(s-7.85)\,\frac{A(s)}{A_{max}}$$

$$\psi_{\lambda_t} = 0 \qquad \text{when} \quad 0 \leq s \leq 14.21$$

$$= \left[1.406\left(\frac{s-14.21}{1.995}\right) - 0.406\left(\frac{s-14.21}{1.995}\right)^2\right] \psi\left(\frac{s-14.21}{1.320}\right) \qquad \text{when} \quad 14.21 \leq s \leq 16.20$$

$$= \psi\left(\frac{s-15.21}{0.660}\right) \qquad \text{when} \quad s \geq 16.20$$

$$\zeta^G = 0 \qquad \text{when} \quad 0 \leq s < 5.81$$

$$= -0.16 \qquad \text{when} \quad 5.81 < s < 15.49$$

$$= 1.0 \qquad \text{when} \quad s > 15.49$$

In the expressions for ψ_λ^L, ψ_λ^m and ψ_{λ_t}, the Küssner functions used are given by equation (A.28). The step-function representation of ζ^G, given by equation (A.62), was used because it was found that, for a long-graded gust, the shape of the ζ^G function has very little effect on the response of the airplane or on the resulting gust loads.

The computing steps required for the application of equations (2.35), (2.26) and (2.32) are illustrated in Table 3.3. In this table, the response of the airplane to a sharp-edged gust is given by

$$\{⑦\}_n = \frac{1}{w/U} \begin{Bmatrix} \bar{y}'' \\ \theta'' \\ \bar{y}' \\ \theta' \\ \theta \end{Bmatrix}_n$$

the loads on the wing, horizontal tail and fuselage by

$$\{⑪\}_n = \frac{1}{a_w \frac{w}{U}} \begin{Bmatrix} C_{L_w} \\ C_{L_t} \\ C_{L_f} \end{Bmatrix}_n$$

and the total load on the airplane by

$$⑫_n = \frac{C_L(n\epsilon)}{a_w \frac{w}{U}}$$

Steps $\{⑧\}$ and ⑬ check each cycle of the recurrence relationship.

To find the gust loads on the example airplane while flying through a long-graded gust, one must integrate the time history of the loads due to a sharp-edged gust in convolution with the desired gust profile. If $B(s)$ is a response or load due to a sharp-edged gust per unit w/U , then the corresponding response or load due to an arbitrary gust profile per unit w_{max}/U is

$$C(s) = \int_0^s B(\sigma)\, F'(s-\sigma)\, d\sigma \qquad (3.7)$$

TABLE 3.3

COMPUTING STEPS FOR NUMERICAL EXAMPLE

	s	0	2	4	6	8	10	12	14	16	18	20	22	24	26	28		58	60
	n	0	1	2	3	4	5	6	7	8	9	10	11	12	13	14		29	30
(1)	$\begin{Bmatrix} f \\ g \end{Bmatrix}$	0 0	0.0194 .0805	0.0243 .0962	0.1606 .3372	0.3932 .5702	0.6221 .5013	0.7885 .3494	0.8620 .3992	0.9232 .3076	0.9846 .0918	1.0163 .0235	1.0348 .0018	1.0467 -.0042	1.0547 -.0052	1.0604 -.0045		1.0749 -.0001	1.0750 -.0001
(2)	$[K]\{①\}_n$	0 0	.000129 .000065	.000164 .000078	.001220 .000255	.003105 .000404	.005097 .000292	.006592 .000122	.007198 .000149	.007765 .000055	.008390 -.000145	.008693 -.000212	.008861 -.000235	.008966 -.000242	.009035 -.000245	.009084 -.000246		.009206 -.000245	.009206 -.000245
(3)	$[E]\{⑦\}_{n-1}$	0 0	0 0	.000013 -.000003	.000026 -.000006	.000083 -.000017	.000190 -.000036	.000301 -.000051	.000402 -.000060	.000511 -.000071	.000608 -.000078	.000679 -.000078	.000747 -.000074	.000817 -.000070	.000892 -.000066	.000972 -.000061		.002784 .000012	.002947 .000017
(4)	$\{②\}_n - \{③\}_n$	0 0	.000129 .000065	.000151 .000080	.001194 .000261	.003022 .000421	.004907 .000328	.006290 .000174	.006796 .000209	.007254 .000126	.007782 -.000067	.008014 -.000134	.008114 -.000160	.008149 -.000172	.008143 -.000179	.008111 -.000184		.006422 -.000258	.006259 -.000263
(5)	$[C]\{④\}_n$	0 0 0 0 0	.000129 .000065 .000129 .000065 .000043	.000151 .000080 .000151 .000080 .000054	.001194 .000261 .001194 .000261 .000174	.003022 .000421 .003022 .000421 .000281	.004907 .000238 .004907 .000328 .000218	.006290 .000174 .006290 .000174 .000116	.006796 .000209 .006796 .000209 .000139	.007254 .000126 .007254 .000126 .000084	.007782 -.000067 .007782 -.000067 -.000045	.008014 -.000134 .008014 -.000134 -.000089	.008114 -.000160 .008114 -.000160 -.000107	.008149 -.000172 .008149 -.000172 -.000115	.008143 -.000179 .008143 -.000179 -.000119	.008111 -.000184 .008111 -.000184 -.000123		.006422 -.000258 .006422 -.000258 -.000172	.006259 -.000263 .006259 -.000263 -.000175
(6)	$[D]\{⑦\}_{n-1}$	0 0 0 0 0	0 0 0 0 0	0 0 .000258 .000130 .000261	0 0 .000560 .000291 .000844	0 0 .002950 .000814 .002471	0 0 .008993 .001656 .005783	0 0 .018806 .002312 .010406	0 0 .031388 .002659 .015724	0 0 .044981 .003077 .021882	0 0 .059488 .003330 .028541	0 0 .075053 .003196 .034932	0 0 .091081 .002928 .040788	0 0 .107310 .002608 .046004	0 0 .123608 .002264 .050532	0 0 .139893 .001906 .054343		0 0 .363544 -.004627 .012414	0 0 .376387 -.005142 .002130
(7)	$\{⑤\}_n + \{⑥\}_n$	0 0 0 0 0	.000129 .000065 .000129 .000065 .000435	.000151 .000080 .000409 .000211 .000314	.001194 .000261 .001755 .000553 .001018	.003022 .000421 .005971 .001235 .002752	.004907 .000328 .013899 .001984 .006002	.006290 .000174 .025097 .002485 .010522	.006796 .000209 .038184 .002868 .015863	.007254 .000126 .052235 .003203 .021966	.007782 -.000067 .067271 .003263 .028496	.008014 -.000134 .083067 .003062 .034843	.008114 -.000160 .099195 .002768 .040682	.008149 -.000172 .115459 .002436 .045890	.008143 -.000179 .131751 .002085 .050413	.008111 -.000184 .148005 .001721 .054220		.006422 -.000258 .369966 -.004884 .012242	.006259 -.000263 .382646 -.005405 .001954
(8)	$[A]\{⑦\}_n = \{①\}_n$	0 0	.0194 .0805	.0243 .0962	.1606 .3372	.3932 .5702	.6221 .5013	.7885 .3494	.8620 .3992	.9232 .3076	.9846 .0918	1.0163 .0235	1.0348 .0018	1.0467 -.0042	1.0547 -.0052	1.0604 -.0045		1.0749 -.0001	1.0750 -.0001
(9)	$\begin{Bmatrix} f_w \\ f_t \\ f_r \end{Bmatrix}_n$	0 0 0	0 0 .0194	0 0 .0243	.1306 .0057 .0243	.3632 .0057 .0243	.5929 .0057 .0235	.7668 .0057 .0160	.8471 .0057 .0092	.8951 .0238 .0043	.9261 .0585 0	.9472 .0691 0	.9620 .0728 0	.9725 .0742 0	.9800 .0747 0	.9855 .0749 0		.9999 .0750 0	1.0000 .0750 0
(10)	$[G]\{⑦\}_n$	0 0 0	.0027 -.0000 0	.0049 -.0002 0	.0061 -.0002 0	.0022 -.0003 0	-.0130 -.0004 0	-.0260 -.0002 0	-.0184 .0001 0	-.0167 .0004 0	-.0243 .0010 0	-.0236 .0020 0	-.0193 .0031 0	-.0130 .0044 0	-.0056 .0057 0	.0029 .0070 0		.2091 .0342 0	.2279 .0364 0
(11)	$\{②\}_n - \{⑩\}_n$	0 0 0	-.0027 .0000 .0194	-.0049 .0002 .0243	.1245 .0059 .0243	.3610 .0060 .0243	.6059 .0061 .0235	.7928 .0059 .0160	.8654 .0056 .0092	.9118 .0234 .0043	.9504 .0575 0	.9708 .0671 0	.9813 .0697 0	.9856 .0698 0	.9856 .0690 0	.9826 .0679 0		.7908 .0408 0	.7721 .0385 0
12	$\Sigma\{⑪\}_n$	0	.0167	.0196	.1547	.3913	.6355	.8147	.8802	.9395	1.0079	1.0379	1.0509	1.0554	1.0546	1.0505		.8317	.8107
13	$2\mu\,⑦_n^{(i)} = ⑫_n$	0	.0167	.0196	.1547	.3913	.6355	.8147	.8803	.9395	1.0080	1.0380	1.0510	1.0554	1.0547	1.0506		.8317	.8107

where

$$F(s) = \frac{W}{W_{max}} \tag{3.8}$$

The application of the trapezoid rule of integration to equation (3.7) yields

$$C_n = \epsilon \left(B_1 F'_{n-1} + B_2 F'_{n-2} + B_3 F'_{n-3} + \cdots + B_{n-1} F'_1 \right) \tag{3.9}$$

provided that $B_0 = F'_0 = 0$. Since there is no gust force at time, $s = 0$, B_0 is always zero. In this case, $F'_0 = 0$ because the customary one-minus-cosine gust profile is used.

A one-minus-cosine gust profile can be represented by

$$F(s) = \frac{1}{2} \left(1 - \cos \pi \frac{s}{s_g} \right) \tag{3.10}$$

Therefore,

$$F'_n = \frac{\pi}{2 s_g} \sin \frac{\pi \epsilon}{s_g} n \tag{3.11}$$

where s_g is the gust gradient distance or the value of s at the gust peak.

The loads on the example airplane flying through a one-minus-cosine gust are computed by applying equation (3.9) to the results obtained in Table 3.3. A gust gradient distance of $s_g = 40$ was used because it was shown in Reference 8 that the structural response of the example airplane is essentially quasi-steady for a gust gradient distance which is that long. The resulting time histories of the loads are shown in Figure 4.6 of Section IV and are described there.

IV. RESULTS, CONCLUSIONS AND RECOMMENDATIONS

4.1 Results

The method of solution presented in Section II was applied to a rigid equivalent of the example airplane of Section III, and the results are presented in Figures 4.1, 4.2, 4.3, 4.4 and 4.5. The effects of unsteady flow on the damping terms were included. Even though the example airplane is actually very flexible, it is felt that these results point out the combined effects of pitching and wing sweep on gust loading.

The two sets of curves in Figure 4.1 show the effect of the pitching degree of freedom on the response of a swept-wing airplane. In this case, neglect of the pitching motion results in an underestimation of the gust loads on the wing and tail. The plot of α in this figure and in those which follow represents the effective angle of attack at the mean geometric chord of the wing.

In Figure 4.2 the gust loads on the example airplane are compared with those on an equivalent unswept-wing airplane. In spite of the gradual build-up of gust forces on the swept wing, the initial entry of the forward inboard portion of the wing produces such a large pitching moment that the gust loads on the swept-wing airplane are larger than those on the unswept-wing airplane. The equivalent unswept-wing airplane was obtained by rotating both wing and tail about the quarter-chord points of their respective mean aerodynamic chords.

The results presented in Figure 4.3 show that an increase in the static stability of the example airplane reduces the gust loads on both the wing and tail.

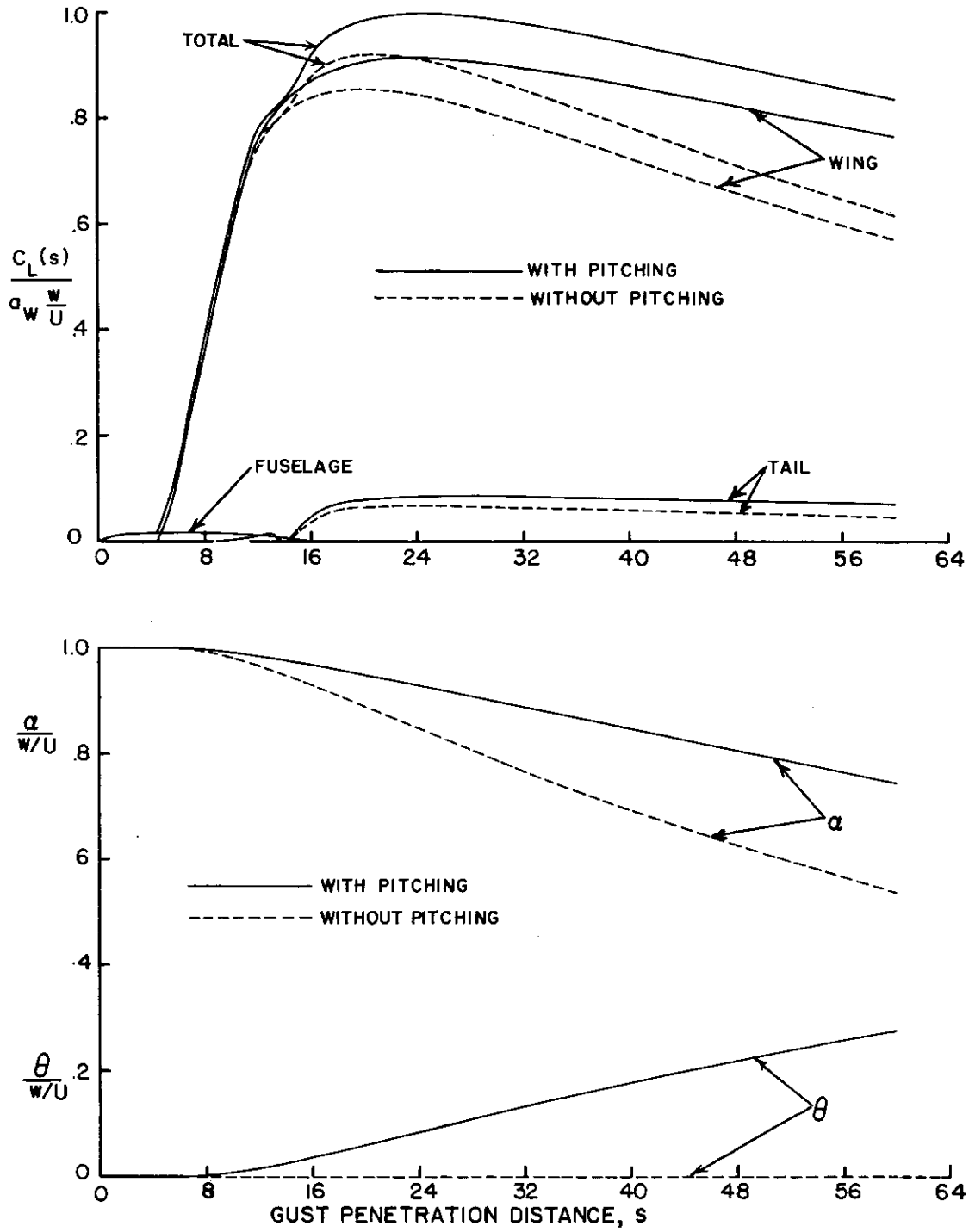

FIGURE 4.1 EFFECT OF PITCHING ON THE RESPONSE OF A RIGID SWEPT-WING AIRPLANE, SHARP-EDGED GUST, $\frac{dC_m}{dC_L} = 0$

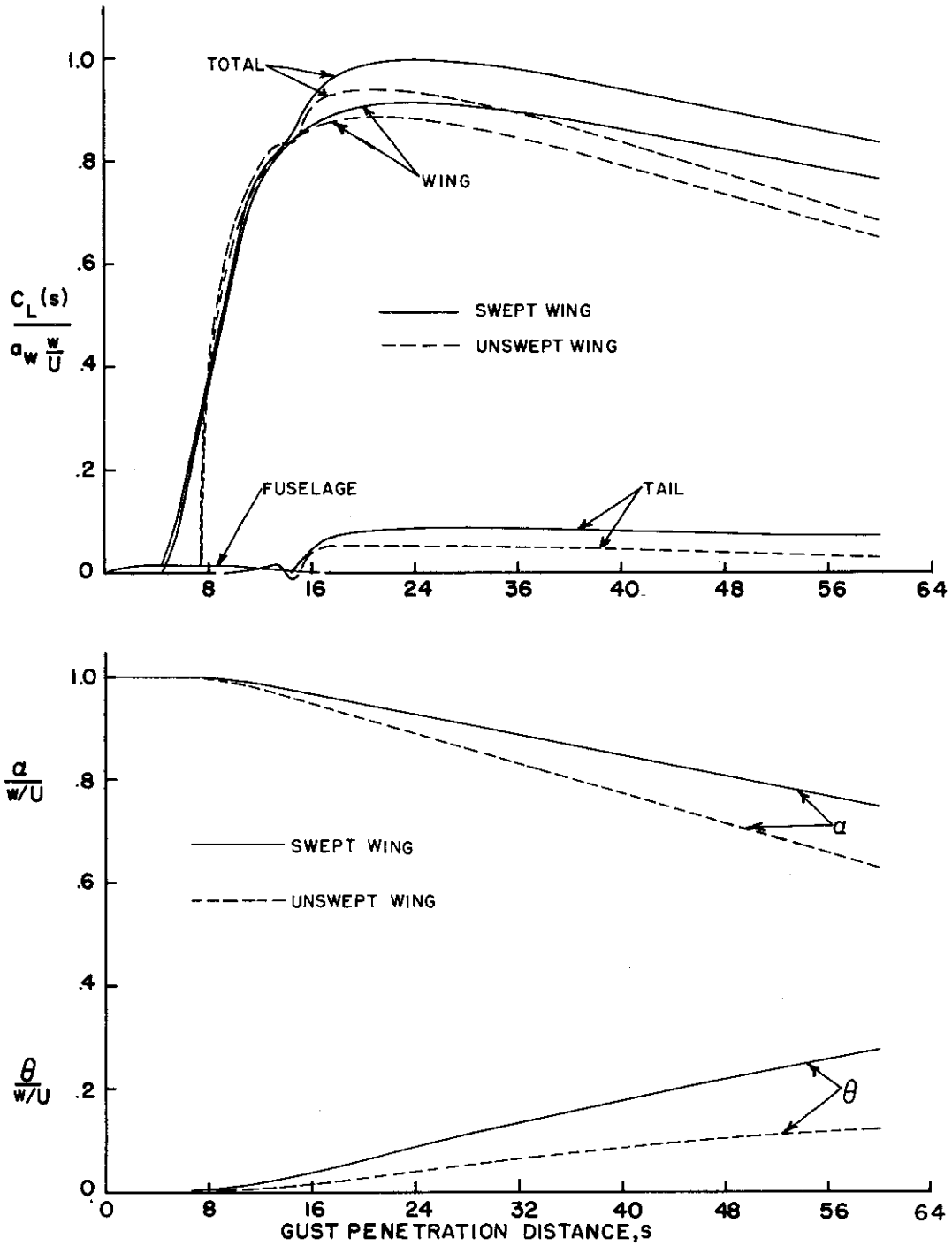

FIGURE 4.2 EFFECT OF SWEEP ON THE RESPONSE OF A RIGID AIRPLANE, SHARP-EDGED GUST, $\frac{dC_m}{dC_L} = 0$

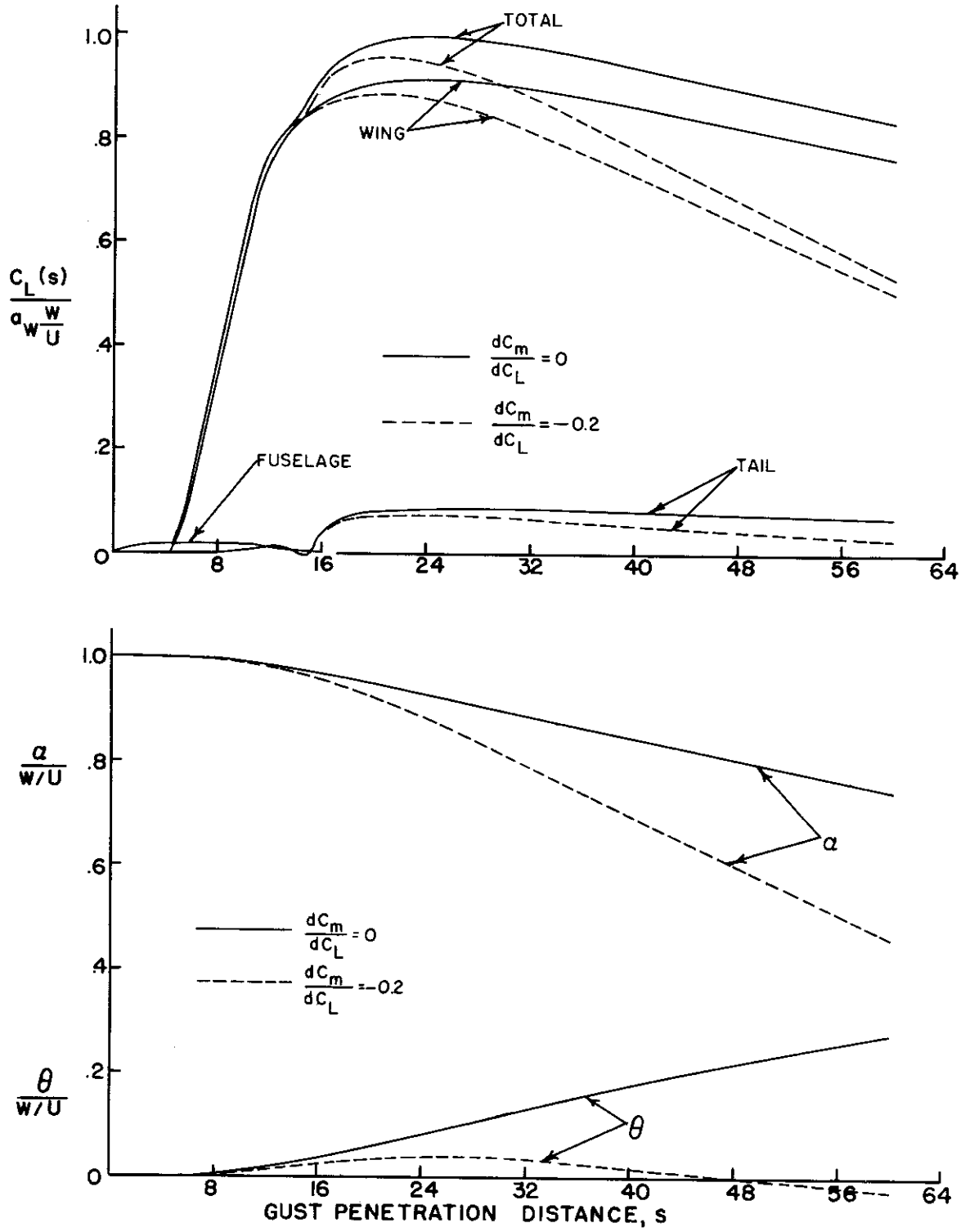

FIGURE 4.3 EFFECT OF STATIC STABILITY ON THE RESPONSE OF A RIGID SWEPT-WING AIRPLANE, SHARP-EDGED GUST

The response of the example airplane to the standard one-minus-cosine gust, i.e., $s_g = 25$, is illustrated in Figure 4.4. These results may be compared with the specifications of Reference 9. The gust load formula in paragraph 4.1.2.1 of that reference gives incremental load factors which are 8% unconservative because the pitching motion of the airplane is accentuated by the sweep of the wing. Paragraph 4.1.2.2.2 implies that the ratio of the maximum incremental tail load to the maximum incremental wing load may be found from the following:

$$\frac{L_t}{L_w} = 1.1 \frac{S_t a_t}{S_w a_w} \left(1 - \frac{d\epsilon}{d\alpha}\right)$$

If the correct wing load for the example airplane is used, the above formula gives a tail load which is 5% conservative. In this case, the incremental tail load is 83% of its maximum when the largest gust load acts on the wing, while the incremental wing load is 87% of its maximum when the tail load reaches its upper limit.

In Figure 4.5 the same comparisons are made for the standard one-minus-cosine gust that were made for the sharp-edged gust in Figures 4.1, 4.2 and 4.3, and the same trends can be observed.

The loads on the example airplane produced by a long-graded gust with quasi-steady flexibility effects included were computed in Section III, and these results are plotted in Figure 4.6. Similar results for the equivalent rigid airplane are shown for comparison. In both cases, the load parameter, $C_L / a_w \frac{w}{U}$, is related to the rigid-airplane lift-curve slope in order to permit a consistent comparison. In this instance, flexibility produces a large alleviation in the gust loads. An approximately equal amount of alleviation was obtained in Reference 8 for the same airplane by an analysis

which did not include the pitching degree of freedom and which considered only the bending flexibility of the wing. But the results of Reference 8 also show that the alleviation of gust loads due to flexibility is less for the standard one-minus-cosine gust. Moreover, when pitching is included, there may be significant dynamic overstresses in the wing.

The dashed curve of Figure 4.7 shows that neglect of the deformations due to inertia gives slightly unconservative results. In computing the results illustrated in Figure 4.7, the downwash function ζ^G given in Figure A.11 was used rather than the step-function approximation to ζ^G employed in Section III. There is no noticeable difference in the resulting gust loads.

4.2 Conclusions and Recommendations

A relatively simple numerical method has been developed for computing the time histories of the gust loads on a rigid swept-wing airplane free to heave and to pitch in response to a discrete gust. The effects of the swept wing and the fuselage penetrating a gust front and the effects of unsteady downwash from the wing on the horizontal tail are included in a simplified manner. The expressions for the growth of lift and pitching moment on swept wings are greatly simplified with little loss of accuracy by using an average gust penetration distance for the entire portion of the wing enveloped by the gust front. This method has been extended to the case of a flexible swept-wing airplane which enters a gust with a gradient distance long enough to consider the structural response as quasi-steady.

Several time histories of the gust loads on an example swept-wing airplane have been computed. These results indicate that, when the effects of

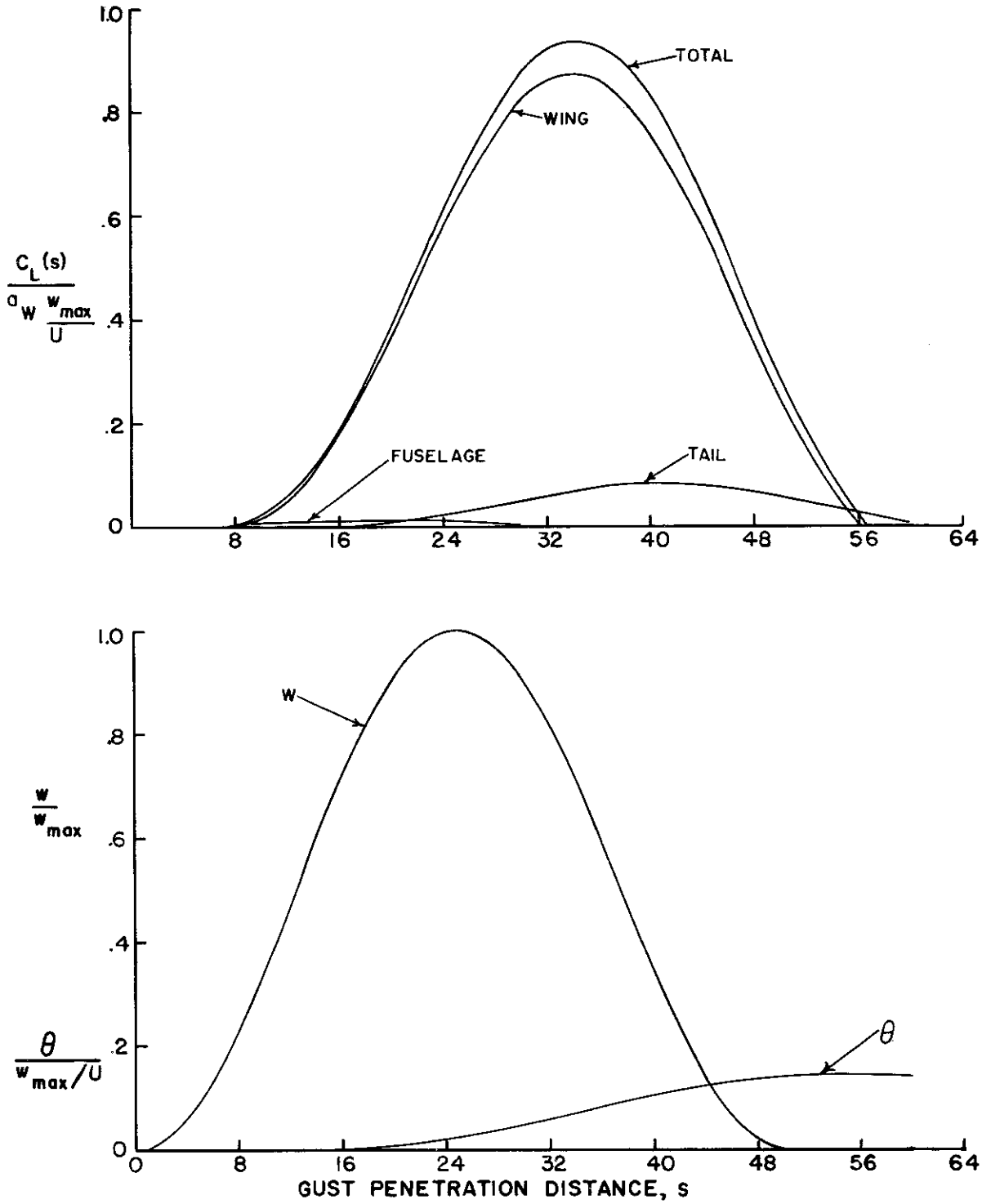

FIGURE 4.4 RESPONSE OF RIGID SWEPT-WING AIRPLANE TO ONE-MINUS-COSINE GUST, $\frac{dC_m}{dC_L} = 0$

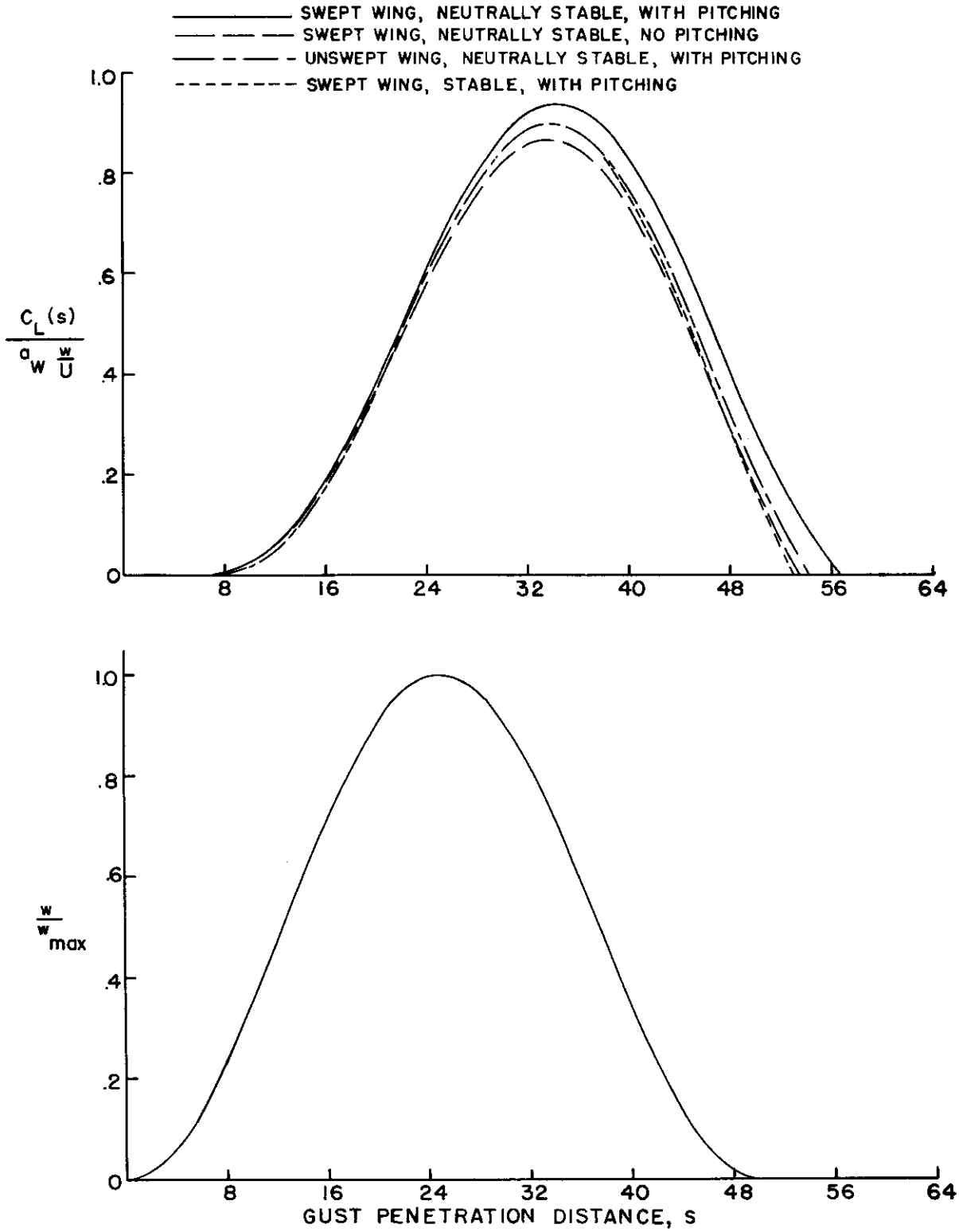

FIGURE 4.5 TOTAL LIFT ON RIGID AIRPLANE, ONE-MINUS-COSINE GUST

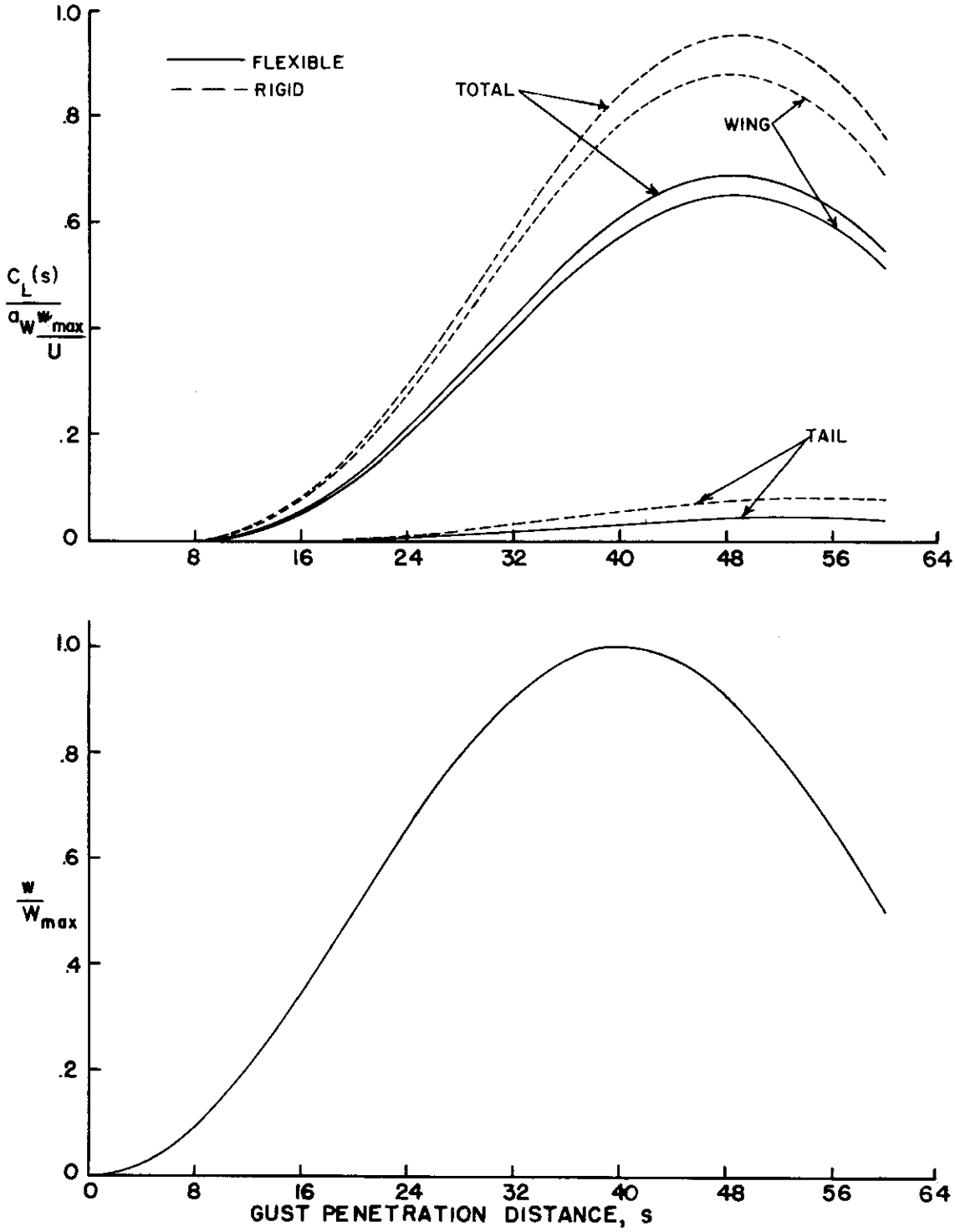

FIGURE 4.6 COMPARISON OF THE LOADS ON THE EXAMPLE AIRPLANE CONSIDERED BOTH AS RIGID AND AS FLEXIBLE, LONG-GRADED GUST

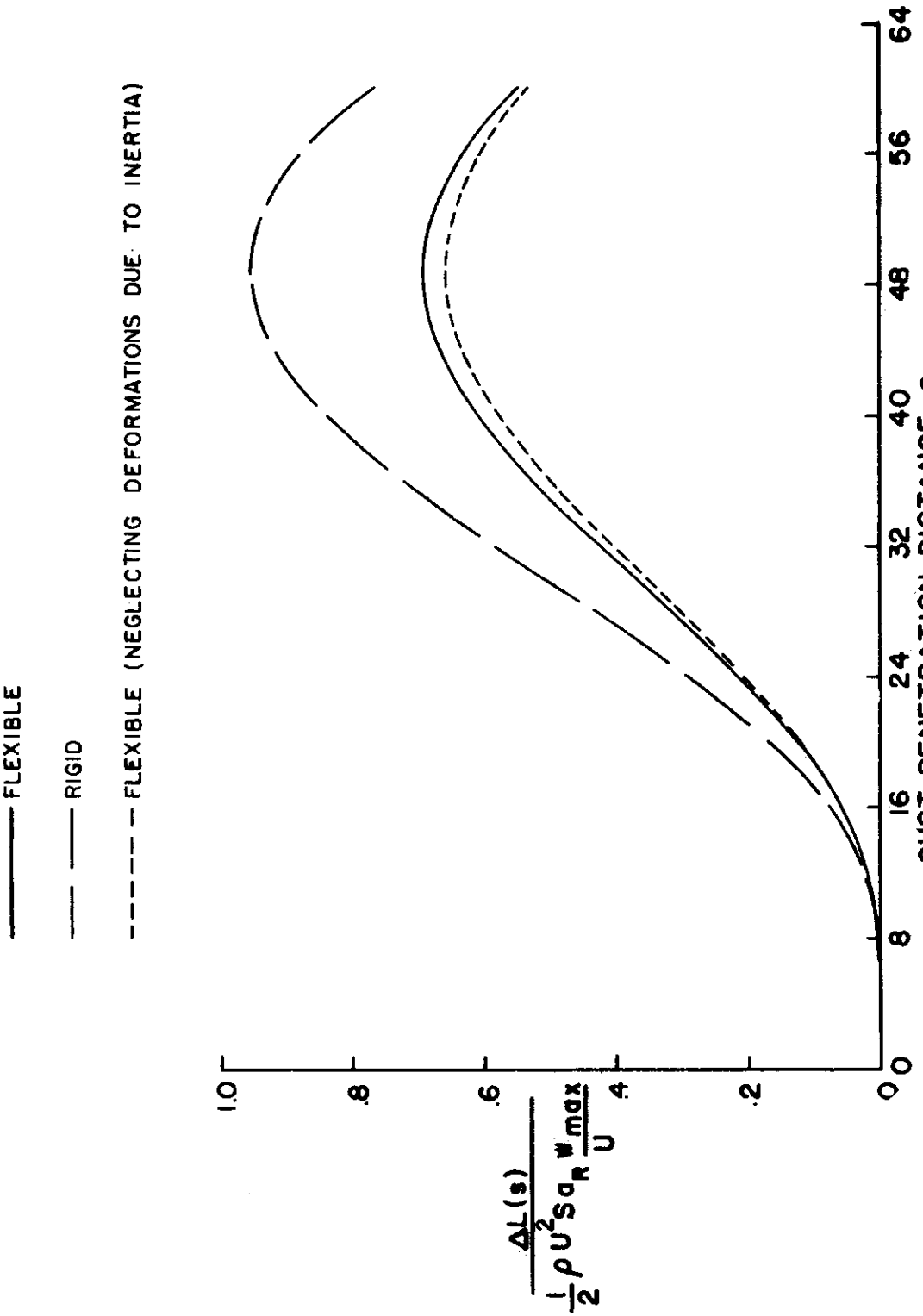

FIGURE 4.7 COMPARISON OF TOTAL LOAD ON THE EXAMPLE AIRPLANE CONSIDERED BOTH AS RIGID AND AS FLEXIBLE, LONG-GRADED GUST

pitching are neglected, the gust loads on a rigid swept-wing airplane are unconservative, particularly the load on the horizontal tail. A comparison of these results with those obtained in previous investigations of unswept-wing airplanes indicates that the pitching degree of freedom is more important for swept-wing airplanes, whereas the center-of-gravity location has less effect on their response. The conclusion is reached in Appendix C that the use of quasi-steady aerodynamics in the damping terms is probably always justified when computing the gust loads on rigid swept-wing airplanes which are free to pitch. When the static deformation of the example airplane penetrating a long-graded gust is considered, there is a large alleviation of gust loads even when pitching motion is included. This alleviation due to flexibility would not, however, be as great when the airplane is flying through a short-graded gust because the structural deformations would lag behind the rigid-body accelerations. Dynamic stresses would also have to be considered for an airplane which encounters a short-graded gust. The present method has been extended to include modes of structural vibration as degrees of freedom and will be reported on at a later date.

From the conclusions noted above, the following recommendations appear justified:

1. The pitching motion of a swept-wing airplane should be included in any gust load analysis.
2. The time history of the gust response must be computed for each airplane configuration. Because of the large number of independent parameters involved when pitching motion is considered, the specification of gust loads by simple charts or

formulas seems doubtful.

3. The center of gravity of the airplane should be in its most aft position because this condition produces the maximum pitching motion and usually the largest gust loads.

REFERENCES

1. Greidanus, J.H. and van de Vooren, A.I. Gust Load Coefficients for Wing and Tail Surfaces of an Aeroplane. National Aeronautical Research Institute, Amsterdam, Report F.28, 1948.

2. Brenner, C.W. and Isakson, G. A Parametric Investigation of Gust Loads on Rigid Airplanes in Two Degrees of Freedom. Navy Contract NOa(s) 8790, Aeroelastic and Structures Research Laboratory, Massachusetts Institute of Technology, October 1952.

3. Mazelsky, B. and Diederich, F.W. A Method of Determining the Effect of Airplane Stability on the Gust load Factor. NACA T.N. 2035, February 1950.

4. Houbolt, J.C. A Recurrence Matrix Solution for the Dynamic Response of Aircraft in Gusts. NACA Rept. 1010, 1951.

5. Houbolt, J.C. and Kordes, E.E. Gust-Response Analysis of an Airplane Including Wing Bending Flexibility. NACA T.N. 2763, August 1952.

6. Mazelsky, B. and Drischler, J.A. Numerical Determination of Indicial Lift and Moment Functions for a Two-Dimensional Sinking and Pitching Airfoil at Mach Numbers 0.5 and 0.6. NACA T.N. 2739, July 1952.

7. Engel, S.J. and McCarthy, J.F., Jr. Effect of Structural Flexibility on Aircraft Loading, Part XIV - An Analogue Study of Horizontal Tail Maneuvering Loads at Various Speeds for a Typical Bomber. AF Technical Report No. 6358, Part XIV, April 1954.

8. Foss, K.A., Sternlight, D. and Pian, T.H.H. Effect of Structural Flexibility on Aircraft Loading, Part XIX - A Parametric Study of the Gust Response of Swept Wing Airplanes Including a Wing-Bending Degree of Freedom. AF Technical Report No. 6358, Part XIX, March 1954.

9. Anonymous. Military Specification - Structural Criteria, Piloted Airplanes - Basic Flight Criteria. MIL - S - 5702 (USAF), December 14,1954.

10. Bisplinghoff, R.L., Isakson, G., Pian, T.H.H., Flomenhoft, H.I. and O'Brien, T.F. An Investigation of Stresses in Aircraft Structures Under Dynamic Loading. Navy Contract NOa(s) 8790, Aeroelastic and Structures Research Laboratory, Massachusetts Institute of Technology, January 1949.

11. Codik, A., Lin, H. and Pian, T.H.H. Effect of Structural Flexibility on Aircraft Loading, Part XII - The Gust Response of a Sweptback Tapered Wing Including Bending Flexibility. AF Technical Report No. 6358, Part XII, October 1953.

12. Pian, T.H.H. and Ashley, H. A Study of Gust Entry of Sweptback Wings. Proceedings of the Second U.S. National Congress of Applied Mechanics, Ann Arbor, Michigan, June 1954 (to be published).

13. Jones, R.T. The Unsteady Lift of a Wing of Finite Aspect Ratio. NACA Rept. 681, 1940.

14. Zbrozek, J. Compressibility Effect on Gust Loads. R.A.E. Tech. Note, Aero. 2254, August 1953.

15. Ashley, H., Zartarian, G. and Neilson, D. Investigation of Certain Unsteady Aerodynamic Effects in Longitudinal Dynamic Stability. AF Technical Report No. 5986, December 1951.

16. Jones, R.T. and Fehler, L.F. Transient Effects of the Wing Wake on the Horizontal Tail. NACA T.N. 771, August 1940.

17. Diederich, F.W. Charts and Tables for Use in Calculations of Downwash of Wings of Arbitrary Plan Form. NACA T.N. 2353, May 1951.

18. Levy, S. and Kroll, W.D. Errors Introduced by Finite Space and Time Increments in Dynamic Response Computation. Proceedings of the First U.S. National Congress of Applied Mechanics, 1951, pp. 1-8.

19. Bisplinghoff, R.L., Isakson, G. and O'Brien, T.F. Gust Loads on Rigid Airplanes with Pitching Neglected. Journal of the Aeronautical Sciences, Vol. 18, No. 1, pp. 33-42, January 1951.

20. Pian, T.H.H. and Winter, P.H. Effect of Structural Flexibility on Aircraft Loading, Part XVI - Estimation of Dynamic Overstress in Straight Wing Airplanes. AF Technical Report 6358, Part XVI, February 1954.

APPENDIX A

UNSTEADY AIR FORCES

A.1 Wing and Tail

(a) Lift on Wing Due to Angle of Attack

According to strip theory, the lift per unit distance along the span of the wing due to a unit jump in angle of attack is

$$\frac{1}{2}\rho U^2 c\, a_w\, \alpha(y)\, \phi(s)$$

where $\phi(s)$ is the Wagner function, which is usually approximated by

$$\phi(s) = 1 - .165\, e^{-.045s} - .335\, e^{-.300s} \tag{A.1}$$

for incompressible two-dimensional flow with

$$s = \frac{Ut}{c/2} \tag{A.2}$$

The integration of this lift distribution across the span yields

$$\begin{aligned} L_w^{\alpha} &= \int_{-\frac{b}{2}}^{\frac{b}{2}} \frac{1}{2}\rho U^2 c\, a_w\, \alpha(y)\, \phi(s)\, dy \\ &= \frac{1}{2}\rho U^2 \frac{b}{2}\, a_w \int_{-1}^{1} c\, \alpha(\eta)\, \phi(s)\, d\eta \end{aligned} \tag{A.3}$$

where

$$\eta = \frac{y}{b/2} \tag{A.4}$$

The three-dimensional value of the lift-curve slope, a_w, is usually chosen in order to have L_w^{α} approach the correct steady-state value.

In equation (A.3), the Wagner function, $\phi(s)$, is a function of the spanwise coordinate, η, because s is inversely proportional to the local

chord of the wing. If, however, the approximation can be made that

$$s = \frac{Ut}{\bar{c}/2} \quad , \tag{A.5}$$

where $\bar{c}$ is the mean geometric chord of the wing, $\phi(s)$ becomes independent of η. Equation (A.5) implies that the rate of growth of lift is constant across the span, and the use of $\bar{c}$ in equation (A.5) gives some kind of an average of the lift growth. With this approximation, $\phi(s)$ can be taken outside the integral sign in equation (A.3). Thus,

$$L_w^{\alpha} = \frac{1}{2} \rho U^2 \frac{b}{2} a_w \phi(s) \int_{-1}^{1} c(\eta)\, \alpha(\eta)\, d\eta \tag{A.6}$$

For a linearly tapered wing, the local chord is given by

$$c(\eta) = \frac{2\bar{c}}{1+\lambda} \left\{ 1 - (1-\lambda)\eta \right\} \tag{A.7}$$

where λ is the taper ratio, i.e., the ratio of the tip chord to the chord at the airplane center line. Substituting in equation (A.6),

$$L_w^{\alpha} = \frac{1}{2} \rho U^2 S_w a_w \phi(s) \frac{2}{1+\lambda} \int_{0}^{1} \left\{ 1 - (1-\lambda)\eta \right\} \alpha(\eta)\, d\eta \tag{A.8}$$

To satisfy two-dimensional thin airfoil theory, the local angle of attack of the wing, $\alpha(\eta)$, must be measured at the three-quarter-chord point (Ref. 10). Therefore, $\alpha(\eta)$ due to motion and attitude is

$$\alpha(\eta) = \theta - \frac{\dot{z}}{U} + \frac{\bar{c}}{2} \left(l_3 - \eta AR \tan \Lambda_3 \right) \frac{\dot{\theta}}{U} \tag{A.9}$$

where

l_3 is the distance which the three-quarter-chord line of the wing lies aft of the airplane center of gravity on the airplane center line and is measured in mean geometric semichords (see Fig. A.1)

Λ_3 is the sweep angle of the three-quarter-chord line of the wing (see Fig. A.1).

or

$$\alpha(\eta) = \theta - \frac{z'}{c/2} + \left(\ell_3 + \eta AR \tan \Lambda_3\right) \theta' \tag{A.10}$$

where the prime mark indicates differentiation with respect to the dimensionless time parameter, s. When the integration indicated by equation (A.8) is carried out, one obtains

$$L_w^{\alpha} = -\frac{1}{2} \rho U^2 S_w a_w \phi(s) \left(\frac{z'}{c/2} - \theta - \bar{\ell}_3 \theta'\right) \tag{A.11}$$

where

$$\bar{\ell}_3 = \frac{2}{1+\lambda} \int_0^1 \{1 - (1-\lambda)\eta\} \left(\ell_3 + \eta AR \tan \Lambda_3\right) d\eta$$

$$= \ell_3 + \frac{1+2\lambda}{3(1+\lambda)} AR \tan \Lambda_3 \tag{A.12}$$

For arbitrary variations of z and θ, the total lift on the wing is

$$L_w^{\alpha}(s) = -\frac{1}{2} \rho U^2 S_w a_w \int_0^s \left\{\frac{2}{c} z''(\sigma) - \theta'(\sigma) - \bar{\ell}_3 \theta''(\sigma)\right\} \phi(s-\sigma)\, d\sigma \tag{A.13}$$

In Reference 11, equation (A.3) was integrated without making the simplifying assumption that the rate of lift growth is constant along the span. These lift-growth functions were defined by

$$I^{(n)}(s_0) = \int_0^1 \eta^n \left[1 - (1-\lambda)\eta\right] \phi \left(\frac{s_0}{1 - (1-\lambda)\eta}\right) d\eta \tag{A.14}$$

where s_0 is measured in wing-root semichords and the superscript n refers to

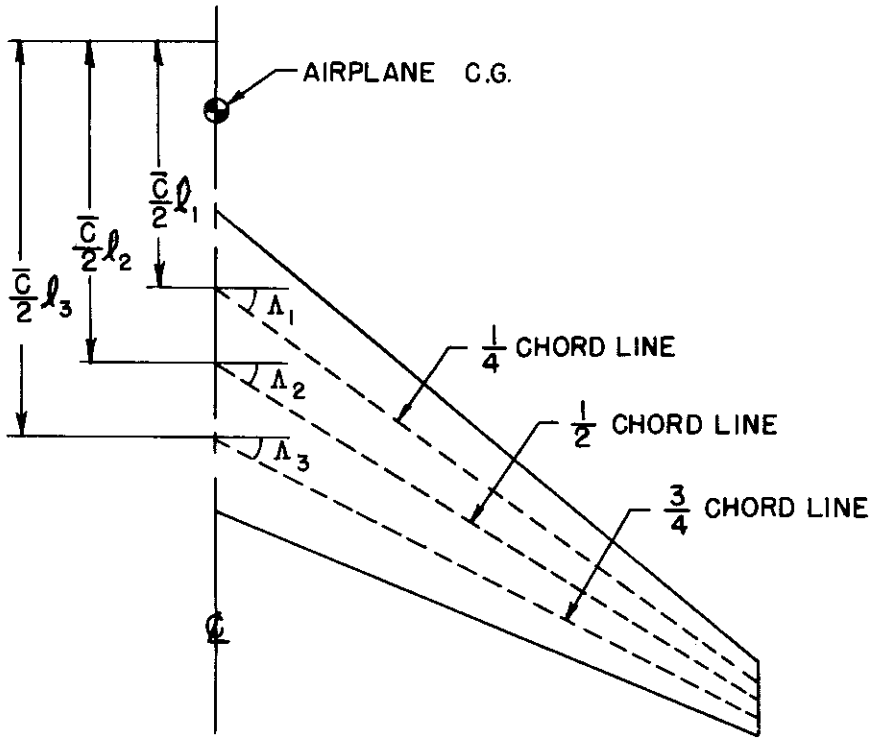

FIGURE A.1 DEFINITIONS OF THE DISTANCES l_1 , l_2 , AND l_3 AND THE SWEEP ANGLES Λ_1 , Λ_2 , AND Λ_3

different parts of some generalized forces associated with a wing free to bend in a parabolic deflection curve. When the above assumption is introduced into equation (A.14), one obtains

$$I^{(n)}(s_o) \cong \phi\left(\frac{2s_o}{1+\lambda}\right)\int_0^1 \eta^n\left[1-(1-\lambda)\eta\right]d\eta$$

$$\cong \frac{1+(n+1)\lambda}{(n+1)(n+2)}\ \phi\left(\frac{2s_o}{1+\lambda}\right) \qquad \text{(A.15)}$$

Figure A.2 presents a comparison of the results obtained from equations (A.14) and (A.15) for the example airplane. It can be seen that the variation in rate of lift growth across the span is a secondary factor even when the lift distribution is weighted by η^4 .

(b) Lift on Tail Due to Angle of Attack

The lift on the horizontal tail due to motion can be obtained from equation (A.13) simply by replacing the wing parameters with the appropriate horizontal tail parameters. As a result,

$$L_t^{\alpha}(s) = -\tfrac{1}{2}\rho U^2 S_t a_t \int_0^s \left\{\frac{2}{\bar{c}} z''(\sigma) - \theta'(\sigma) - \left[l_t + \frac{1}{\gamma}\right]\theta''(\sigma)\right\}\phi(\gamma s - \gamma\sigma)\,d\sigma \qquad \text{(A.16)}$$

where

l_t is the distance which the tail aerodynamic center lies aft of the airplane center of gravity, measured in mean geometric wing semichords

γ is the ratio $\bar{c}_w / \bar{c}_t$.

(c) Pitching Moment on the Wing Due to Angle of Attack

According to two-dimensional thin airfoil theory, the lift on the wing

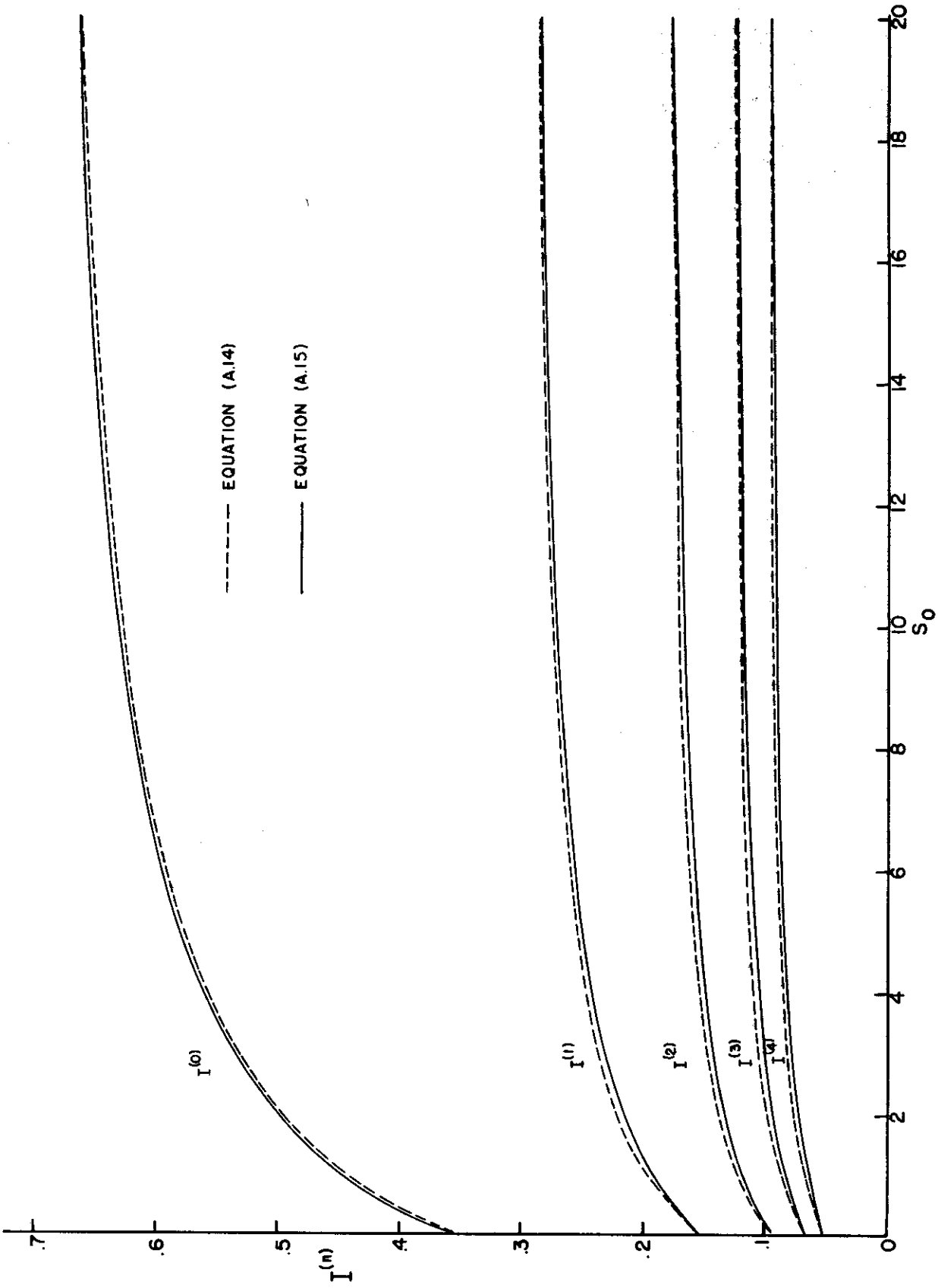

FIGURE A.2 COMPARISON OF EQUATIONS (A.14) AND (A.15), $\lambda = 0.42$

effectively acts at the quarter-chord line, and thus, the pitching moment (positive, nose up) on a strip of the wing about the airplane center of gravity due to a unit jump in angle of attack is

$$-\frac{\bar{c}}{2}\left(l_1 + \eta\, AR \tan\Lambda_1\right)\left(\tfrac{1}{2}\rho U^2 c\, a_w\, \alpha(y)\, \phi(s)\right)$$

where

l_1 is the distance which the wing quarter-chord line lies aft of the airplane center of gravity on the airplane center line, measured in mean geometric semichords (see Fig. A.1).

Λ_1 is the sweep angle of the wing quarter-chord line (see Fig. A.1).

The total pitching moment on the wing is then

$$m_w^{\alpha} = -\tfrac{1}{2}\rho U^2 S_w \frac{\bar{c}}{2}\, a_w\, \phi(s)\, \frac{2}{1+\lambda}\int_0^1 \left(l_1 + \eta\, AR \tan\Lambda_1\right)\left[1-(1-\lambda)\eta\right]\alpha(\eta)\, d\eta \qquad (A.17)$$

When $\alpha(\eta)$ given by equation (A.10) is substituted into equation (A.17), the pitching moment becomes

$$m_w^{\alpha} = \tfrac{1}{2}\rho U^2 S_w \frac{\bar{c}}{2}\, a_w\, \phi(s)\left[l_w\left(\frac{\bar{z}'}{\bar{c}/2} - \theta\right) - \bar{l}_2\,\theta'\right]\phi(s) \qquad (A.18)$$

where

$$l_w = \frac{2}{1+\lambda}\int_0^1 \left(l_1 + \eta\, AR \tan\Lambda_1\right)\left[1-(1-\lambda)\eta\right] d\eta$$

$$= l_1 + \frac{1+2\lambda}{3(1+\lambda)}\, AR \tan\Lambda_1 \qquad (A.19)$$

$$\bar{l}_2 = \frac{2}{1+\lambda}\int_0^1 \left(l_1 + \eta\, AR \tan\Lambda_1\right)\left(l_3 + \eta\, AR \tan\Lambda_3\right)\left[1-(1-\lambda)\eta\right] d\eta$$

$$= l_w \bar{l}_3 + \frac{1}{18}\left[1 + \frac{2\lambda}{(1+\lambda)^2}\right] AR^2 \tan\Lambda_1 \tan\Lambda_3 \qquad (A.20)$$

The moment arm $l_w \frac{\bar{c}}{2}$ is the distance which the wing aerodynamic center lies aft of the airplane center of gravity, and the strip theory value given by equation (A.19) can be replaced by a more realistic value.

For arbitrary variations of z and θ, the total pitching moment on the wing is

$$m_w^{\alpha} = \frac{1}{2}\rho U^2 S_w \frac{\bar{c}}{2} a_w \int_0^s \left\{ l_w \left(\frac{2}{\bar{c}} z''(\sigma) - \theta'(\sigma) \right) - \bar{l}_2 \theta''(\sigma) \right\} \phi(s-\sigma)\, d\sigma \qquad (A.21)$$

(d) Pitching Moment on Tail Due to Angle of Attack

The pitching moment on the horizontal tail due to motion can be obtained by multiplying its lift by the moment arm $l_t \frac{\bar{c}}{2}$. From equation (A.16), this procedure gives

$$m_t^{\alpha} = \frac{1}{2}\rho U^2 S_t a_t l_t \frac{\bar{c}}{2} \int_0^s \left\{ \frac{2}{\bar{c}} z''(\sigma) - \theta'(\sigma) - \left[l_t + \frac{1}{\gamma} \right] \theta''(\sigma) \right\} \phi(\gamma s - \gamma\sigma)\, d\sigma \qquad (A.22)$$

(e) Lift on Wing Due to Gust Penetration

According to strip theory, the lift on a wing strip of unit span due to the penetration of a sharp-edged gust is

$$\frac{1}{2}\rho U^2 c\, a_w \frac{w}{U} \psi(s)$$

where

w is the vertical gust velocity

$\psi(s)$ is the Küssner lift-growth function.

The Küssner function is defined in such a way that s must be measured from the leading edge of the strip. If the front of the sharp-edged gust is taken to be perpendicular to the airplane center line and if the gust penetration distance s is measured from the apex of the swept wing in mean geometric semichords, the total lift on the wing is (see Ref. 12)

$$L_w^G = \tfrac{1}{2}\rho U^2 S_w a_w \frac{w}{U} \frac{2}{1+\lambda} \int_0^{\eta^*} [1-(1-\lambda)\eta] \Psi\left(\frac{(1+\lambda)(s-\beta\eta)}{2[1-(1-\lambda)\eta]}\right) d\eta \qquad (A.23)$$

where

$$\eta^* = \frac{s}{\beta}, \quad \text{when} \quad s < \beta$$

$$= 1, \quad \text{when} \quad s > \beta$$

$$\beta = AR \tan \Lambda_0$$

Λ_0 is the sweep angle of the leading edge of the wing.

The distance $\beta \frac{\bar{c}}{2}$ is the streamwise distance from the apex of the wing to the leading edge of the tip chord.

The results of integrating equation (A.23) in closed form, given in Reference 12, are quite complicated and cumbersome, and their extension to the case of an arbitrarily deformed elastic swept wing would be very difficult. It has been found, however, that equation (A.23) can be integrated easily if the following two approximations are made:

(1) Assume, as was done previously for the lift due to motion, that the rate of lift growth is independent of the local chord.

(2) Assume that an average gust penetration distance can be used for that portion of the wing which is enveloped by the gust.

From Figure A.3, it can be seen that the average penetration distance is $s/2$ when the wing has partially penetrated the gust front, i.e., $s < \beta$, and is $s - \frac{\beta}{2}$ after the wing has completely penetrated the front, i.e., $s > \beta$.

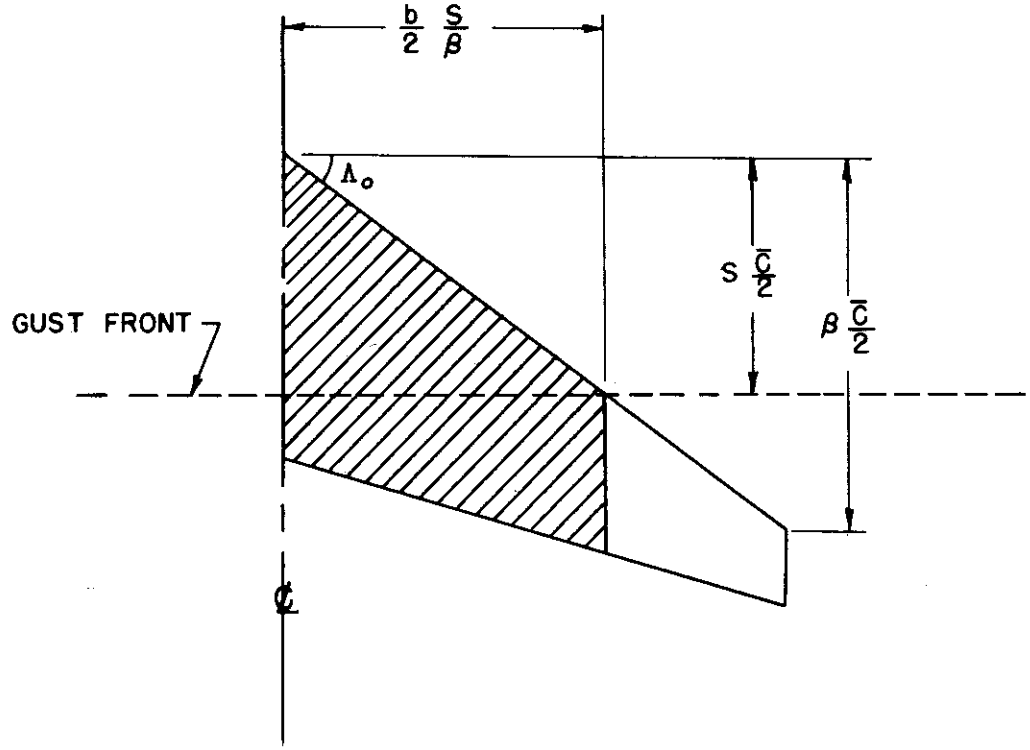

FIGURE A.3 PENETRATION OF GUST FRONT BY SWEPT WING

After making these two approximations, equation (A.23) reduces to

$$L_w^G = \tfrac{1}{2}\rho U^2 S_w a_w \frac{w}{U}\,\psi\!\left(\tfrac{s}{2}\right)\frac{2}{1+\lambda}\int_0^{\frac{s}{\beta}}\left[1-(1-\lambda)\eta\right]d\eta\,, \qquad \text{when } s \le \beta$$

$$= \tfrac{1}{2}\rho U^2 S_w a_w \frac{w}{U}\,\psi\!\left(s-\tfrac{\beta}{2}\right)\frac{2}{1+\lambda}\int_0^{1}\left[1-(1-\lambda)\eta\right]d\eta\,, \qquad \text{when } s \ge \beta \tag{A.24}$$

Or

$$L_w^G = \tfrac{1}{2}\rho U^2 S_w a_w \frac{w}{U}\,\frac{2-(1-\lambda)\frac{s}{\beta}}{1+\lambda}\,\frac{s}{\beta}\,\psi\!\left(\tfrac{s}{2}\right), \qquad \text{when } s \le \beta$$

$$= \tfrac{1}{2}\rho U^2 S_w a_w \frac{w}{U}\,\psi\!\left(s-\tfrac{\beta}{2}\right), \qquad \text{when } s \ge \beta \tag{A.25}$$

For an arbitrary variation of gust velocity in the streamwise direction, the variation of the total lift on the wing is

$$L_w^G(s) = \tfrac{1}{2}\rho U^2 S_w a_w \int_0^s \frac{w'(\sigma)}{U}\, \psi_\lambda^L(s-\sigma)\, d\sigma \qquad \text{(A.26)}$$

where

$$\psi_\lambda^L(s) = \frac{2-(1-\lambda)\frac{s}{\beta}}{1+\lambda}\,\frac{s}{\beta}\,\psi\left(\frac{s}{2}\right), \qquad \text{when} \quad s \le \beta$$

$$= \psi\left(s-\frac{\beta}{2}\right), \qquad \text{when} \quad s \ge \beta$$

In Reference 11, equation (A.23) was integrated without making any simplifying assumptions, and the resulting lift-growth functions were defined by

$$\psi_n(s_0) = \int_0^{\eta^*} [1-(1-\lambda)\eta]\,\eta^n\,\psi\left(\frac{s_0-\beta_0\eta}{1-(1-\lambda)\eta}\right) d\eta \qquad \text{(A.27)}$$

where s_0 and β_0 are measured in wing-root semichords and η^n is a weighting factor which is used to obtain generalized forces for a wing free to bend in a parabolic deflection curve. When the simplifying assumptions noted above are applied to equation (A.27), one obtains

$$\psi_n(s_0) \cong \left(\frac{1}{n+1} - \frac{1-\lambda}{n+2}\,\frac{s_0}{\beta_0}\right)\left(\frac{s_0}{\beta_0}\right)^{n+1}\psi\left(\frac{s_0}{1+\lambda}\right), \qquad \text{when} \quad s_0 \le \beta_0$$

$$\cong \frac{1+(n+1)\lambda}{(n+1)(n+2)}\,\psi\left(\frac{2s_0-\beta_0}{1+\lambda}\right) \qquad \text{when} \quad s_0 \ge \beta_0 \qquad \text{(A.28)}$$

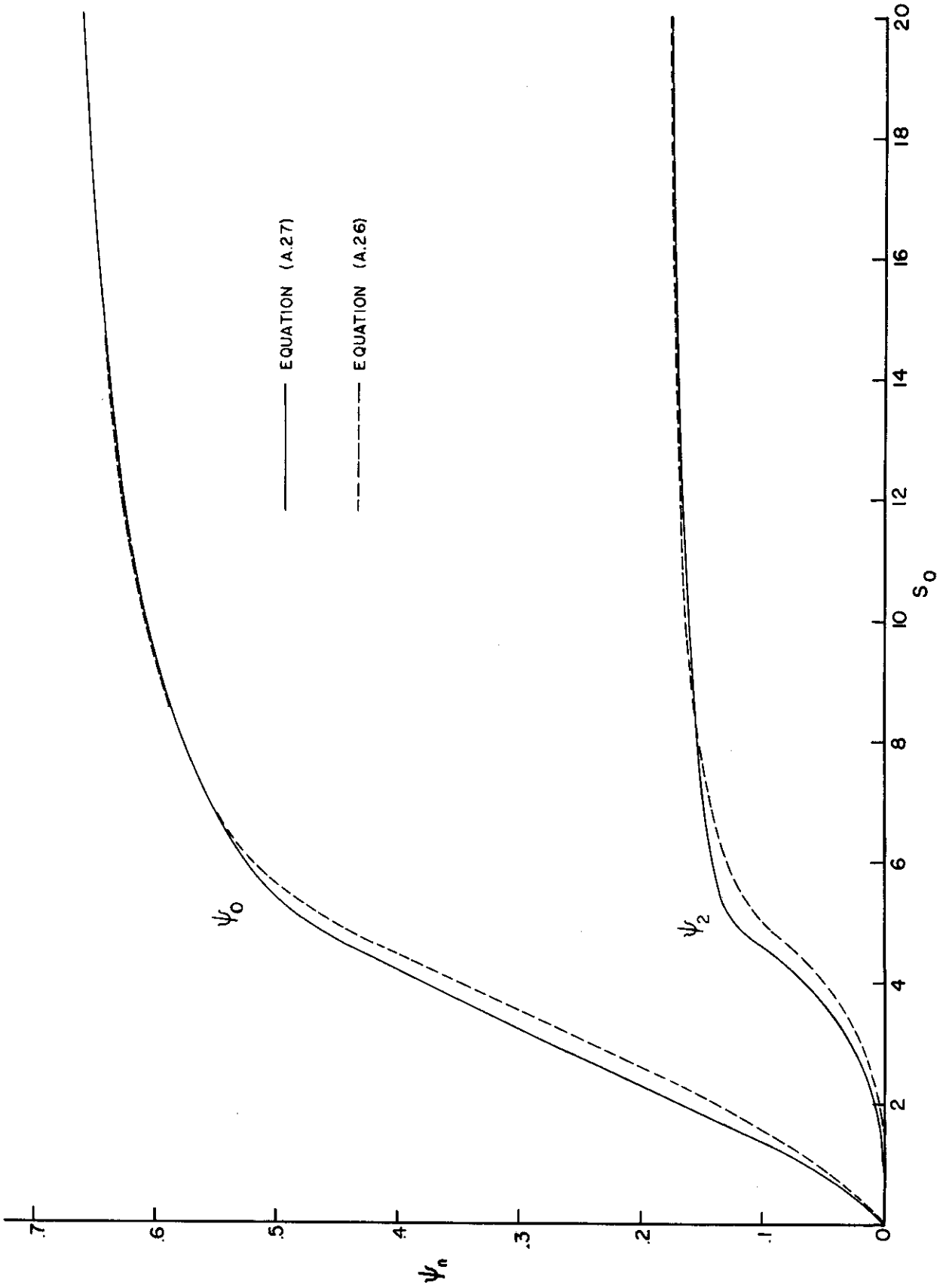

FIGURE A.4 COMPARISON OF EQUATIONS (A.26) AND (A.27), $\beta_0 = 4.91$, $\lambda = 0.42$

Figure A.4 offers a comparison of the results obtained by applying equations (A.27) and (A.28) to the example airplane of the present report. This figure shows that the simplifying assumptions made in this section produce slightly conservative and useful results.

Reference 12 presents a "semi-three-dimensional-theory" for the computation of the lift build-up on a swept wing. This theory is based on the lift distribution of an infinite swept wing which penetrates a sharp-edged gust. This unsteady flow problem is shown to be equivalent to a steady-flow problem that involves an infinite swept wing with an angle-of-attack discontinuity at a spanwise station. A comparison between the two theories which was made in Reference 12 has been reproduced in Figure A.5, and it shows that the "semi-three-dimensional-theory" predicts a much more rapid rate of lift growth than does strip theory.

In Reference 13 exponential expressions for the Küssner function were derived for finite elliptic unswept wings. These results also yield a more rapid rate of lift build-up than does strip theory. Although there is no logical way to transform an aspect-ratio correction to the Küssner function for an elliptic wing into a corresponding correction for a swept wing, Figure A.5 discloses that the arbitrary use of the Küssner functions of Reference 13 in equation (A.26) gives a curve which lies between those given by the "semi-three-dimensional" and strip theories. If, as has been suggested, these two theories represent the upper and lower bounds, respectively, between which the actual lift lies, the present method may yield quite realistic results.

The aforesaid Küssner functions for elliptic wings can be expressed by the formula,

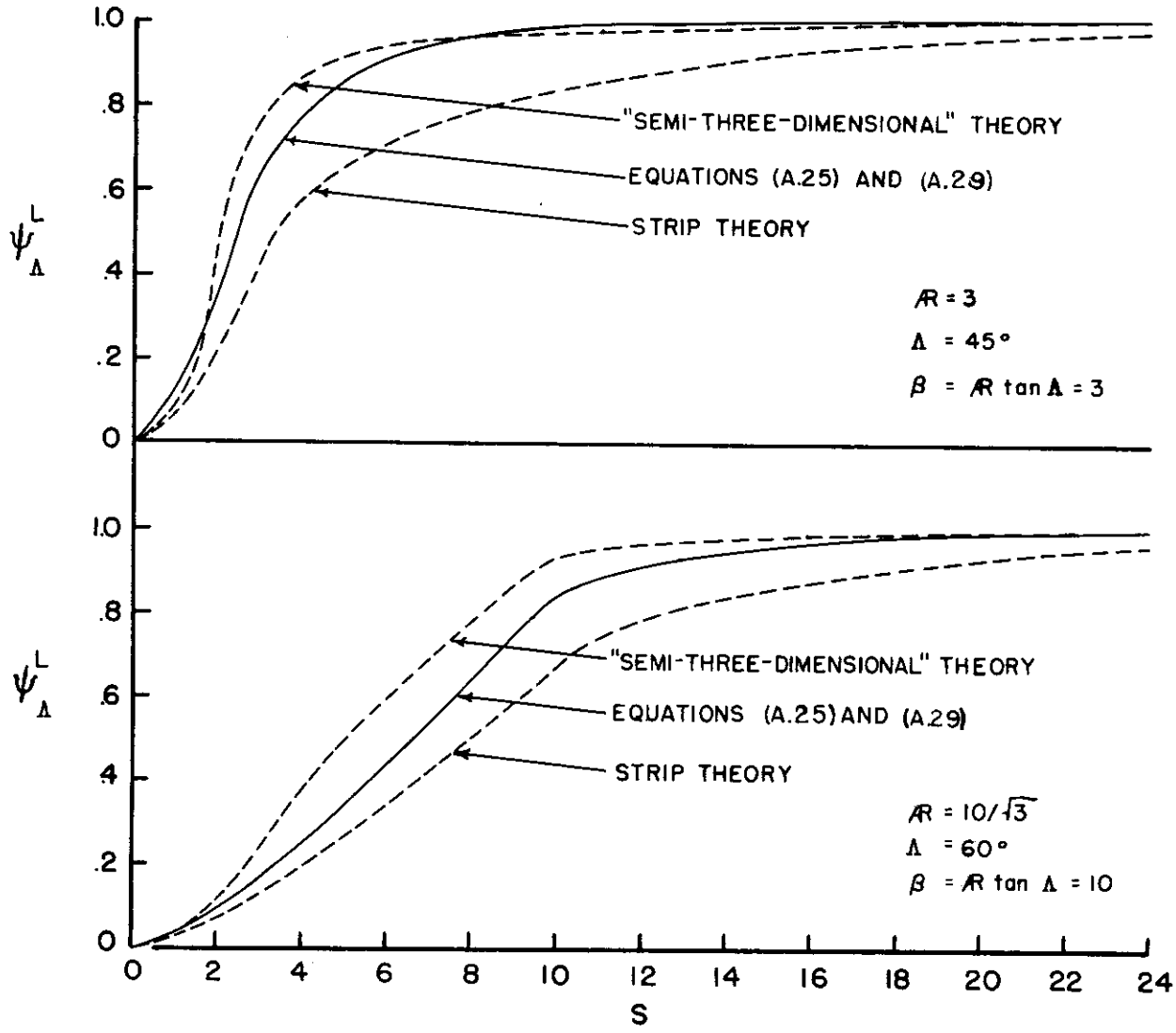

FIGURE A.5 COMPARISON OF DIFFERENT METHODS FOR FINDING THE LIFT GROWTH ON SWEPTBACK WINGS

$$\psi(s) = 1 - a_1 e^{-\lambda_1 s} - a_2 e^{-\lambda_2 s} - a_3 e^{-\lambda_3 s} \qquad (A.29)$$

where the a- and λ- coefficients are given in the following table:

TABLE A.1

COEFFICIENTS FOR EQUATION (A.29)

AR	3	6	∞
a_1	.679	.448	.236
a_2	0	.272	.513
a_3	.227	.193	.171
λ_1	.438	.228	.058
λ_2	- -	.569	.364
λ_3	2.51	2.36	2.42

In equation (A.29), s is measured in mean geometric semichords instead of in root semichords as in Reference 13. In Figure A.6 the coefficients of Table A.1 have been plotted against the reciprocal of the aspect ratio. Interpolation is simple because the resulting lines are almost straight.

Similar exponential expressions for the Kussner function in two-dimensional subsonic compressible flow are given in Reference 6; one cannot, however, use the results of both References 6 and 13 in equation (A.26) at the same time. Furthermore, the results of Reference 14 indicate that the use of incompressible lift-growth functions together with a steady-state lift-curve slope corrected for compressibility yields conservative results for subcritical Mach numbers. It should be pointed out that compressibility effects can

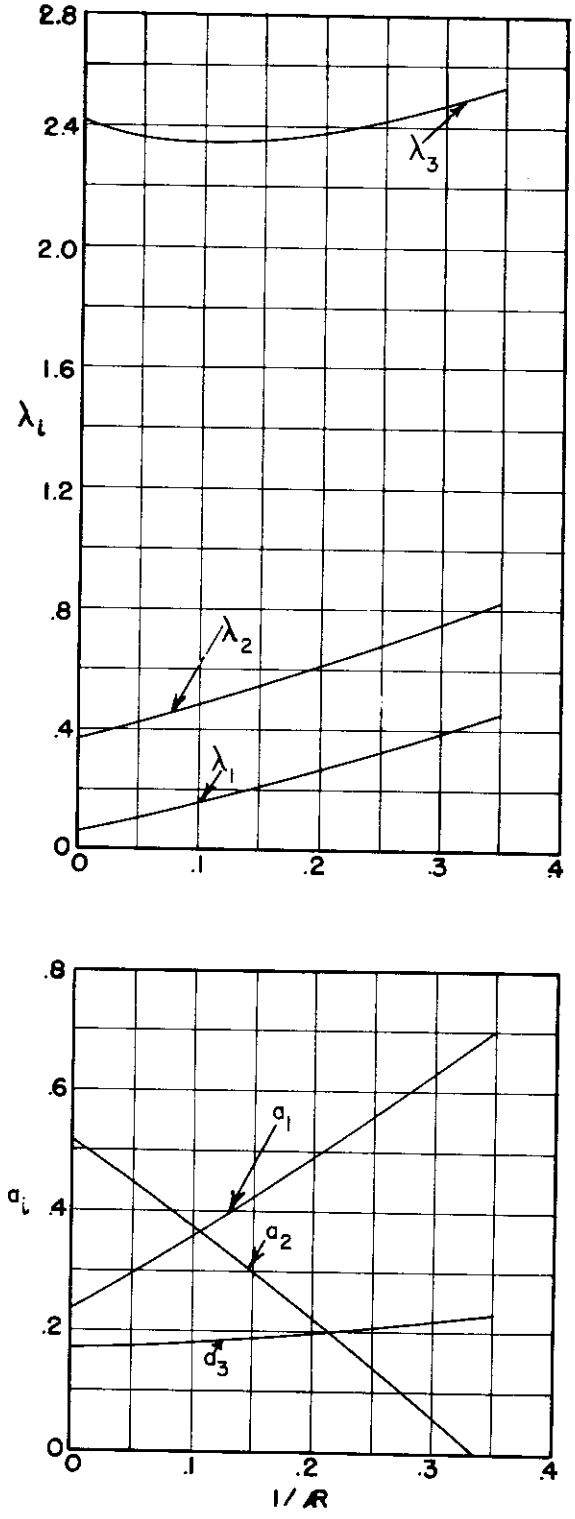

FIGURE A.6 COEFFICIENTS FOR EQUATION (A.29)

be included in the "semi-three-dimensional" theory of Reference 12 for subsonic as well as supersonic speeds.

(f) Lift on Tail Due to Gust Penetration

The lift on the horizontal tail due to gust penetration is obtained by modifying equation (A.26) to give

$$L_t^G(s) = \tfrac{1}{2}\rho U^2 S_t\, a_t \int_0^s \frac{w'(\sigma)}{U}\, \psi_{\lambda_t}(s-\sigma)\, d\sigma \qquad \text{(A.30)}$$

where

$$\psi_{\lambda_t}(s) = \frac{2-(1-\lambda_t)\frac{\gamma s}{\beta_t}}{1+\lambda_t}\,\frac{\gamma s}{\beta_t}\,\psi\left(\frac{\gamma s}{2}\right) \quad , \text{ when } \quad s \le \frac{\beta_t}{\gamma}$$

$$= \psi\left(\gamma s - \frac{\beta_t}{2}\right) \quad , \text{ when } \quad s \ge \frac{\beta_t}{\gamma}$$

and where

$$\beta_t = R_t \tan \Lambda_{0_t}$$

$$\gamma = \frac{\bar{c}_w}{\bar{c}_t}$$

(g) Pitching Moment on Wing Due to Gust Penetration

In addition to the assumptions made with regard to L_w^G in subsection A.1 (e) above, another assumption must be made about the pitching moment growth in order to keep a comparable simplicity. It will be assumed here that, for a sharp-edged gust, the center of pressure of the lift on the wing is on the quarter-chord line at a spanwise distance given by the centroid of the chord distribution on the gust-enveloped portion of the wing, i.e., the shaded area in Figure A.3. Therefore, the wing pitching moment about the airplane center of gravity due to a sharp-edged gust becomes

$$m_w^G = -\left(l_1 + \frac{3 - 2(1-\lambda)\frac{s}{\beta}}{6 - 3(1-\lambda)\frac{s}{\beta}} \frac{s}{\beta} \tan \Lambda_1\right) \frac{\bar{c}}{2} L_w^G \quad , \text{ when } s \leq \beta$$

$$= -l_w \frac{\bar{c}}{2} L_w^G \quad , \text{ when } s \geq \beta \qquad \text{(A.31)}$$

where the parameters l_1, Λ_1 and l_w are defined in subsection A.1 (c) above. Then, for a gust which varies arbitrarily in the streamwise direction,

$$m_w^G(s) = -l_1 \frac{\bar{c}}{2} L_w^G(s) - \frac{1}{2}\rho U^2 S_w \frac{\bar{c}}{2} (l_w - l_1) a_w \int_0^s \frac{w'(\sigma)}{U} \psi_\Lambda^m(s-\sigma)\, d\sigma \qquad \text{(A.32)}$$

where

$$\psi_\Lambda^m = \frac{3 - 2(1-\lambda)\frac{s}{\beta}}{1 + 2\lambda} \left(\frac{s}{\beta}\right)^2 \psi\left(\frac{s}{2}\right) \quad , \text{ when } s \leq \beta$$

$$= \psi\left(s - \frac{\beta}{2}\right) = \psi_\Lambda^L(s) \quad , \text{ when } s \geq \beta$$

It should be noted that the pitching moment about the intersection of the quarter-chord line and the plane of symmetry for a sharp-edged gust is given by

$$\frac{m_w^G(s)}{m_w^G(\infty)} = \psi_\Lambda^m(s) \qquad \text{(A.33)}$$

Figure A.7 provides a comparison of the pitching moment growths as calculated by equation (A.3), the "semi-three-dimensional" theory (Ref. 12), and strip theory. Once again, the present method gives intermediate results.

(h) Pitching Moment on Tail Due to Gust Penetration

When the fore-and-aft variation of the center of pressure on the horizontal tail is small compared with the tail length, $l_t \frac{\bar{c}}{2}$, the pitching moment of the tail about the airplane center of gravity due to a gust is simply

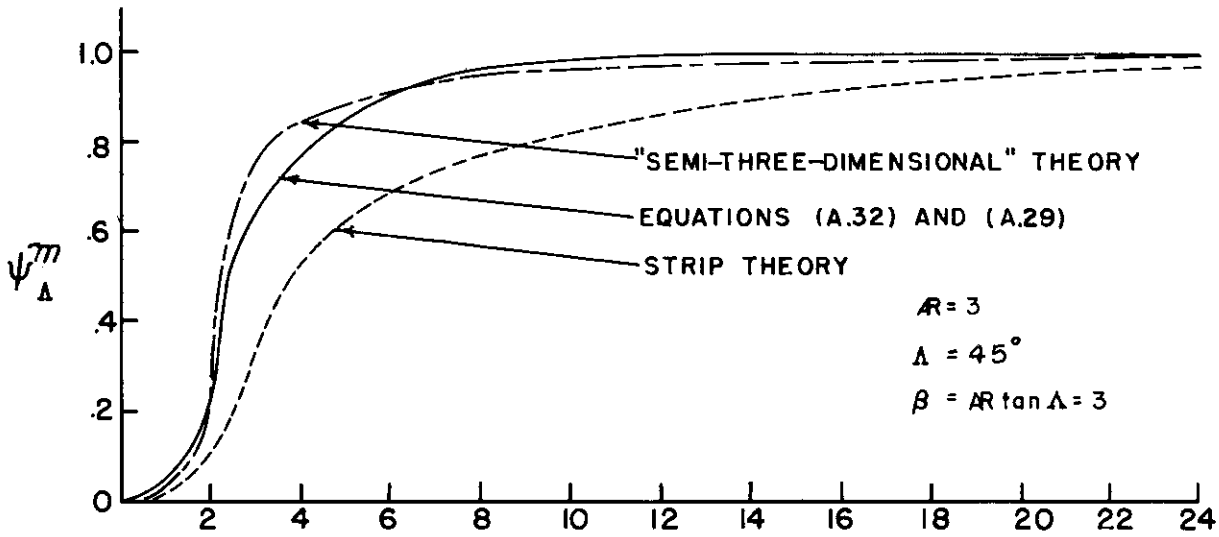

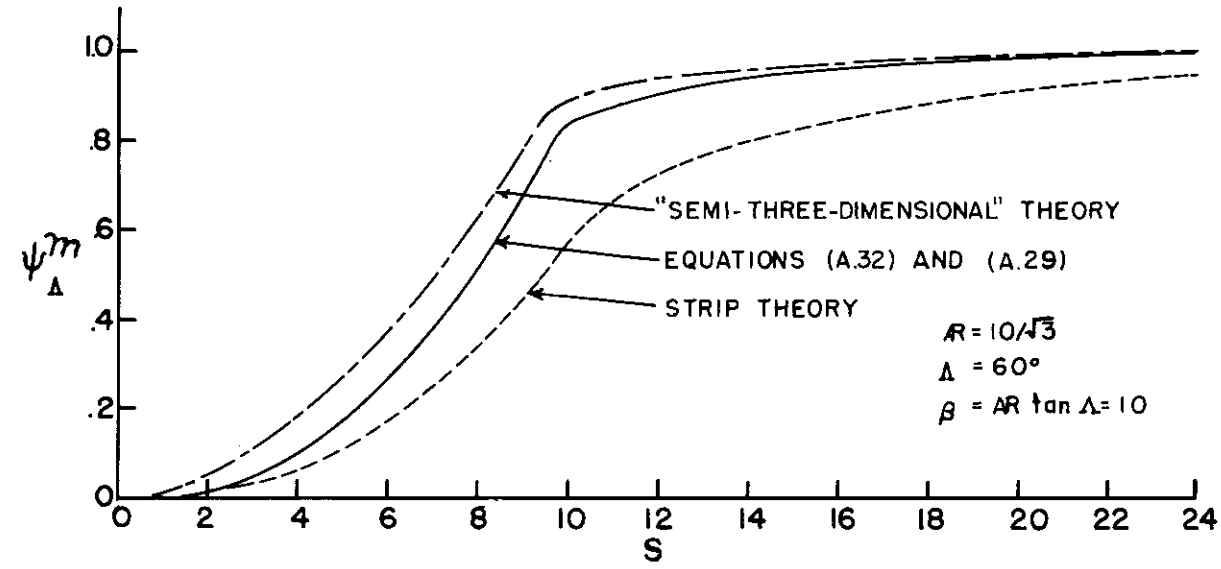

FIGURE A.7 COMPARISON OF DIFFERENT METHODS FOR FINDING THE PITCHING-MOMENT GROWTH ON SWEPTBACK WINGS

$$m_t^G(s) = -l_t \frac{\bar{c}}{2} L_t^G(s)$$

$$= -\frac{1}{2}\rho U^2 S_t a_t \int_0^s \frac{w(\sigma)}{U} \psi_{\Lambda_t}(s-\sigma)\, d\sigma \qquad (A.34)$$

(i) Lift on Wing Due to Apparent Mass

By strip theory the force on a wing strip of unit span due to the apparent mass of the surrounding air is $\pi\rho\left(\frac{c}{2}\right)^2$ multiplied by the acceleration of this strip normal to its midpoint relative to the surrounding air (Ref. 10). The lift per unit span on the wing is then

$$\pi\rho\left(\frac{c}{2}\right)^2\left[-\ddot{z} + U\dot{\theta} + \left(l_2 + \eta AR \tan\Lambda_2\right)\frac{\bar{c}}{2}\ddot{\theta}\right]$$

where

l_2 is the distance which the wing midchord line lies aft of the airplane center of gravity on the airplane center line and is measured in mean geometric semichords (see Fig. A.1)

Λ_2 is the sweep angle of the wing midchord line (see Fig. A.1).

The integration of this lift distribution across the span of a linearly tapered wing yields a total lift of

$$L_w^A = \pi\rho b\left(\frac{\bar{c}}{2}\right)^2\left[1 + \frac{1}{3}\left(\frac{1-\lambda}{1+\lambda}\right)^2\right]\left[-\ddot{z} + U\dot{\theta} + k_1\frac{\bar{c}}{2}\ddot{\theta}\right] \qquad (A.35)$$

where

$$k_1 = l_2 + \frac{1+2\lambda+3\lambda^2}{4(1+\lambda+\lambda^2)} AR \tan\Lambda_2$$

Except for a part of the lift due to $U\dot{\theta}$, this lift is noncirculatory and no Prandtl-type aspect-ratio correction should be applied.

(j) Lift on Tail Due to Apparent Mass

If equation (A.35) is modified to give the total lift on the horizontal tail due to apparent mass effects, then

$$L_t^A = \pi\rho \frac{b_t}{\gamma^2}\left(\frac{\bar{c}}{2}\right)^2\left[1 + \frac{1}{3}\left(\frac{1-\lambda_t}{1+\lambda_t}\right)^2\right]\left[-\ddot{z} + U\dot{\theta} + \left(l_t + \frac{1}{2\gamma}\right)\frac{\bar{c}}{2}\ddot{\theta}\right] \qquad (A.36)$$

(k) Pitching Moment on Wing Due to Apparent Mass

From Reference 10, the distribution of pitching moment along the wing due to apparent mass is

$$\pi\rho\left(\frac{c}{2}\right)^2\left[\frac{\bar{c}}{2}\left(l_2 + \eta AR\tan\Lambda_2\right)\ddot{z} - \frac{\bar{c}}{2}\left(l_3 + \eta AR\tan\Lambda_3\right)U\dot{\theta}\right.$$

$$\left.-\left(\frac{\bar{c}}{2}\right)^2\left(l_2 + \eta AR\tan\Lambda_2\right)^2\ddot{\theta} - \frac{1}{8}\left(\frac{c}{2}\right)^2\ddot{\theta}\right]$$

and the integration of this distribution over the span of the wing yields

$$m_w^A = \pi\rho b\left(\frac{\bar{c}}{2}\right)^3\left[1 + \frac{1}{3}\left(\frac{1-\lambda}{1+\lambda}\right)^2\right]\left[k_1\ddot{z} - k_2 U\dot{\theta} - k_3\frac{\bar{c}}{2}\ddot{\theta}\right] \qquad (A.37)$$

where

$$k_1 = l_2 + \frac{1+2\lambda+3\lambda^2}{4(1+\lambda+\lambda^2)} AR\tan\Lambda_2$$

$$k_2 = l_3 + \frac{1+2\lambda+3\lambda^2}{4(1+\lambda+\lambda^2)} AR\tan\Lambda_3$$

$$k_3 = \frac{3(1+\lambda+\lambda^2+\lambda^3+\lambda^4)}{10(1+\lambda+\lambda^2)(1+\lambda)^2} + l_2^2 + \frac{1+2\lambda+3\lambda^2}{2(1+\lambda+\lambda^2)} l_2 AR \tan \Lambda_2 + \frac{1+3\lambda+6\lambda^2}{10(1+\lambda+\lambda^2)} AR^2 \tan^2 \Lambda_2$$

(l) Pitching Moment on Tail Due to Apparent Mass

Modification of equation (A.36) to give the pitching moment on the horizontal tail about the airplane center of gravity due to apparent mass effects yields

$$m_t^A = \pi \rho \frac{b_t}{\gamma^2} \left(\frac{\bar{c}}{2}\right)^3 \left(l_t + \frac{1}{2\gamma}\right) \left[1 + \frac{1}{3}\left(\frac{1-\lambda_t}{1+\lambda_t}\right)^2\right] \left[\ddot{z} - U\dot{\theta} - \left(l_t + \frac{1}{2\gamma}\right)\frac{\bar{c}}{2}\ddot{\theta}\right] \quad \text{(A.38)}$$

A.2 Fuselage

It is shown in Reference 15 that, for a very slender body with an elliptic cross section, the apparent mass per unit length is ρA, where A is the local cross-sectional area of an equivalent body of revolution, i.e., one with the same local width. The lift per unit length on a slender fuselage is then the rate of change of momentum of this apparent mass,

$$\frac{d}{dt}(\rho A U \alpha) = \rho U^2 \left(\frac{dA}{dx}\alpha + A\frac{\partial \alpha}{\partial x}\right) + \rho A \frac{\partial}{\partial t}(U\alpha) \quad \text{(A.39)}$$

In the following analysis, the first term on the right-hand side of equation (A.39) is designated as the lift due to angle of attack and the second term

as the lift due to apparent mass.

(a) Lift and Pitching Moment on Fuselage Due to Angle of Attack

From equation (A.39), the total lift on the fuselage due to angle of attack is

$$L_f^{\alpha} = \rho U^2 \int_0^{l_f \frac{\bar{c}}{2}} \left(\frac{dA}{dx} \alpha + A \frac{\partial \alpha}{\partial x} \right) dx \tag{A.40}$$

where

l_f is the length of the fuselage in mean geometric semichords,

The angle of attack at each section of the fuselage is

$$\alpha(x,t) = \theta - \frac{\dot{z}}{U} + \left(x - \frac{\bar{c}}{2} l_{CG} \right) \frac{\dot{\theta}}{U} \tag{A.41}$$

where

l_{CG} is the distance which the airplane center of gravity lies aft of the nose of the fuselage.

The substitution of equation (A.41) into equation (A.40) gives

$$L_f^{\alpha} = \rho U^2 \int_0^{l_f \frac{\bar{c}}{2}} \left\{ \left[\theta - \frac{\dot{z}}{U} + \left(x - \frac{\bar{c}}{2} l_{CG} \right) \frac{\dot{\theta}}{U} \right] \frac{dA}{dx} + A \frac{\dot{\theta}}{U} \right\} dx$$

$$= \rho U^2 \left[\left(\theta - \frac{\dot{z}}{U} - \frac{\bar{c}}{2} l_{CG} \frac{\dot{\theta}}{U} \right) A \right]_0^{l_f \frac{\bar{c}}{2}} + \rho U^2 \frac{\dot{\theta}}{U} \left[Ax - \int A \, dx \right]_0^{l_f \frac{\bar{c}}{2}} + \rho U^2 \frac{\dot{\theta}}{U} \int_0^{l_f \frac{\bar{c}}{2}} A \, dx \tag{A.42}$$

$$= 0$$

Similarly, the pitching moment on the fuselage is

$$m_f^{\alpha} = -\rho U^2 \int_0^{l_f \frac{\bar{c}}{2}} \left(\frac{dA}{dx} \alpha + A \frac{\partial \alpha}{\partial x} \right) \left(x - \frac{\bar{c}}{2} l_{CG} \right) dx$$

$$= -\rho U^2 \int_0^{l_f \frac{\bar{c}}{2}} \left\{ \left[\theta - \frac{\dot{z}}{U} + \left(x - \frac{\bar{c}}{2} l_{CG} \right) \frac{\dot{\theta}}{U} \right] \frac{dA}{dx} x + A \frac{\dot{\theta}}{U} x \right\} dx + \frac{\bar{c}}{2} l_{CG} L_f^{\alpha}$$

$$= -\rho U^2 \left(\theta - \frac{\dot{z}}{U} - \frac{\bar{c}}{2} l_{CG} \frac{\dot{\theta}}{U} \right) \left[Ax - \int A dx \right]_0^{l_f \frac{\bar{c}}{2}} \qquad \text{(A.43)}$$

$$-\rho U^2 \frac{\dot{\theta}}{U} \left[Ax^2 - 2 \int Ax\, dx \right]_0^{l_f \frac{\bar{c}}{2}} - \rho U^2 \frac{\dot{\theta}}{U} \int_0^{l_f \frac{\bar{c}}{2}} Ax\, dx$$

This equation reduces to

$$m_f^{\alpha} = \frac{1}{2} \rho U^2 S_w \bar{c} \frac{dC_{m_f}}{d\alpha} \left[\theta - \frac{\dot{z}}{U} + \frac{\bar{c}}{2} \left(\bar{l}_f - l_{CG} \right) \frac{\dot{\theta}}{U} \right] \qquad \text{(A.44)}$$

where

$$\frac{dC_{m_f}}{d\alpha} = \frac{2 V_f}{S_w \bar{c}}$$

$$V_f = \int_0^{l_f \frac{\bar{c}}{2}} A\, dx = \text{total volume of the equivalent body of revolution}$$

$$\frac{\bar{c}}{2} \bar{l}_f = \frac{\int_0^{l_f \frac{\bar{c}}{2}} Ax\, dx}{V_f} = \text{distance from the nose of fuselage to the centroid of the volume of the equivalent body of revolution.}$$

The expression given for $\frac{dC_{m_f}}{d\alpha}$ is not very realistic because of the large interference from the wings. Although this interference is not quasi-steady, a more accurate steady-state value for $\frac{dC_{m_f}}{d\alpha}$ should probably be used.

(b) Lift and Pitching Moment on Fuselage Due to Apparent Mass

From equation (A.39), the total lift on the fuselage due to apparent mass is

$$L_f^A = \rho \int_0^{l_f \frac{\bar{c}}{2}} A \frac{\partial}{\partial t}(U\alpha)\, dx \tag{A.45}$$

and from equation (A.41),

$$\frac{\partial}{\partial t}(U\alpha) = U\dot{\theta} - \ddot{z} + \left(x - \frac{\bar{c}}{2} l_{CG}\right)\ddot{\theta} \tag{A.46}$$

The substitution of equation (A.46) into equation (A.45) gives

$$\begin{aligned} L_f^A &= \rho \int_0^{l_f \frac{\bar{c}}{2}} \left[U\dot{\theta} - \ddot{z} + \left(x - \frac{\bar{c}}{2} l_{CG}\right)\ddot{\theta}\right] A\, dx \\ &= \rho V_f \left[U\dot{\theta} - \ddot{z} + \frac{\bar{c}}{2}\left(\bar{l}_f - l_{CG}\right)\ddot{\theta}\right] \end{aligned} \tag{A.47}$$

Similarly, the pitching moment on the fuselage due to apparent mass is

$$\begin{aligned} m_f^A &= -\rho \int_0^{l_f \frac{\bar{c}}{2}} \left[U\dot{\theta} - \ddot{z} + \left(x - \frac{\bar{c}}{2} l_{CG}\right)\ddot{\theta}\right]\left(x - \frac{\bar{c}}{2} l_{CG}\right) A\, dx \\ &= -\rho \frac{\bar{c}}{2} \bar{l}_f V_f \left[U\dot{\theta} - \ddot{z} - \frac{\bar{c}}{2} l_{CG}\ddot{\theta}\right] - \rho \ddot{\theta} \int_0^{l_f \frac{\bar{c}}{2}} A x^2 dx + \frac{\bar{c}}{2} l_{CG} L_f^A \\ &= \rho V_f \left[\frac{\bar{c}}{2}\left(\bar{l}_f - l_{CG}\right)\left(\ddot{z} - U\dot{\theta}\right) - \left(\frac{\bar{c}}{2}\right)^2 \left\{k_f^2 + \left(\bar{l}_f - l_{CG}\right)^2\right\}\ddot{\theta}\right] \end{aligned} \tag{A.48}$$

where

$$\left(\frac{\bar{c}}{2}\right)^2 k_f^2 = \frac{\int_0^{\ell_f \frac{\bar{c}}{2}} A \left(x - \frac{\bar{c}}{2}\bar{\ell}_f\right)^2 dx}{V_f} =$$

the square of the radius of gyration of the volume of the equivalent body of revolution.

(c) Lift and Pitching Moment on Fuselage Due to Gust Penetration

By analogy with equation (A.39), the lift per unit length on a slender fuselage due to a vertical gust of velocity, $w(x,t)$, is

$$\frac{d}{dt}(\rho A w) = \rho U\left(\frac{dA}{dx} w + A \frac{\partial w}{\partial x}\right) + \rho A \frac{\partial w}{\partial t} \qquad \text{(A.49)}$$

Since, however, the gust velocity profile acts as a traveling wave,

$$w(x,t) = w(x - Ut)$$

and

$$U \frac{\partial w}{\partial x} + \frac{\partial w}{\partial t} = 0$$

equation (A.49) reduces to

$$\frac{d}{dt}(\rho A w) = \rho U^2 \frac{w}{U} \frac{dA}{dx} \qquad \text{(A.50)}$$

Thus, the total lift on the fuselage when it penetrates a sharp-edged gust is

$$L_f^G = \rho U^2 \frac{w}{U} \int_0^{s\frac{\bar{c}}{2}} \frac{dA}{dx} dx = \rho U^2 \frac{w}{U} A(s)$$

where $A(s)$ is the cross-sectional area of the equivalent body of revolution at the gust front. The total pitching moment about the airplane center of gravity is

$$m_f^G = -\rho U^2 \frac{w}{U} \int_0^{s\frac{\bar{c}}{2}} \frac{dA}{dx}\left(x - \frac{\bar{c}}{2}\ell_{CG}\right) dx$$

$$= -\rho U^2 \frac{w}{U}\left[Ax - \int A\,dx - \frac{\bar{c}}{2}\ell_{CG}\int dA\right]_0^{s\frac{\bar{c}}{2}} \qquad \text{(A.51)}$$

(Cont.)

$$m_f^G = \rho U^2 \frac{w}{U} \left[V(s) - \frac{\bar{c}}{2} (s - l_{CG}) A(s) \right] \qquad \text{(A.51) (cont.)}$$

Finally, for an arbitrary gust profile,

$$L_f^G = \frac{1}{2} \rho U^2 (2 A_{max}) \int_0^s \frac{w'(\sigma)}{U} \psi_f^L (s - \sigma) \, d\sigma \qquad \text{(A.52)}$$

and

$$m_f^G = \frac{1}{2} \rho U^2 S_w \bar{c} \frac{dC_{m_f}}{d\alpha} \int_0^s \frac{w'(\sigma)}{U} \psi_f^m (s - \sigma) \, d\sigma \qquad \text{(A.53)}$$

where

$$\psi_f^L = \frac{A(s)}{A_{max}}$$

$$\psi_f^m = \frac{V(s)}{V_f} - \frac{\frac{\bar{c}}{2} A_{max}}{V_f} (s - l_{CG}) \frac{A(s)}{A_{max}}$$

A_{max} is the maximum cross-sectional area

V_f is the total volume.

The slope of the moment curve for the fuselage, $\frac{dC_{m_f}}{d\alpha}$, used in equation (A.53), is defined in subsection A.2(a) above as

$$\frac{dC_{m_f}}{d\alpha} = \frac{2 V_f}{S_w \bar{c}}$$

As before, the effect of steady-state interference from the wing can be included in $\frac{dC_{m_f}}{d\alpha}$ even though wing interference probably has a large effect on ψ_f^m as well.

A.3 Unsteady Downwash at Tail

For a constant angle of attack of the wing, the lift on the horizontal tail due to the downwash from the wing is usually written as

$$L_{tw} = -\frac{1}{2}\rho U^2 S_t a_t \frac{d\epsilon}{d\alpha}\alpha_w \tag{A.54}$$

where $\frac{d\epsilon}{d\alpha}$ is the downwash parameter used in aircraft stability analyses and is the rate of change of effective downwash angle at the horizontal tail with respect to the angle of attack of the wing. For a time variation in angle of attack of the wing, equation (A.54) can be modified as follows:

$$L^{\alpha}_{tw} = -\frac{1}{2}\rho U^2 S_t a_t \frac{d\epsilon}{d\alpha}\int_0^s \alpha'(\sigma)\, \zeta^{\alpha}(s-\sigma)\, d\sigma \tag{A.55}$$

and for entry of the wing into a gust, it becomes

$$L^{G}_{tw} = -\frac{1}{2}\rho U^2 S_t a_t \frac{d\epsilon}{d\alpha}\int_0^s \frac{w'(\sigma)}{U}\, \zeta^{G}(s-\sigma)\, d\sigma \tag{A.56}$$

where

$\zeta^{\alpha}(s)$ is a normalized lift-growth function for the tail after a step increase in angle of attack of the wing

$\zeta^{G}(s)$ is a normalized lift-growth function for the tail after entry of the wing into a sharp-edged gust.

It remains to determine the indicial lift-growth functions, $\zeta^{\alpha}(s)$ and $\zeta^{G}(s)$.

The lift-growth on an elliptic tail due to the downwash from an elliptic wing, corresponding to $\zeta^{\alpha}(s)$, was derived in Reference 16 through the use of an unsteady lifting-line theory. This result, however, is not directly applicable to a swept-wing airplane. In References 1 and 2, the unsteady downwash at the tail is found by assuming that the spanwise distribution of bound vorticity is constant at a particular instant of time. This assumption

results in a relatively simple analytical expression for the time variation of downwash at the tail after an abrupt change in circulation on the wing, but the extension of this technique to swept-wing airplanes is complicated and of doubtful validity.

In the present report, the downwash at the tail of the example swept-wing airplane was computed through the use of a vortex lattice system similar to that used in Reference 17 for the steady downwash at the tail. In this system, the circularion on the wing is represented by several discrete vortices of span $b/20$ located on the quarter-chord line of the wing. As shown in Figure A.8, after a step increase in circulation, a rectangular vortex loop of length $s\frac{z}{2} + \frac{3}{4}c$ is formed if the wake vortex is considered to start at the trailing edge. The downwash at the tail caused by each vortex loop can be found from the tables of Reference 17 by superimposing two of the horseshoe vortices of that reference. In the present calculations, the horizontal tail was assumed to be located above the wing wake at a distance of 1/20th of the wing span.

After the indicial downwash had been found for each discrete vortex, the results were added together in proportion to the steady-state spanwise lift distribution to give the total indicial downwash at the tail. The downwash was computed at the apex of the swept horizontal tail because the downwash field was assumed to act as a gust which travelled over the horizontal tail. In the case of gust entry of the wing, the results must be staggered according to the value of s which corresponds to the position of the gust front relative to the leading edge of the wing at each discrete vortex.

To obtain the lift growth on the horizontal tail due to downwash from the wing, the indicial downwash must be integrated in superposition with the

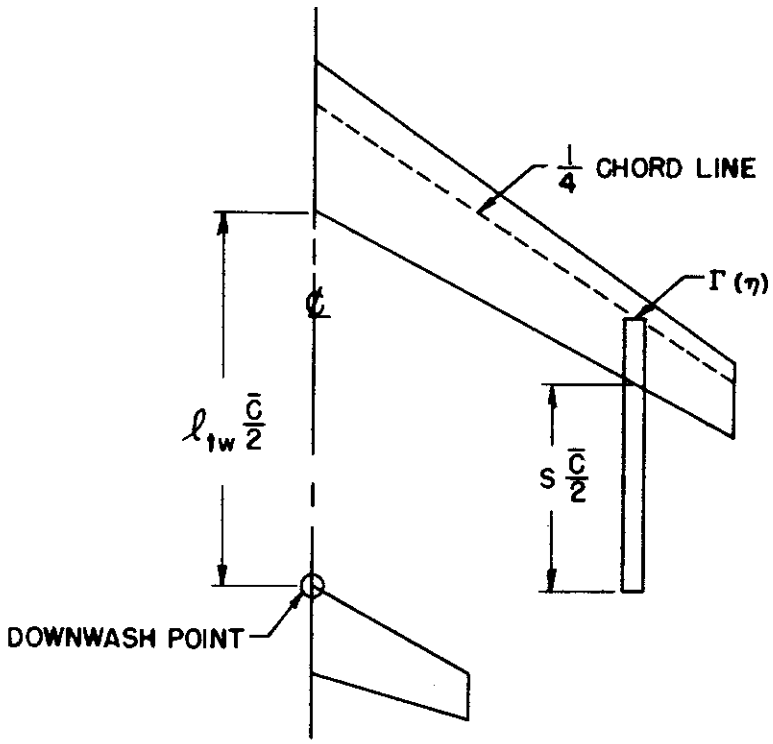

FIGURE A.8 VORTEX LATTICE SYSTEM FOR COMPUTING THE UNSTEADY DOWNWASH

actual circulation growth on the wing and then with the Küssner function for the swept tail. This results in the following expressions for the functions $\zeta^{\alpha}(s)$ and $\zeta^{G}(s)$:

$$\zeta^{\alpha}(s) = \frac{1}{w_{\eta}(\infty)} \int_0^s \psi'_{\Lambda_t}(s-\sigma) \int_0^{\sigma} w_{\eta}(\sigma') \, \psi'(\sigma-\sigma') \, d\sigma' \, d\sigma \qquad (A.57)$$

and

$$\zeta^{G}(s) = \frac{1}{w_{f}(\infty)} \int_{0}^{s} \psi'_{\Lambda_t}(s-\sigma) \int_{0}^{s} w_{f}(\sigma') \chi'(\sigma - \sigma') \, d\sigma' \, d\sigma \qquad \text{(A.58)}$$

where

$w_f(s)$ is the variation in downwash at the apex of the horizontal tail due to a step change in circulation on the wing

$\psi(s)$ is the Küssner function which describes the growth in circulation on the wing due to a step increase in angle of attack

$\chi(s)$ is the circulation-growth function for a wing which enters a sharp-edged gust

$\psi_{\Lambda_t}(s)$ is the lift-growth function for horizontal tail entry into a sharp-edged gust (equation (A.30)).

The circulation-growth function $\chi(s)$ has been derived by Ashley and Brenner (Ref. 2), and, in present calculations, it has been approximated by the expression

$$\chi(s) = 1 - .20e^{-.050s} - .80e^{-.28s} - .234se^{-s} \qquad \text{(A.59)}$$

A comparison between this approximate expression and the exact formulation given in Reference 2 is shown in Figure A.9.

The integrations indicated by equations (A.57) and (A.58) were carried out numerically for the example swept-wing airplane as well as for an equivalent unswept-wing airplane obtained by rotating both the wing and tail about the quarter-chord points of their respective mean aerodynamic chords. These results are given in Figures A.10 and A.11. Some of the parameters involved in the results for the swept-wing airplane are

$AR_w = 9.43$ $\qquad \Lambda_{l_t} = 32.8^\circ$

$AR_t = 4.06$ $\qquad \lambda_w = 0.42$

$\Lambda_{l_w} = 35^\circ$ $\qquad \lambda_t = .423$

$l_{tw} = 7.08$ (see Fig. A.8)

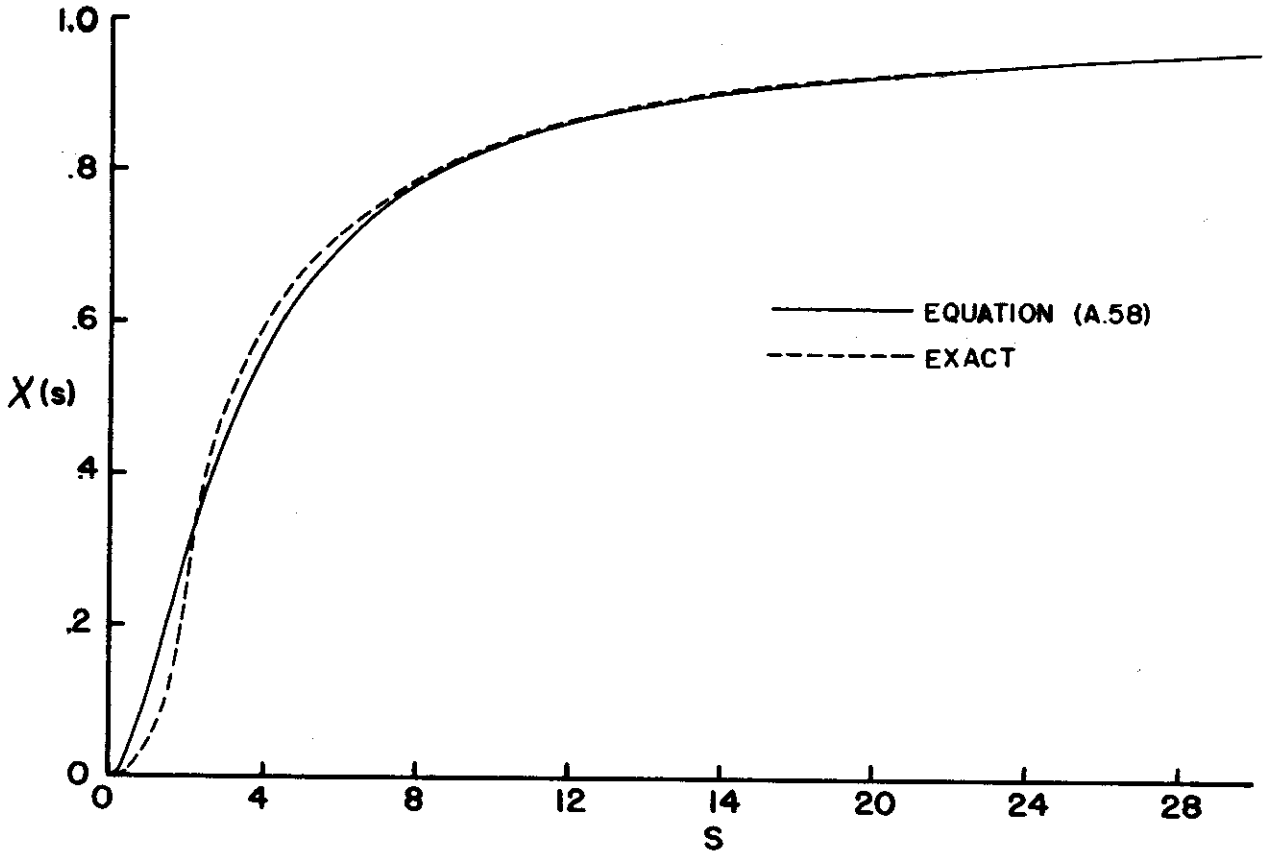

FIGURE A.9 THE CIRCULATION-GROWTH FUNCTION, $\chi(s)$

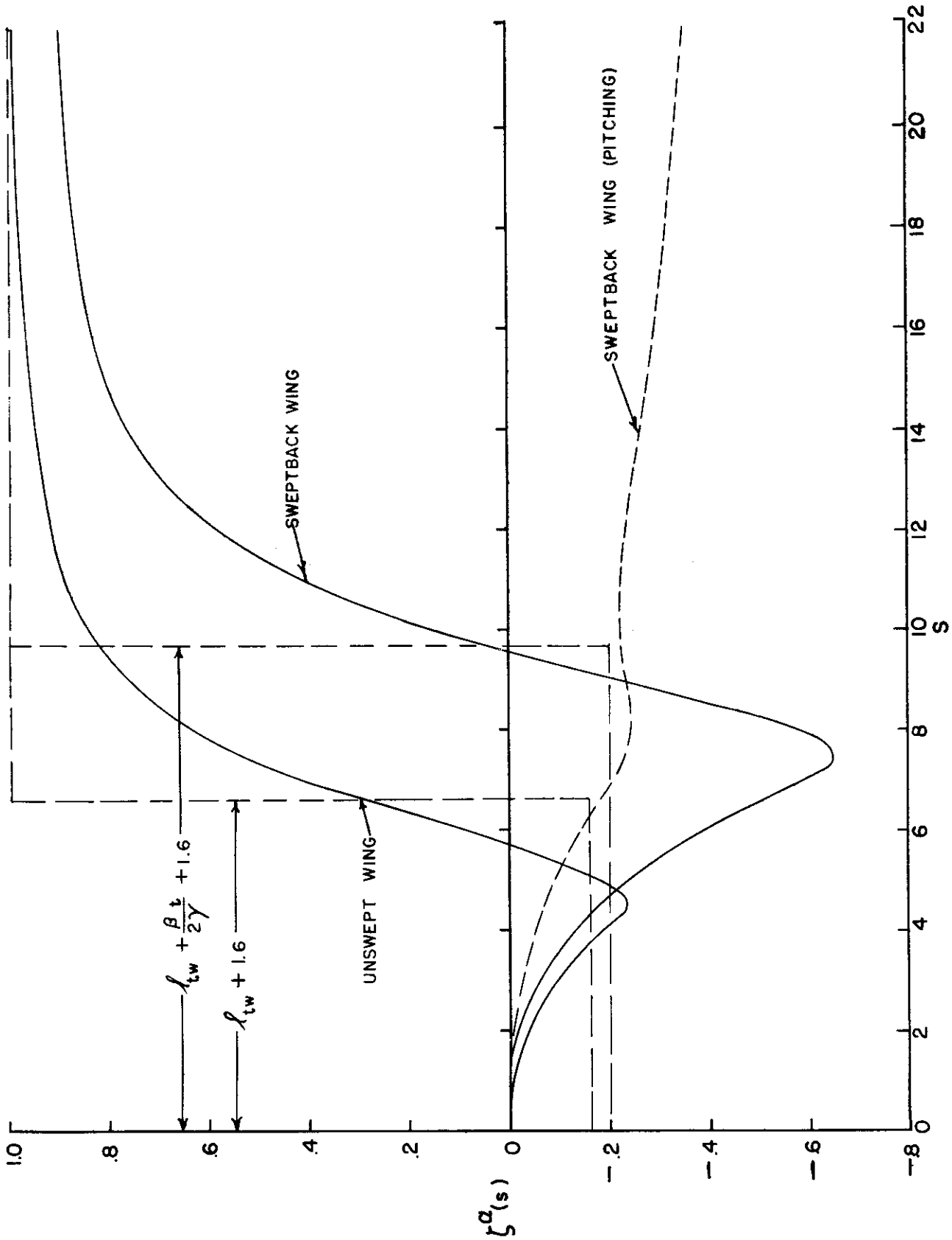

FIGURE A.10 LIFT ON TAIL DUE TO DOWNWASH AFTER AN ABRUPT CHANGE IN WING ANGLE OF ATTACK

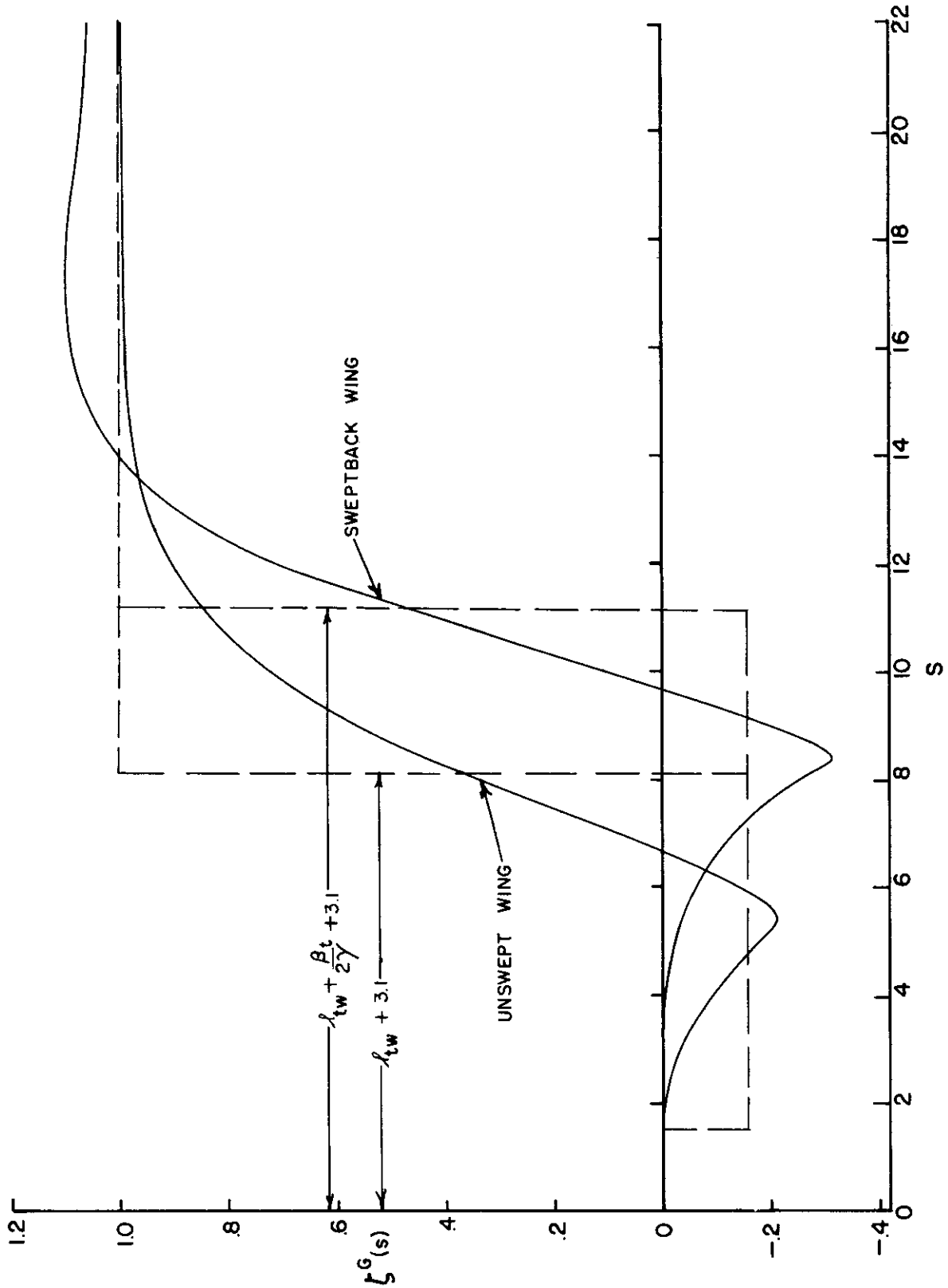

FIGURE A.11 LIFT ON TAIL DUE TO DOWNWASH AFTER ENTRY OF WING INTO A SHARP-EDGED GUST

In Figure A.10, the dashed curve, designated as "sweptback wing (pitching)", is the lift growth on the tail due to a linearly varying angle of attack of the wing which is obtained when the swept wing has a pitching velocity about its root. Although the steady-state downwash on the tail is essentially constant across its span for a constant angle of attack of the wing, it was found that the steady-state downwash for a linear angle of attack is negative at the root and positive at the tip so that the total lift on the tail is very small. Therefore, the lift on the tail due to the pitching velocity of the wing about its root will be assumed negligible.

It is suggested in Reference 16 that, due to the relatively slow motion of the airplane, the $\zeta^{\alpha}(s)$ function can be approximated by step functions for practical purposes. Such an approximation was used in Reference 3 not only for $\zeta^{\alpha}(s)$ but also for $\zeta^{G}(s)$, and the following expressions were recommended:

$$\begin{aligned} \zeta^{\alpha}(s) &= -0.16, \text{ when } s < l_{tw} + 1.6 \\ &= 1.0, \text{ when } s > l_{tw} + 1.6 \end{aligned} \tag{A.60}$$

and

$$\begin{aligned} \zeta^{G}(s) &= 0, \text{ when } s < 1.5 \\ &= -0.16, \text{ when } 1.5 < s < l_{tw} + 3.1 \\ &= 1.0, \text{ when } s > l_{tw} + 3.1 \end{aligned} \tag{A.61}$$

where

l_{tw} is the distance which the tail leading edge lies aft of the wing trailing edge on the airplane center line, measured in mean geometric semichords.

It can be seen that equations (A.60) and (A.61) are reasonable representations of the curves in Figures A.10 and A.11 for the unswept configurations. For the sweptback wing, however, the following modifications are probably better:

$$\zeta^{\alpha}(s) = -0.20, \text{ when } s < l_{tw} + \frac{\beta_t}{2\gamma} + 1.6$$

$$= 1.0 \text{ , when } s > l_{tw} + \frac{\beta_t}{2\gamma} + 1.6 \qquad \text{(A.62)}$$

and

$$\zeta^{G}(s) = 0 \text{ , when } s < 1.5$$

$$= -0.16, \text{ when } 1.5 < s < l_{tw} + \frac{\beta_t}{2\gamma} + 3.1 \qquad \text{(A.63)}$$

$$= 1.0 \text{ , when } s > l_{tw} + \frac{\beta_t}{2\gamma} + 3.1$$

The factor of $\beta_t/2\gamma$ has been included to take into account the lag in lift due to the sweep of the horizontal tail.

A.4 Total Air Forces Due to the Gust

The total lift and pitching moment growth on a constrained airplane entering a sharp-edged gust is obtained by adding the expressions for the air forces on the individual components of the airplane which have been given in the preceding sections of this appendix. Thus, the total lift is given by

$$L^{G}(s) = \frac{1}{2}\rho U^2 S_w a_w f(s) \qquad \text{(A.64)}$$

where

$$f(s) = \frac{W}{U}\left\{\psi_{\lambda}^{L} + \frac{2A_{max}}{S_w a_w}\psi_f^{L} + P_t\,\psi_{\lambda_t} - P_t\frac{d\epsilon}{d\alpha}\zeta^{G}\right\} \qquad \text{(A.65)}$$

and the total pitching moment about the airplane center of gravity, by

$$m^{G}(s) = \frac{1}{2}\rho U^2 S_w \frac{\bar{c}}{2} a_w g(s) \qquad \text{(A.66)}$$

where

$$g(s) = \frac{w}{U}\left\{-l_1 \psi_\lambda^L - (l_w - l_1)\psi_\lambda^m + \frac{2}{a_w}\frac{dC_{mf}}{d\alpha}\psi_f^m - l_t P_t \psi_{\lambda_t} + l_t P_t \frac{d\epsilon}{d\alpha}\zeta^G\right\} \tag{A.67}$$

The tail parameter, P_t , is defined by

$$P_t = \frac{S_t a_t}{S_w a_w} \tag{A.68}$$

Results for other gust profiles can be obtained by the use of Duhamel's integral. Since the dimensionless time s is measured from the time that the gust front strikes the nose of the fuselage in equations (A.65) and (A.67), the gust functions, ψ_λ^L , ψ_λ^m , ψ_{λ_t} , and ζ^G , must be translated accordingly. For example, the function ψ_λ^L was defined in Section A.1 such that $s = 0$ at the time when the gust front strikes the apex of the wing.

The nature of the forcing functions, $f(s)$ and $g(s)$, is illustrated in Figures A.12, A.13 and A.14. In Figure A.12, the lift and moment growths on the example swept-wing airplane considered as rigid are shown when its center of gravity location is such as to give neutral static stability, and it will be seen that there is a significant pitching moment produced by the fuselage even before the wing has entered the gust front. Figure A.13 presents a comparison of the lift and moment growths for the example swept-wing airplane and an equivalent unswept-wing airplane. The equivalent unswept-wing airplane was obtained by rotating both the wing and tail about the quarter-chord points of their respective mean aerodynamic chords. This figure illustrates the large pitching moment produced by the initial entry of the forward inboard portions of the wing into the gust front. Figure A.14 shows that, for swept-wing air-

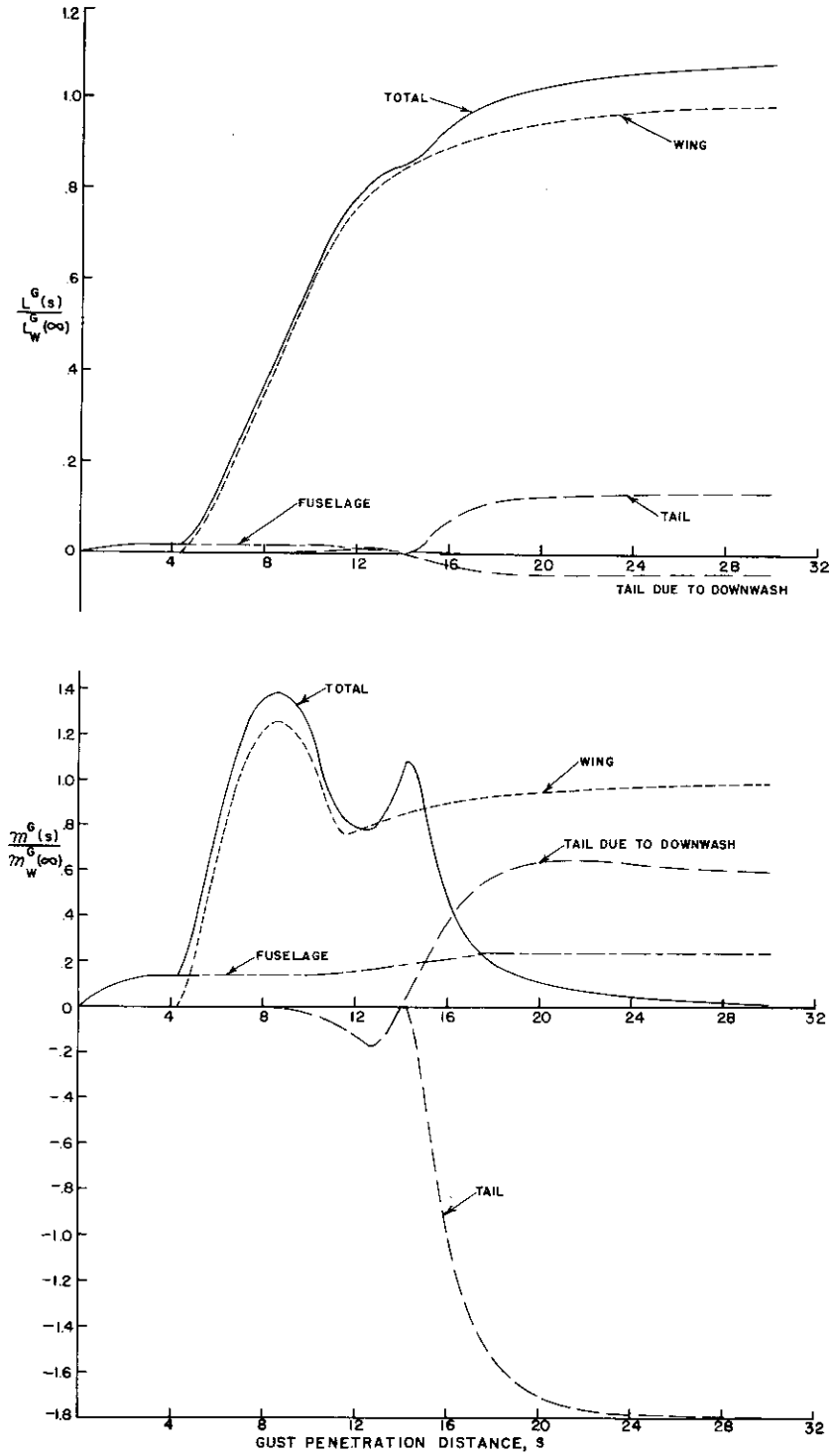

FIGURE A.12 LIFT AND MOMENT GROWTHS ON CONSTRAINED EXAMPLE SWEPT-WING AIRPLANE AFTER ENTRY INTO A SHARP-EDGED GUST, NEUTRALLY STABLE

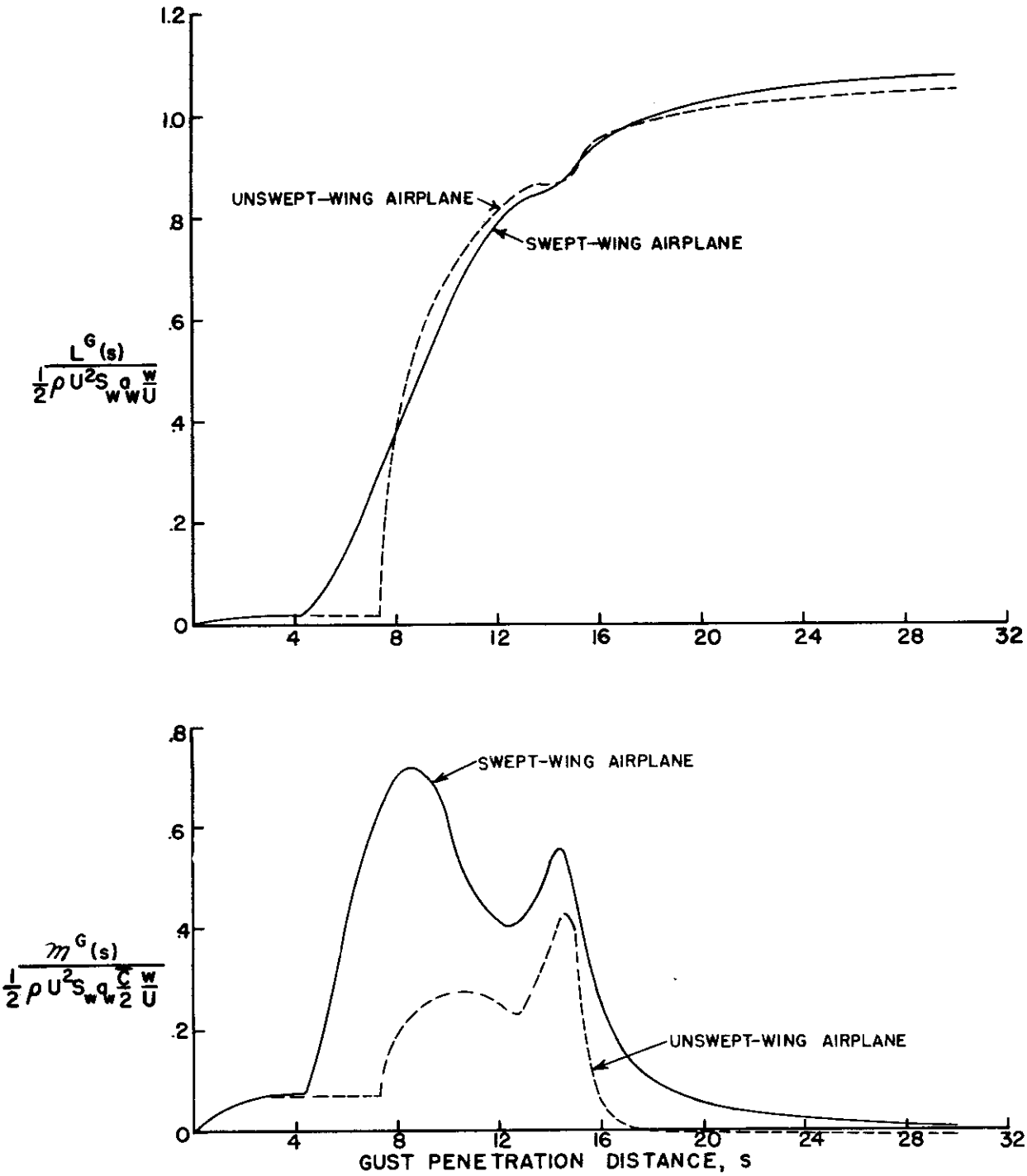

FIGURE A.13 LIFT AND MOMENT GROWTHS ON CONSTRAINED AIRPLANES, SHARP-EDGED GUST, NEUTRALLY STABLE

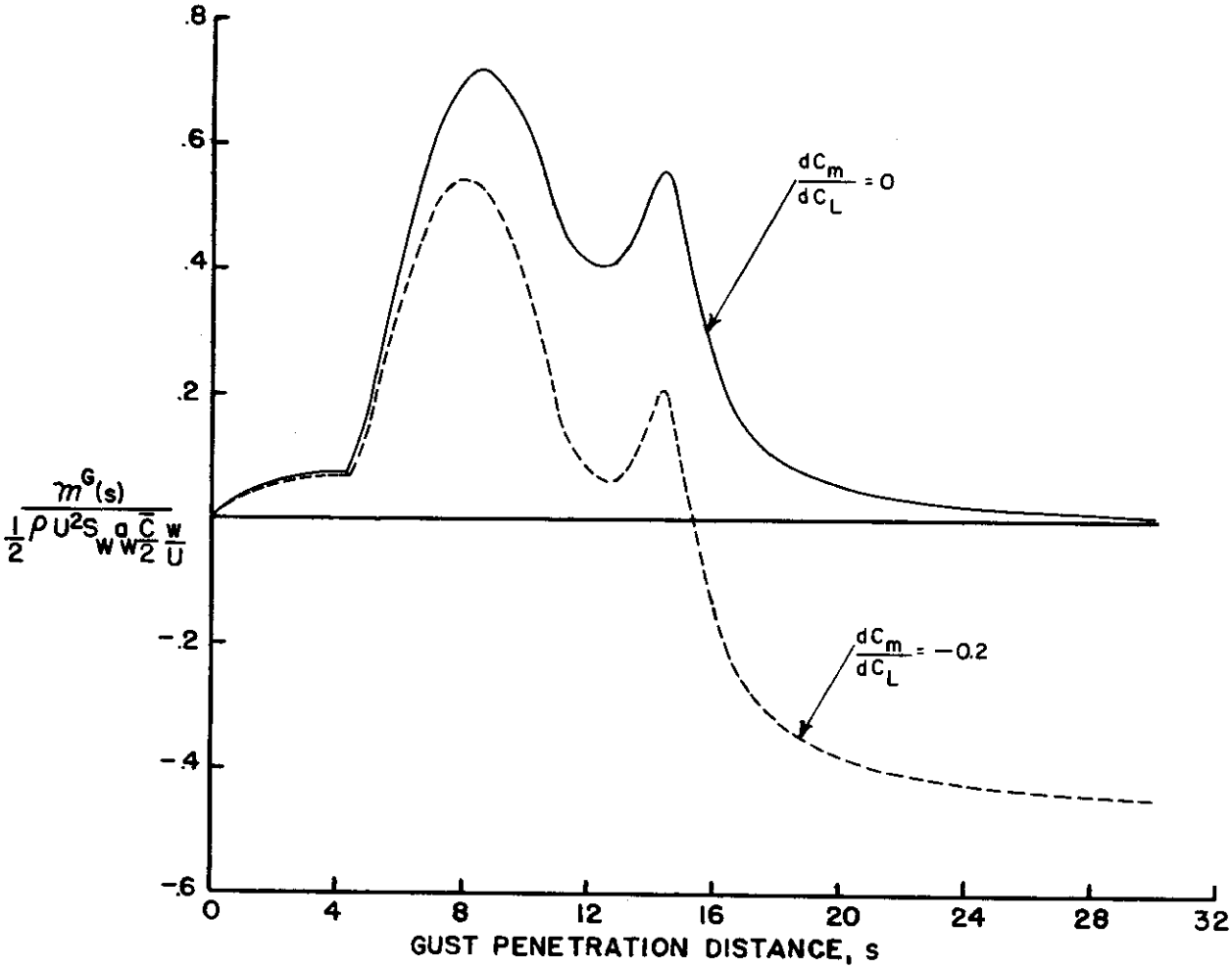

FIGURE A.14 EFFECT OF STATIC STABILITY ON THE PITCHING MOMENT GROWTH FOR THE EXAMPLE SWEPT-WING AIRPLANE

planes, the static stability does not have much effect on the initial phase of the pitching-moment growth and that variations in static stability probably have less effect on the gust loads than they do in the case of unswept-wing airplanes.

APPENDIX B

ACCURACY OF THE NUMERICAL INTEGRATION TECHNIQUE

The purpose of this appendix is to determine the accuracy, convergence and stability of the numerical integration technique of Section II which was used to solve the equations of motion derived in Section I. Levy and Kroll (Ref. 18) investigated the accuracy, convergence and stability of the fourth-difference numerical integration formula used by Houbolt (Ref. 4) to solve a a dynamic gust response problem, and an analogous approach to the problem is used in this appendix.

The integration formulas used in Section II are

$$\dot{z}_n = \dot{z}_{n-1} + \frac{h}{2}\left(\ddot{z}_n + \ddot{z}_{n-1}\right) \tag{B.1}$$

and

$$z_n = z_{n-1} + h\,\dot{z}_{n-1} + \frac{h^2}{6}\ddot{z}_n + \frac{h^2}{3}\ddot{z}_{n-1} \tag{B.2}$$

These formulas give the velocity $\dot{z}$ and the displacement z at the time $t = nh$ in terms of the acceleration $\ddot{z}$ at the time $t = nh$ and the acceleration, velocity and displacement at the previous discrete time $t = (n-1)h$. Equations (B.1) and (B.2) are based on the approximation of the acceleration time history by straight-line segments of length h.

To investigate the approximations inherent in equations (B.1) and (B.2), these formulas can be applied to the homogeneous solution of a simple spring-mass system whose equation of motion is

$$\ddot{z} + \omega^2 z = 0 \tag{B.3}$$

when the natural frequency of vibration of the system is ω . The substitution of equation (B.2) into (B.3) yields

$$\left(1 + \frac{1}{6}\omega^2 h^2\right)\ddot{z}_n = -\frac{1}{3}\omega^2 h^2 \ddot{z}_{n-1} - \omega^2 h \dot{z}_{n-1} - \omega^2 z_{n-1} \qquad \text{(B.4)}$$

A point-by-point solution of equation (B.3) for z , $\dot{z}$ and $\ddot{z}$ is then obtained by the alternate use of equations (B.4), (B.1) and (B.2). In such a simple case, however, a closed-form solution can be obtained with the present numerical method by applying the calculus of finite differences. Let

$$\ddot{z} = A\beta^n \qquad \text{(B.5)}$$

$$\dot{z} = B\beta^n \qquad \text{(B.6)}$$

and

$$z = C\beta^n \qquad \text{(B.7)}$$

The substitution of these expressions into equations (B.4), (B.1) and (B.2) gives

$$\left(1 + \frac{1}{6}\omega^2 h^2\right)A\beta^n + \frac{1}{3}\omega^2 h^2 A\beta^{n-1} + \omega^2 h B\beta^{n-1} + \omega^2 C\beta^{n-1} = 0 \qquad \text{(B.8)}$$

$$B\beta^{n-1}(\beta - 1) = \frac{1}{2}hA\beta^{n-1}(\beta + 1) \qquad \text{(B.9)}$$

and

$$C\beta^{n-1}(\beta - 1) = hB\beta^{n-1} + \frac{1}{6}A\beta^{n-1}(\beta + 2) \qquad \text{(B.10)}$$

respectively. These equations can be combined into one equation,

$$(1 + \tfrac{1}{6}\omega^2h^2)\beta^2 - 2(1 - \tfrac{1}{3}\omega^2h^2)\beta + (1 + \tfrac{1}{6}\omega^2h^2) = 0 \qquad \text{(B.11)}$$

The solution of equation (B.11) for β is

$$\beta = \frac{1 - \frac{1}{3}\omega^2h^2}{1 + \frac{1}{6}\omega^2h^2} \pm \sqrt{\left(\frac{1 - \frac{1}{3}\omega^2h^2}{1 + \frac{1}{6}\omega^2h^2}\right)^2 - 1} \qquad \text{(B.12)}$$

When, for example, $h = \sqrt{2}/\omega$,

$$\beta = 0.2500 \pm 0.9682\,i$$

and, therefore,

$$z = C_1\,(.25 + .9682\,i)^n + C_2\,(25 - .9682\,i)^n \qquad \text{(B.13)}$$

or

$$z = C_1 \sin 1.3181n + C_2 \cos 1.3181n \qquad \text{(B.14)}$$

Since $n = \omega t/\sqrt{2}$,

$$z = C_1 \sin .932\,\omega t + C_2 \cos .932\,\omega t \qquad \text{(B.15)}$$

The exact analytical solution of equation (B.3) is

$$z = C_1 \sin \omega t + C_2 \cos \omega t \qquad \text{(B.16)}$$

Thus, when the increment $h = 0.225\,T$, which is a little less than one quarter of the natural period of vibration, this numerical method gives a solution which oscillates with a frequency of $0.932\,\omega$ rather than of ω .

In Reference 18, the fourth-difference equation

$$\ddot{z}_n = \frac{1}{h^2}\left(2 z_n - 5 z_{n-1} + 4 z_{n-2} - z_{n-3}\right) \qquad (B.17)$$

was applied to equation (B.3), and the results which were obtained are given in Table B.1, together with comparable results obtained with the present method. Table B.1 also presents the results obtained by the use of the following parabolic integration formulas:

$$\dot{z}_n = \dot{z}_{n-1} + \frac{h}{12}\left(5 \ddot{z}_n + 8 \ddot{z}_{n-1} - \ddot{z}_{n-2}\right) \qquad (B.18)$$

$$z_n = z_{n-1} + h \dot{z}_{n-1} + \frac{h^2}{24}\left(3 \ddot{z}_n + 10 \ddot{z}_{n-1} - \ddot{z}_{n-2}\right) \qquad (B.19)$$

These formulas have the same basis as Simpson's rule and should be more accurate than the linear integration formulas, namely, equations (B.1) and (B.2), which are based on the trapezoidal rule of integration.

The solutions obtained by all of the three numerical methods can be written as

$$z = C_1 e^{\gamma_2 \omega t} + e^{\gamma_3 \omega t}\left(C_2 \sin \gamma_1 \omega t + C_3 \cos \gamma_1 \omega t\right) \qquad (B.20)$$

and the γ coefficients are listed in Table B.1.

Table B.1 shows that all of the methods converge to the exact solution as the increment h approaches zero and that the integration methods converge more rapidly than the difference method. Also, when the increment h is a little larger than half the natural period of vibration, the numerical integration solutions "blow up", i.e., they become hyperbolic rather than sinusoidal.

TABLE B.1

COMPARISON OF RESULTS FROM USE OF NUMERICAL METHODS ON SIMPLE SPRING-MASS SYSTEM

h	γ	FOURTH DIFFERENCE	LINEAR INTEGRATION	PARABOLIC INTEGRATION
0	γ_1	1.0	1.0	1.0
	γ_2	$-\infty$	$-\infty$	$-\infty$
	γ_3	0	0	0
$\sqrt{0.1}/\omega =$ 0.0503 T	γ_1	.961	0.996	0.9999
	γ_2	-2.32	$-\infty$	-17.37
	γ_3	-.0095	0	.00065
$\sqrt{2}/\omega =$ 0.225 T	γ_1	.712	.932	.973
	γ_2	-.701	$-\infty$	-1.988
	γ_3	-.139	0	.036
$\sqrt{10}/\omega =$ 0.503 T	γ_1	.457	.834	.872
	γ_2	-.400	$-\infty$	-.689
	γ_3	-.193	0	.078
$\sqrt{98}/\omega =$ 1.575 T	γ_1	.183	HYPERBOLIC	HYPERBOLIC
	γ_2	-.180		
	γ_3	-.142		

Since the present report is concerned with equations of motion which contain damping terms, the three numerical methods are applied to a simple spring-mass-damper system described by

$$\ddot{z} + 2\zeta\dot{z} + (\omega^2 + \zeta^2)z = 0 \tag{B.21}$$

where

ζ is a damping coefficient

ω is the damped frequency.

The analytical solution of equation (B.21) is

$$z = e^{-\zeta\omega t}(C_1 \sin\omega t + C_2 \cos\omega t) \tag{B.22}$$

while the numerical solutions are given by Table B.2 for $\zeta = \frac{1}{4}\omega$. These results show that the inclusion of damping does not have much effect on the relative accuracy, convergence and stability of the three methods.

The linear integration formulas, equations (B.1) and (B.2), were chosen for the solution of the equations of motion in Section II because they are simpler to use than the parabolic integration formulas and give results of comparable accuracy. The linear integration method is more accurate than the fourth-difference method and is probably as easy to apply numerically. In the linear integration method, z_n , $\dot{z}_n$ and $\ddot{z}_n$ must be carried in the step-by-step numerical process, but all of these quantities are usually required in a gust-load analysis. Thus, it is only necessary to refer back one time increment in the step-by-step process. In the fourth-difference method, only z_n need be carried in the numerical process, but the resulting recurrence formulas refer back to z_{n-1} , z_{n-2} and z_{n-3} . As a result, there is difficulty in starting the numerical process, i.e., in satisfying the initial

conditions. In the analysis of a system with many degrees of freedom, it is often difficult to avoid the use of a time increment which is large in comparison with the period of vibration of one of the higher modes, and the fourth-difference method has the advantage that it does not "blow up". But it does not seem logical to include higher modes of vibration when their effects cannot be taken into account by the numerical solution.

As a further check on the accuracy of the numerical method of Section II, the method has been applied to the single-degree-of-freedom gust load problem for which analytical solutions are given in Reference 19. In the notation of the present report, the equation of motion in Reference 19 is

$$(2\mu + \tfrac{1}{2})\, z'' + \int_0^s z''(\sigma)\, \phi(s-\sigma)\, d\sigma = \psi(s) \qquad \text{(B.23)}$$

This equation represents the entry of an unswept-wing airplane into a sharp-edged gust. Only the lift on the wing is considered, and the airplane is restrained from pitching.

Equation (B.23) was solved by the numerical technique of Section II, and the results are presented in Table B.3 for $\mu = 35.6$ and for different values of the dimensionless time increment, ϵ. These results illustrate the rapid convergence of this numerical method to the exact solution, i.e., $\epsilon = 0$. In this particular case, results which are accurate to three significant figures are obtained when $\epsilon = 2$.

The accuracy of the numerical solutions presented in Section IV is illustrated in Table B.4. The results represented by the solid curves (with pitching) of Figure 4.1 were computed with integration intervals of $\epsilon = 1$ and $\epsilon = 2$, and the numerical values obtained at a gust penetration distance of $s = 24$ are given in Table B.4. The convergence of the numerical method is apparently as good in this case as in the simpler gust loading problem described previously.

TABLE B.2

COMPARISON OF RESULTS FROM USE OF NUMERICAL METHODS ON SPRING-MASS-DAMPER SYSTEM, $\zeta = \frac{1}{4}\omega$

h	γ	FOURTH DIFFERENCE	LINEAR INTEGRATION	PARABOLIC INTEGRATION
0	γ_1	1.0	1.0	1.0
	γ_2	$-\infty$	$-\infty$	$-\infty$
	γ_3	-.250	-.250	-.250
$\sqrt{0.1}/\omega =$ 0.0503 T	γ_1	.959	.997	1.0007
	γ_2	-2.15	$-\infty$	-14.73
	γ_3	-.223	-.246	-.2496
$\sqrt{2}/\omega =$ 0.225 T	γ_1	.651	.952	1.031
	γ_2	-.644	$-\infty$	-2.417
	γ_3	-.200	-.189	-.193
$\sqrt{10}/\omega =$ 0.503 T	γ_1	.407	.900	HYPERBOLIC
	γ_2	-.365	$-\infty$	
	γ_3	-.184	-.093	
$\sqrt{98}/\omega =$ 1.575 T	γ_1	.165	HYPERBOLIC	HYPERBOLIC
	γ_2	-.156		
	γ_3	-.112		

TABLE B.3

CONVERGENCE OF THE NUMERICAL METHOD

FOR THE SIMPLE GUST LOAD PROBLEM, $\mu = 35.6$

	ACCELERATION RATIO, $2\mu\frac{s}{c}$			
s \ ϵ	2	1	$\frac{1}{2}$	0
0	0	0	0	0
2	.5392	.5380	.5377	.5376
4	.6740	.6725	.6721	.6720
6	.7351	.7334	.7330	.7328
8	.7717	.7700	.7695	.7694
10	.7940	.7922	.7917	.7916
12	.8058	.8041	.8036	.8035
14	.8099	.8082	.8078	.8076
16	.8082	.8064	.8060	.8058
18	.8019	.8002	.7998	.7996
20	.7923	.7907	.7902	.7901

TABLE B.4

ACCURACY OF THE NUMERICAL METHOD

FOR A TWO-DEGREES-OF-FREEDOM GUST PROBLEM, $s = 24$

ϵ	1	2
$\frac{C_L}{a_w \frac{w}{U}}$	0.9949	0.9951
$\frac{C_{L_w}}{a_w \frac{w}{U}}$	.9121	.9123
$\frac{C_{L_t}}{a_w \frac{w}{U}}$	.0839	.0838
$\frac{C_{L_f}}{a_w \frac{w}{U}}$	-.0010	-.0010
$\frac{\theta}{w/U}$	.0850	.0851
$\frac{\alpha}{w/U}$	.9284	.9285

APPENDIX C

EFFECTS OF NEGLECT OF UNSTEADY FLOW IN THE DAMPING TERMS

In the latter part of Section II, the simplification of neglecting the effects of unsteady flow in the damping terms is found to reduce greatly the complexity of the numerical method of that section. This simplification is primarily due to the replacement of the Wagner function, $\phi(s)$, by a unit step function.

Some indication of the errors involved is illustrated by Figure C.1. The gust loads on the example airplane considered as rigid and free to pitch were computed both with and without unsteady flow effects in the damping terms, and the results are given in this figure. Neglect of unsteady flow effects resulted in an underestimate of the peak wing load of about 1% and of the peak tail load of less than 1%. By contrast, Figure 4.1 showed that the neglect of the pitching degree of freedom resulted in an underestimation of the peak wing load of about 7% and of the peak tail load of 20%. Thus, it appears that unsteady flow in the damping terms has only a secondary effect on the gust loads on a rigid airplane which is free to pitch.

In an attempt to determine the generality of the above conclusion, the same simplification was made in the simple gust load problem described by equation (B.23). When the lift due to motion is considered quasi-steady, equation (B.23) becomes

$$2\mu \zeta'' + e \zeta' = \psi(s) \qquad (C.1)$$

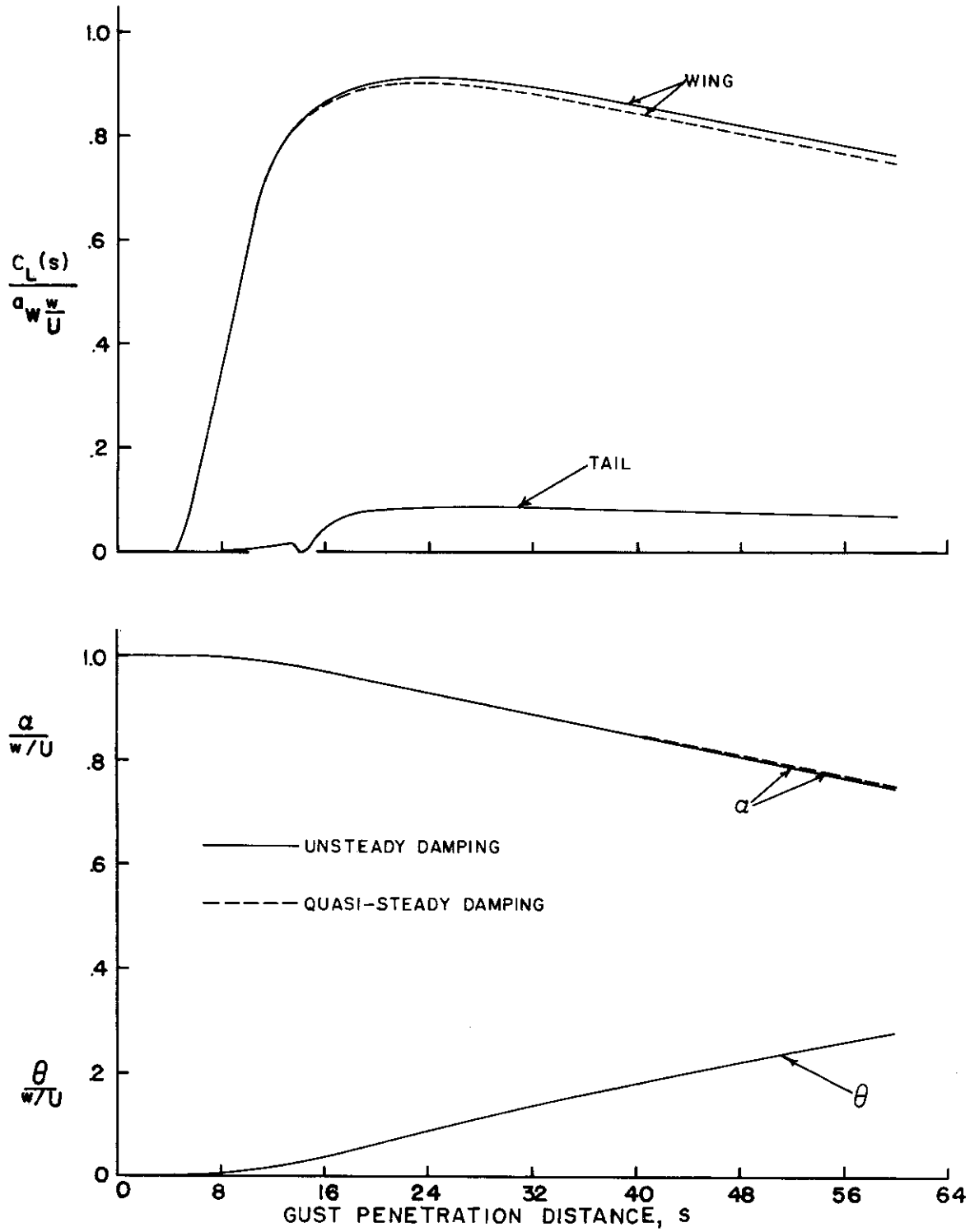

FIGURE C.1 EFFECT OF NEGLECTING UNSTEADY FLOW IN THE DAMPING TERMS, PITCHING MOTION INCLUDED, SHARP-EDGED GUST

The efficiency factor e was introduced after the manner of Reference 20 to approximate the reduction in damping due to unsteady flow effects. In Figure C.2 the effects of the efficiency factor e and the mass parameter μ on the error in the peak gust load are shown.

When an efficiency factor of $e = 1$ is used, the error in the peak gust load is always unconservative and is largest when the mass parameter is small. Also, the error is larger in this simple case than it is when the effects of wing sweep and pitching are included because the lifts due to the heaving and pitching motions tend to cancel each other. The error is always conservative when $e = 0.75$, and perhaps such an efficiency factor should be included in the simplified method of Section II.

Figures C.3 and C.4 show that the use of quasi-steady damping results in errors which are more unconservative at high subsonic speeds than for cases in which the flow is incompressible. An efficiency factor of $e = 0.75$ would, however, give good results. The Wagner function for a Mach number of $M = 0.7$, obtained from Reference 6, was normalized as follows:

$$\phi(s) = 1 - .364\, e^{-.0536s} - .405\, e^{-.357s} + .419\, e^{-.902s} \qquad (C.2)$$

The compressible-flow results of Figures C.3 and C.4 do not include the effects of compressibility on the lift-curve slope nor those on the Küssner function because only the effects of unsteady flow on the damping terms are compared.

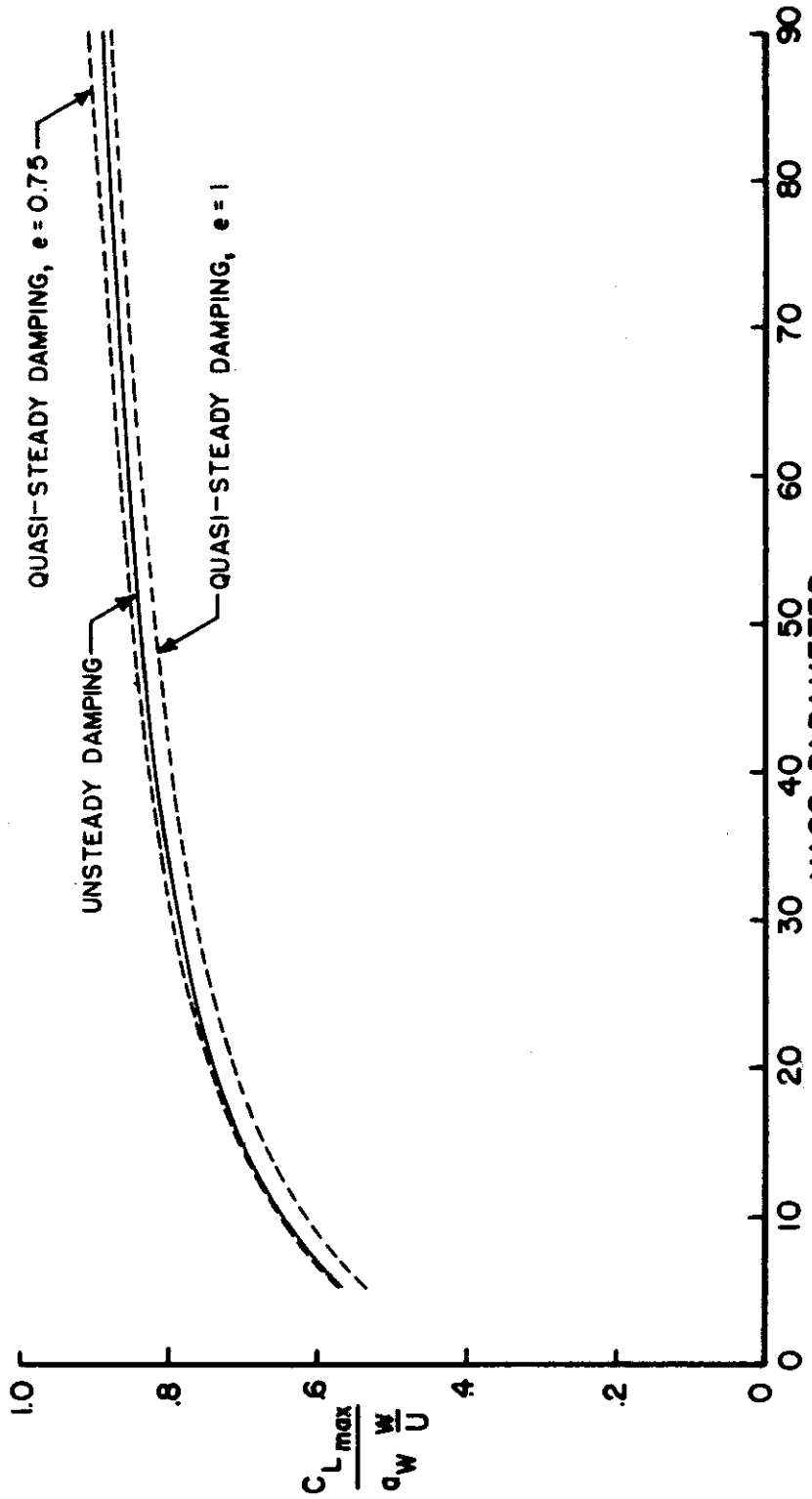

FIGURE C.2 EFFECT OF NEGLECTING UNSTEADY FLOW IN THE DAMPING TERMS, SINGLE DEGREE OF FREEDOM, SHARP-EDGED GUST

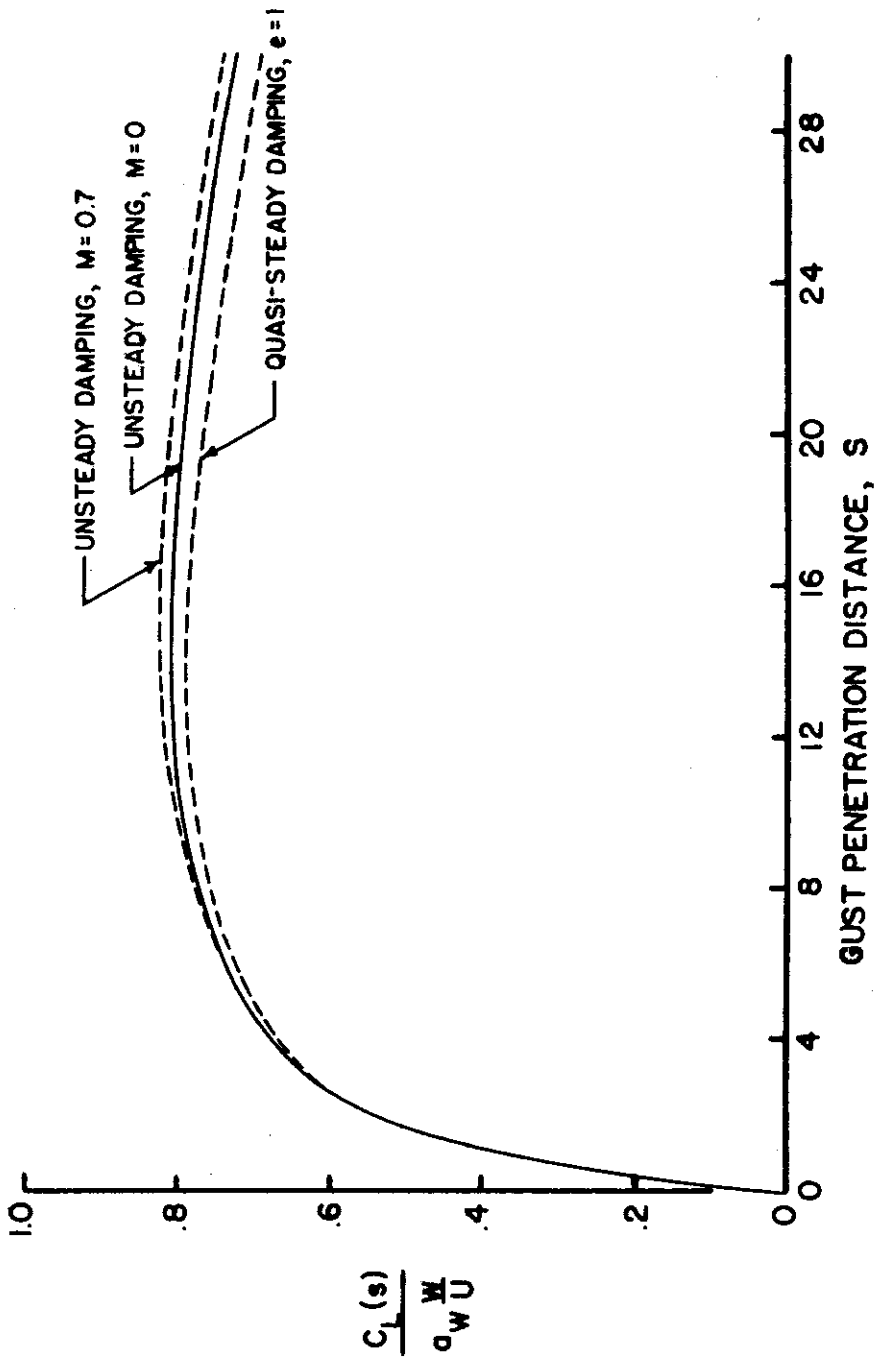

FIGURE C.3 EFFECT OF NEGLECTING UNSTEADY FLOW IN THE DAMPING TERMS, SINGLE DEGREE OF FREEDOM, SHARP-EDGED GUST, $\mu = 35.6$

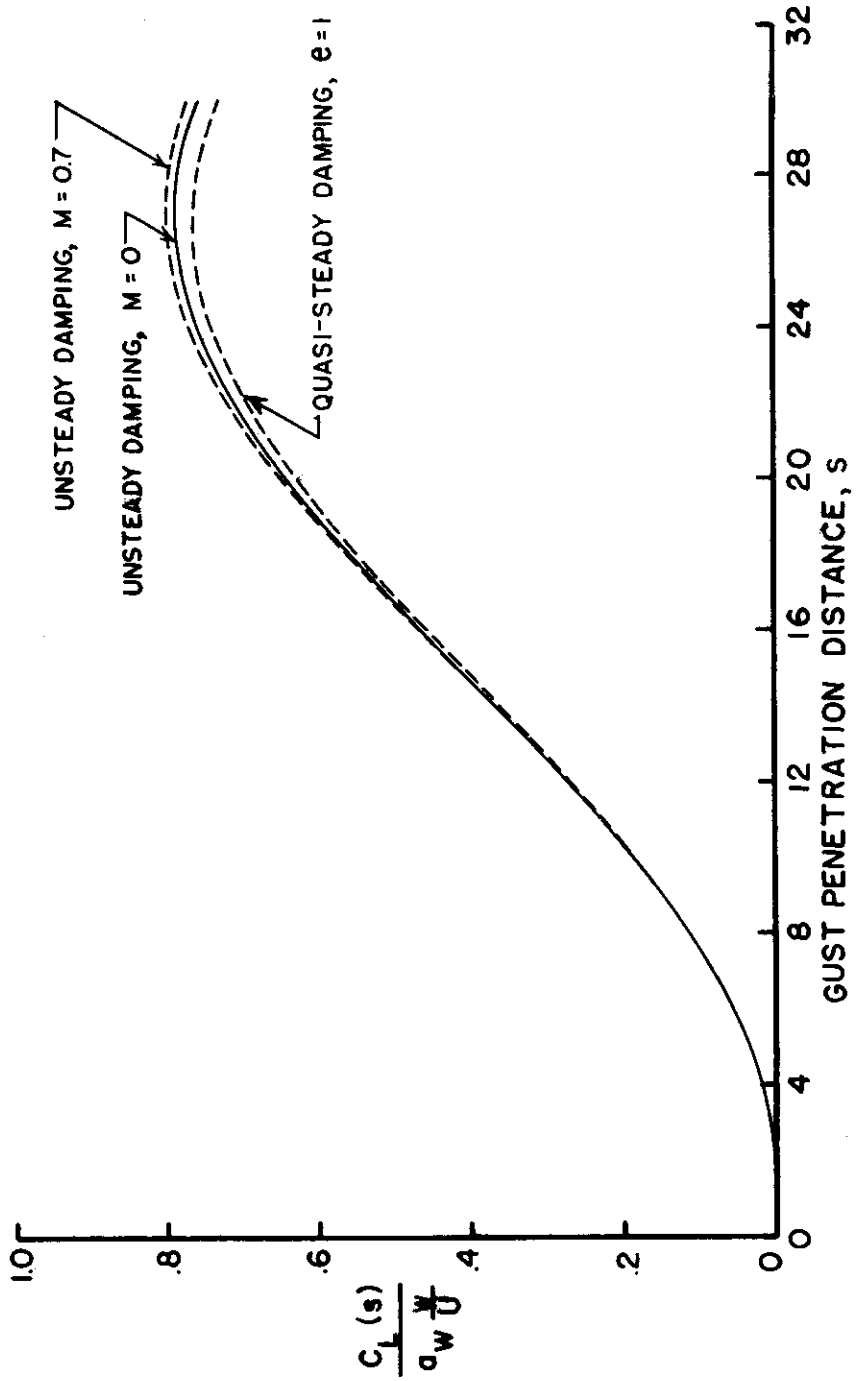

FIGURE C.4 EFFECT OF NEGLECTING UNSTEADY FLOW IN THE DAMPING TERMS, SINGLE DEGREE OF FREEDOM, ONE-MINUS-COSINE GUST, $s_g = 25$, $\mu = 35.6$